UiT The Arctic University of Norway

Faculty of Science and Technology
Department of Geology

# *Gas seeps in the Barents Sea – how does the geology influence the natural and well related seeps?*

**Hieu Khanh Nguyen**

*GEO-3900 Master Thesis in Geology*
*July 2021*

# ABSTRACT

This thesis examined gas flares found in the Cruise log 20-2 from CAGE and correlated them to subsurface seismic data in south of Barents Sea. The cruise log passed several hydrocarbon discoveries/fields such as Goliat, Caurus/Langlitinden, Norvarg and Wisting/Hanssen. The aim of the thesis is to investigate the relationship between shallow geology and the observed gas flares and seabed leakages.

Multibeam echosounder data and Water Column Imaging (WCI) is used to hunt the flares along the cruise, 12 flare locations are detected mostly over the hydrocarbon discoveries/fields. Well data is also used to investigate if or how some of the flares might be connected to the drilling activities. However, not all amplitude anomalies in the WCI are gas flares, thus a protocol to define gas flares in WCI is applied.

Tectonic movements and uplift in the study area cause faulting and fault reactivation, which open migration pathways from reservoir levels and fluids escape towards the seabed. Additionally, erosion and removal of as much as 2km sediments reduce the overburden pressure, causing the reservoir fluids to expand and escape. Repeated glaciation events during the last ice age formed an unconformity surface (URU) where many potential shallow gas accumulations locate. Shallow accumulation/seismic anomaly along the URU is the main target of this thesis.

Some of the observed gas flares are closely related to hydrocarbon wells in the study area, gas might migrate through well-induced fractures along the wellpath. The relationship between deeper gas accumulations, hydrocarbon wells, shallow gas accumulation and potential leakage of gas into the water column is not straight forward. More empirical data and investigations needs to be applied to increase the knowledge of these interrelated and complicated processes.

# PREFACE

This 60 ETC thesis is the final work of a 2-year Master's program in Petroleum Geology at UiT – The Arctic University of Tromso. The thesis is supervised by Stig-Morten Knutsen and two secondary supervisor Rune Mattingsdal from NPD and Pavel Russerov from CAGE. Seismic data is provided by NPD and Water Column multibeam data is provided by CAGE.

# ACKNOWLEDGEMENT

I would like to express my appreciation to my supervisors and my lecturers who have been incredibly supportive during my study in Norway. In the time of the pandemic, many strange things did impact everyone and limited the time of personal interactive. However, all the staff in the Department of Science and Technology as well as UiT have shown great support and motivate me on my thesis.

I would like to thank Mr. Knutsen for being so educative and orienting to me, motivating me on this thesis. Rune Mattingsdal and Pavel Russerov as secondary supervisors have helped me on the datasets and guide me the advanced techniques in processing data.

I also would like to thank the Board of Geology department, particularly Kai Mortensnes for allowing me more opportunity to finish my thesis remotely and successfully.

# TABLE OF CONTENTS

## Contents

# 1 INTRODUCTION

The objective of this thesis is to look for seepage locations by spotting gas bubble features (as known as gas flares) in the water column and determine their correlation with subsurface features, such as faulting, seismic anomalies, indicators of shallow gas accumulation and potential migration pathways of found gas seeps. Subsequently, observations of seismic anomalies, thickness maps, potential faults/weak zones at the flares' location will be made to explain how geology influence seepages in water column.

Greenhouse gases (GHGs), consisting of anthropogenic and halogenated gases, are mainly referred to carbon dioxide ($CO_2$) to cause atmospheric temperature increase by trapping infrared radiation. Additionally, other GHGs such as methane ($CH_4$), nitrous oxide ($N_2O$) as well as halogenated compounds (CFCs, HFCs and PFCs) concentration have been observed to increase in the atmosphere which are proven to enhance the greenhouse effect (European Environment Agency, 1999). Apart from man-made GHGs emissions through energy combustion, land use, deforestation, … naturally occurred emissions such as degassing of magma, contact metamorphism of carbonate rocks, biogenic breakdown of oil and gas, leakage of matured type III kerogen in sedimentary basins,… (IEA, 2005) are also note-worthy because they happen at a constant pace in millions of years scale are difficult to control. The leakages of natural gas into the Earth's atmosphere can be a direct injection of methane into the atmosphere in both on- and off-shore environments which contributes to the global warming.

Within this thesis, gas emissions from seepages in marine environment are focused. Seepages of natural gas consist mainly of methane, ethane and propane, they contribute to inject these gases into the atmosphere.

# 2 STUDY AREA AND GEOLOGICAL SETTINGS

## 2.1 Study area

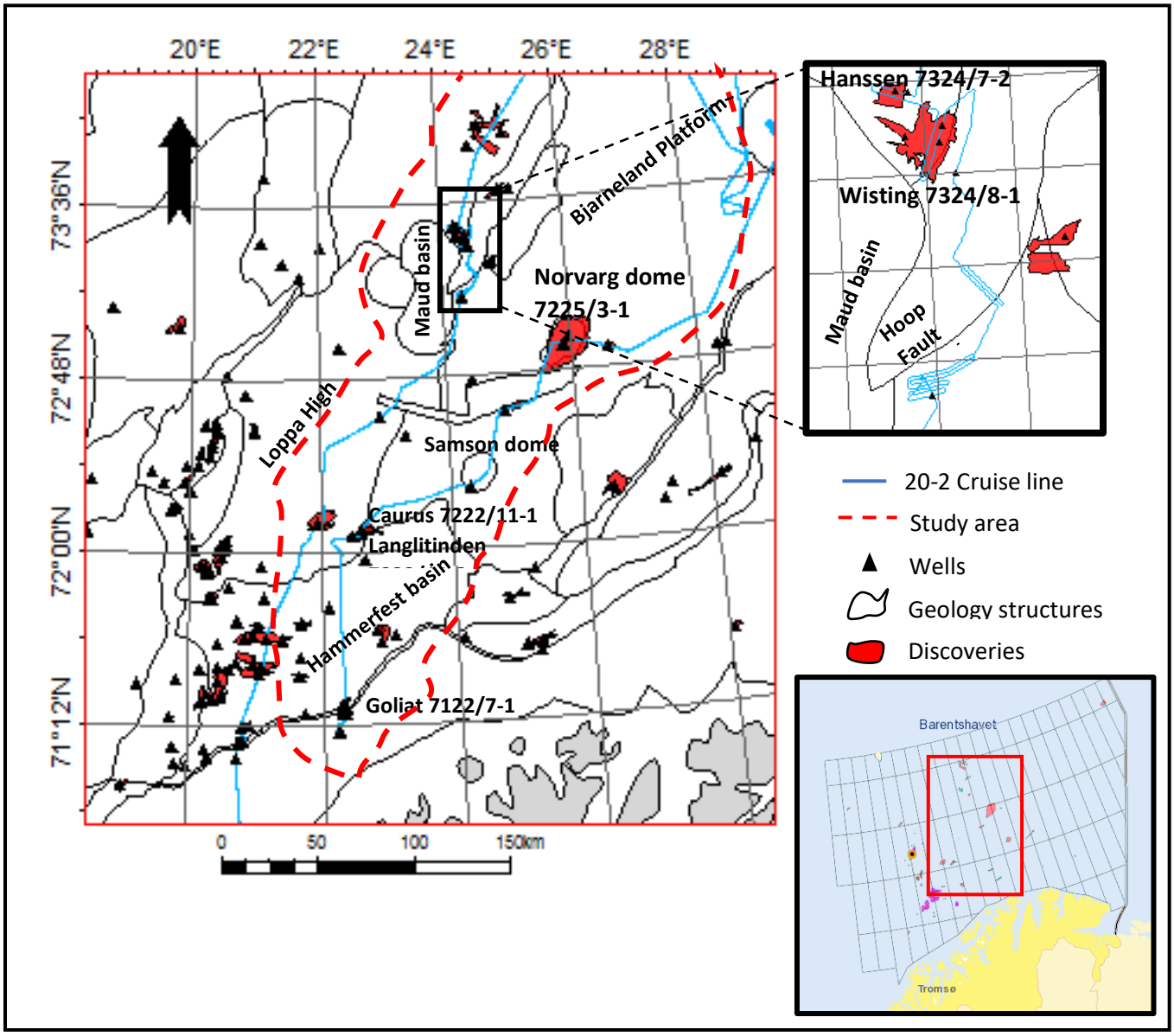


*Figure 2.1 Study area (within red dash line) in south of Norwegian Barents Sea following the gas flare hunting cruise 20-2 from CAGE (blue line). The region includes several petroleum fields/discoveries with well data available on NPD.no*

The study area is in south of Norwegian Barents Sea (south of 74º34'N), it follows a gas flare hunting cruise from Center for Arctic Gas Hydrate, Environment and Climate (CAGE) and is delineated by red dash line in Figure 2.1. Main structural elements included in the study are NE edge of Hammerfest Basin, SE end of Loppa High, Bjarmeland Platform, Samson Dome, Swaen

Graben Norvarg Dome and Hoop Fault Complex. The study area also encounters petroleum discoveries and exploration wells namely Caurus (7222/11-1), Langlitinden (7222/11-2), Arenaria (7224/6-1), Ververis (7226/2-1), Hanssen (7324/7-1), Wisting (7234/8-1) and well 7224/7-1 over Samson Dome.

*Water depths*

Figure 2.2 illustrates the bathymetric map of the Barents Sea using applied temperature and salinity profiles from the World Ocean Database, according to the authors, "the Barents Sea is relatively shallow with bottom depth varying from 50 to 500 meters"(Hjelmervik et al., 2015). Examinations the wells available within the study area (figure 2.2, within red delineation), water depths vary from 266m to 377m in the Bjarmeland Platform, NE Hammerfest Basin and SE Loppa High areas, whereas deeper water depths of 390m to 413m are reported in the Hoop Fault Complex area.

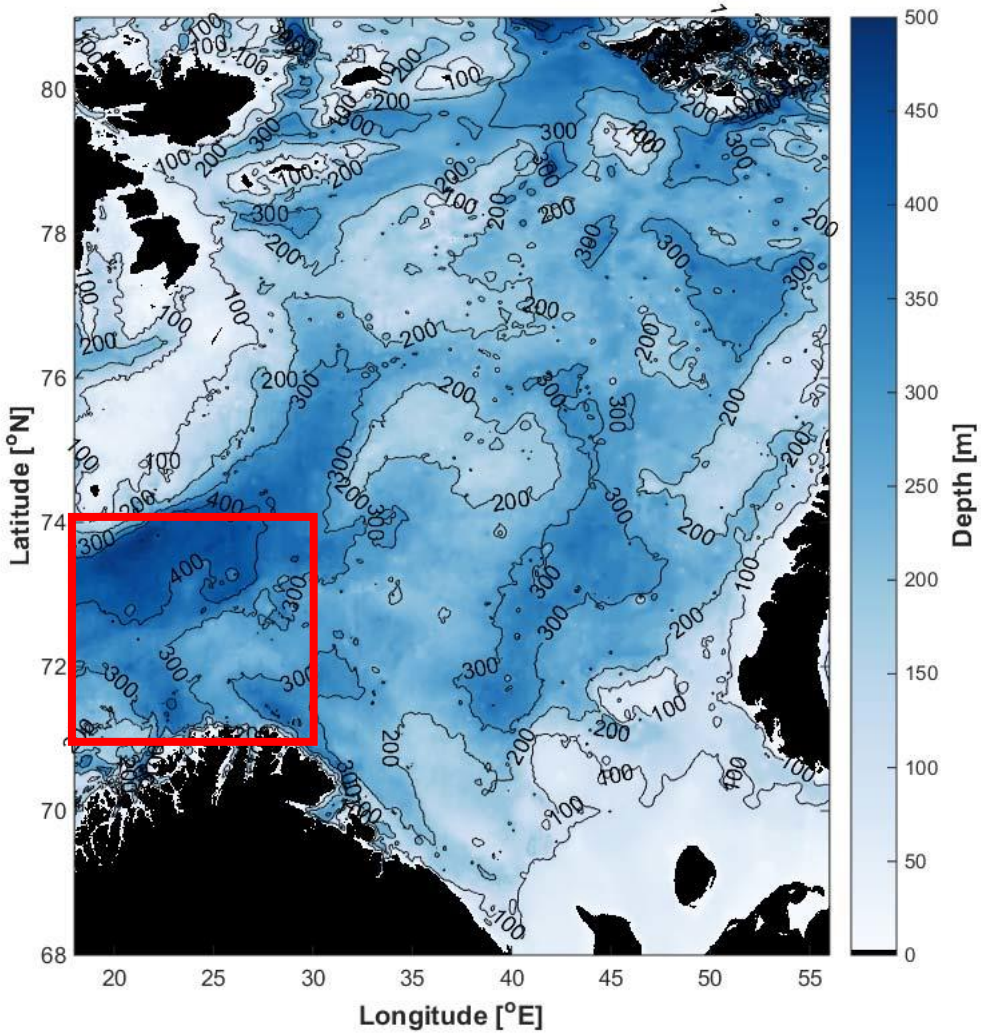


*Figure 1.2 Barents Sea bathymetric map, the delineated red box is in south of the Barents Sea and is where the study area is included within. Modified from Hjelmervik et al., 2015*

## 2.2 Main geological elements

*Hammerfest Basin* in present time is known by Loppa High to the north, the Troms-Finmark Platform to the south and deep Tromso Basin to the west. The Hammerfest Basin is believed to initiate its formation with a compressional event back in the Caledonian Orogeny (490-390 million year ago, ma). One noticeable element in the Hammerfest Basin is the formation of Late Jurassic succession from oceanic, organic-rich shale deposits, which became one of the most successful play in the Barents Sea (Berglund et al., 1986).

*Loppa High* is a ridge structure developing during the Late Paleozoic, when the Atlantic rifting between Greenland and Norway initiated (Sayago et al., 2018). It is characterized by a N-S orientation and experienced a complex geological history with series of uplift/subsidence and subsequent tilting and erosion. Upper Paleozoic siliciclastics, evaporates and carbonate deposits overlay Late Carboniferous rift platform, gradual onlap during Early and Middle Triassic continued the deposition and the following thick Upper Triassic Snadd FM succession. On the southern crest of the Loppa High, Middle Triassic claystone is overlain by the erosion of Paleogene Sotbakken GP shale (NPD(a), 2014).

*The Bjarmeland Platform* is a massive area to the NE of the Loppa High, the platform initiated in the Late Carboniferous to Permian and was subsequently tilted the Paleozoic and Mesozoic sequences towards the south by Paleogene tectonics. To the north of the platform in present time, unconsolidated Pleistocene sediments overlie older succession, while in the south and west, salt tectonics (Samson Dome) divide the platform into minor highs and small-scale basins (NPD(a), 2014).

In the center of the study area, there are 2 large salt structures (*Samson Dome and Norvarg Dome*) and *Swaen Graben*. The Swaen graben runs across the 2 salt domes and is restricted to post-Carboniferous levels. The graben was suggested to be caused by compactional stresses in the post-Carboniferous sedimentary beddings rooted from formation of the Samson and Norvarg Dome (Gudlaugsson et al., 1998). Samson Dome and Norvarg formed in response of the extension of post-salt Mesozoic sequences and then reactivated during Late Cretaceous and Early Tertiary. It has been described to have “elliptic to circular geometry, with a diameter of ~18km”. The salt movement in Samson Dome is studied to be moderate, and the main reason for the movement is suggested to due to the abundant and considerable overburden over Upper Palaeozoic evaporites (Breivik et al., 1995; Gabrielsen et al., 1990; Mattos et al., 2016).

The *Hoop Fault Complex* locates in the SW Barents Sea, it is characterized as a deep-seated weak zone that cuts across the Loppa High and Bjarmeland Platform and separates Maud Basin from the Mercurius High. The complex initiated during regional rifting in Early Carboniferous – Late Permian and went through a minor rifting event in the Triassic and Cretaceous creating faults in the complex (A. Mahajan et al., 2014; R.H. Gabrielsen et al., 1993).

*Glaciation, Uplift and erosion*

The region highlights the uplift and erosion along the Barents Sea history. The process initiated since late-Cretaceous (75ma) under the effects of the rifting of Greenland towards the Barents shelf and subsequent doming activities during the Eurekan Orogeny causing uplift and erosion to a wide part of Barents shelf including Bjornoya and Svalbard. Continuous plate rifting and seafloor-spreading in Eocence (55ma) contributes to the uplift of the area between Greenland and the Barents shelf, it is followed by a gradual period of uplift and erosion by plate reorganization in post-Eurekan time (Oligocene, 33ma) and volcanism. Global sea level fluctuations also might have been responsible for controlling sedimentation rate and erosion during this period. The latest uplift and erosion phase was governed by the last glaciation in Plio-Pleistocene (5ma), repeated glaciations during this time caused the glacial isostatic adjustment by the loading and deloading of icesheets with various thicknesses and extents (Lasabuda et al., 2021; Mitrovica & Vermeersen, 2002).

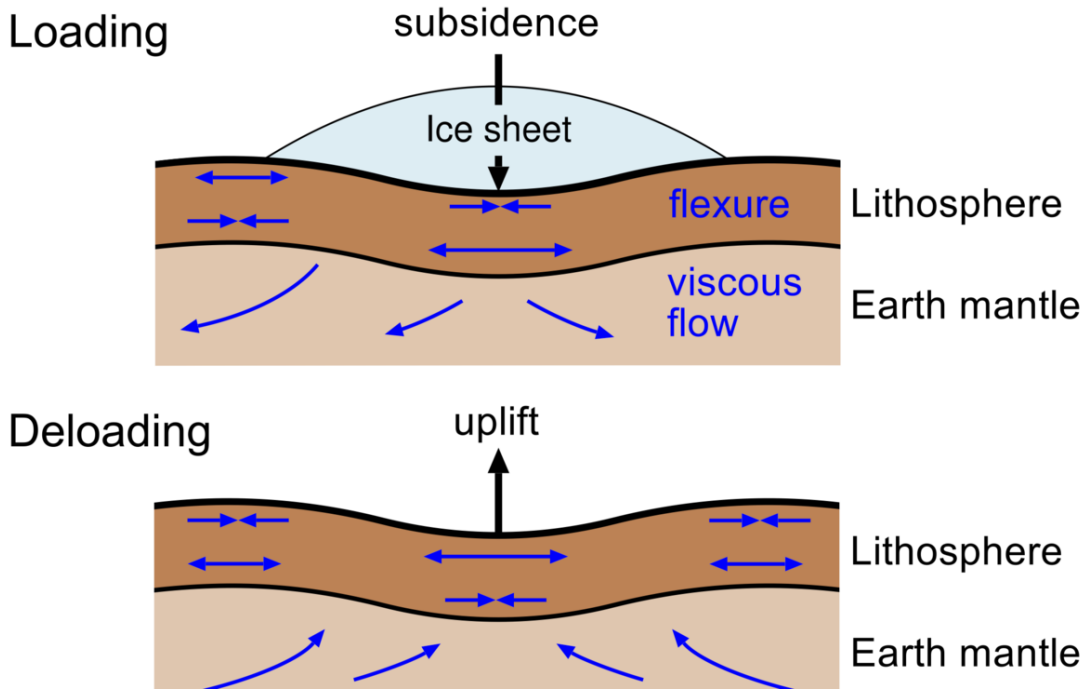


*Figure 2 Illustration of Glacial Isostatic Adjustment (Mitrovica & Vermeersen, 2002)*

Net erosion during the Cenozoic of main structures in the Barents Sea determined by different methods was summarized by Lasabuda et al. (2021) combining with other previous studies (Figure 2.3). The results for Hammerfest Basin, Loppa High and Bjarmeland Platform are specifically concerned in this thesis because they are included in the study area, and for the uplift

- erosion may put effects to leakages of petroleum through faults/fractures and shallow fluid accumulations. The net erosion in the Barents Sea estimated by different methods resulted in varying values, but the average number for Hammerfest Basin is around 1500m, while in Loppa High and Bjarmeland Platform is about 2000m.

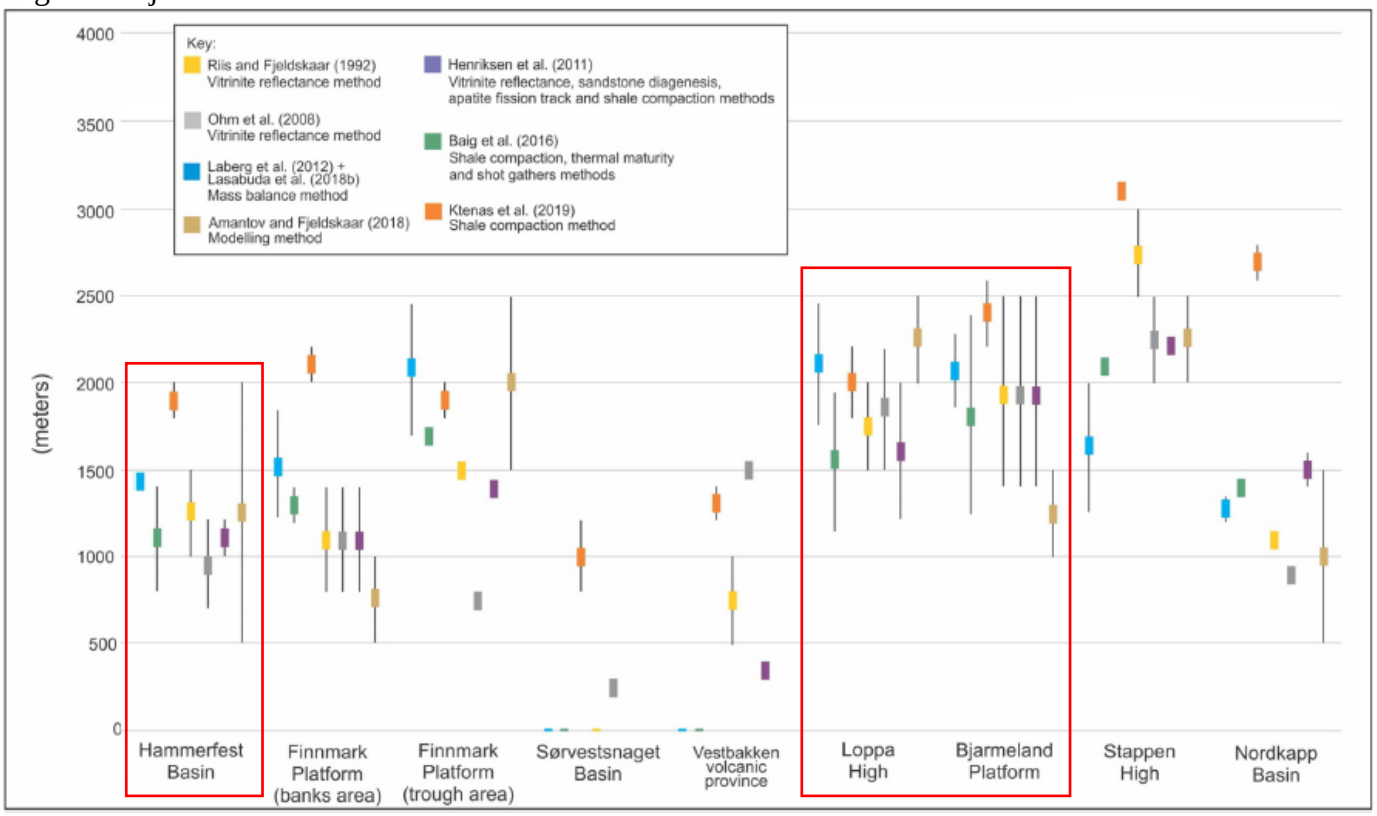


*Figure 2.3 Cenozoic net erosion ranges (not box-whisker plot) in the SW Barents Sea compiled from various references. Results to be concerned in the study area are delineated within red boxes. Modified from Lasabuda et al., 2021.*

Also the Pleistocene repeated glaciations in regional scale in the Barents Sea caused series of erosion and created a widespread unconformity across most of the Barents Sea, which is referred to Upper Regional Unconformity (URU) (Müller et al., 2019; Vorren et al., 1989). The URU morphology typically features glacially over-eroded troughs, it might occur in (mid-) Oligocene in relation to fluvial processes and subsequently be modified by Plio-Pleistocene glacial activities (Vorren et al., 1986, 1989).

## 2.3 Stratigraphy

For the purpose of this thesis is to find out the linkage between the gas flares in water column and their shallow subsurface behaviors, mostly shallow formations (above URU horizon) are used as

a reference to spot potential seismic anomalies in place. However, deeper stratigraphy units are also the targets to determine faults that act as fluid migration pathways, geomorphological features (i.e channels, sand boxes, trough mouths, …) that can be gas accumulations and especially in petroleum fields/discoveries, petroleum-bearing levels (e.g Upper Jurassic succession in the Barents Sea).

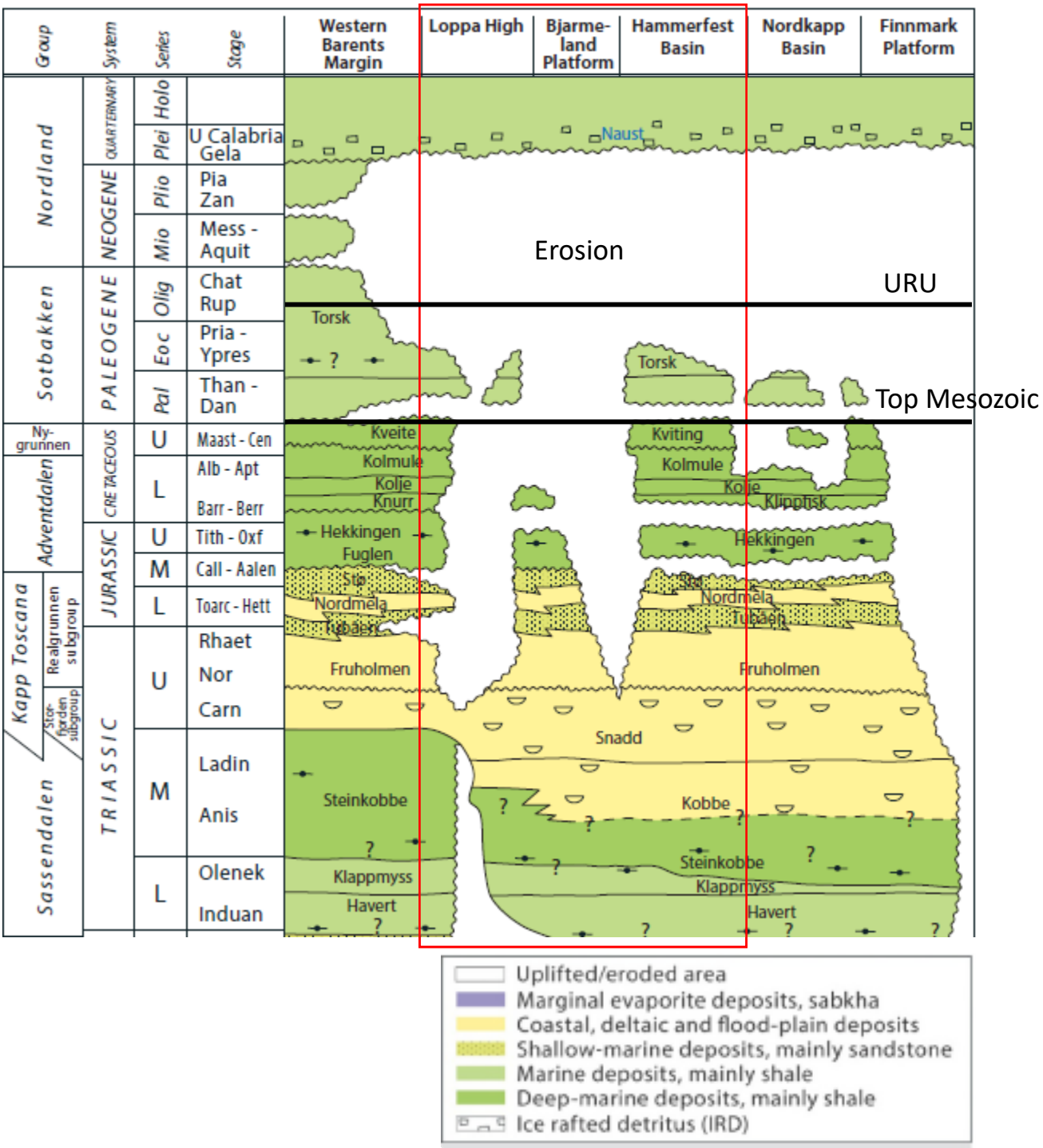


*Figure 2.4 Lithostratigraphy for major elements in the Barents Sea (NPD(a), 2014) with the included elements are delineated within the red box. Modified from NPD(a), 2014 and legends from Lasabuda et al., 2021. The URU surface represents the base of series of glaciation events and the "Top Mesozoic" surface represents top of Mesozoic and older strata, which are interpreted and shown in Chapter 5.*

## Mesozoic

*The Sassendalen Group (Lower and Middle Triassic)*

The Sassendalen Group consists of four formations Harvert-, Klappmyss-, Steinkobbe- and Kobbe formations, and is limited by Upper Paleozoic mixed siliciclastic and carbonate sequences and at the base of Fruholmen Formation (Realgrunnen Subgroup). The formations in the Sassendalen Group are mainly medium to dark grey shale with little grey siltstone and some thin sandstone layers indicating a shallow to open marine depositional environments (NPD(b), 2014).

*The Kapp Toscana Group (Lower Triassic and Middle Jurassic) – Realgrunnen Subgroup*

The Kapp Toscana Group is divided into 2 subgroups: the Storfjorden and Realgrunnen

The Storfjorden subgroup includes the Snadd Formation, above the Kobbe Formation of the Sassendalen Group and below the Fruholmen Formation basal shales. The formation represents distal marine environments with coarse basal grey shale interbedded with grey siltstones and sandstones (NPD(c), 2014).

The Realgrunnen subgroup is the most successful levels for petroleum exploration in the Barents Sea. Within this thesis, the subgroup is mentioned in Goliat field (7122/7-1), Norvarg (7225/3-1), Ververis (7226/2-1), Hanssen (7324/7-2) and Wisting (7234/8-1) discoveries. The subgroup consists of Fruholmen-, Tubaen-, Nordmela- and Sto Formations. The main lithology is pale grey sandstone with thin shale and coal appear occasionally. The lower boundary is the Fruholmen Formation shale while the upper boundary is Fulgen- and Hekkingen Formations shales and the subgroup experienced erosion at the top. The formation of the subgroup characterizes near-shore deltaic environments controlled by shallow marine, coastal deltaic and fluviodeltaic deposits (NPD(c), 2014).

*The Adventdalen Group (Middle Jurassic to Lower Cretaceous)*

The Adventdalen Group is divided into the Fulgen-, Hekkingen-, Knurr-, Kolje- and Kolmule Formations in which the Upper Jurassic Hekkingen Formation is considered one of the most successful source rocks in the Norwegian Continental Shelf (Hansen et al., 2020). The group's lithology is mainly dark marine mudstones, in specific places, there are deltaic and shelf sandstones and carbonate. Whereas, the Hekkingen Formation lithology is shale and mudstone with somewhat thin limestone, dolomite, siltstone and sandstone interbeds. Both Fulgen- and

Hekkingen Formations characterize as good source rock and cap rocks simultaneously (NPD(d), 2014).

### 2.3.1 Cenozoic

*The Sotbakken Group (Late Paleocene to Middle Eocene)*

The group only has Torsk Formation as a subdivision, the lithology is mostly claystones, with minor siltstone, tuffaceous and carbonate interbeds. The formation represents outer sublittoral to deep shelf environments (NPD(e), 2014).

*The Nordland Group (Late Pliocene to Pleistocene/Holocene)*

The Nordland Group consists of the Kai-, Molo-, Naust- and Utsira Formations. The group's lithology is dominated by grey to greyish-green, soft to firm, blocky, non-calcareous clays grade into sand with sand contents increases upwards. The formations characterize bathyal to glacial marine environments (NPD(f), 2014).

# 3 DATASET

## 3.1 Seismic data

Seismic surveying is the most important method in subsurface geophysical data acquisition. The method takes advantage of wave propagation through media, which have acoustic velocity ($v$) and density ($\rho$), the two parameters make up a physical property of media called *acoustic impedance (vp)*. There are two types of wave: *P* (push, compressional) *wave* moves in the propagation direction while *S* (shake, shear) *wave* moves perpendicularly to the propagation direction. In seismic surveying, primary *P wave* is mainly concerned because S-waves do not propagate through water. However, because some of the P-wave energy is converted into S-wave, in marine systems, S-waves can be recorded using ocean-bottom seismometers (OBS) or ocean-bottom cables (OBC). When a wave travels through a boundary of two media with different acoustic impedances, some of the energy is reflected into the upper media, and depending on the incident angle, some of the wave energy will be refracted to the lower medium or refracted along the interface between the 2 media.

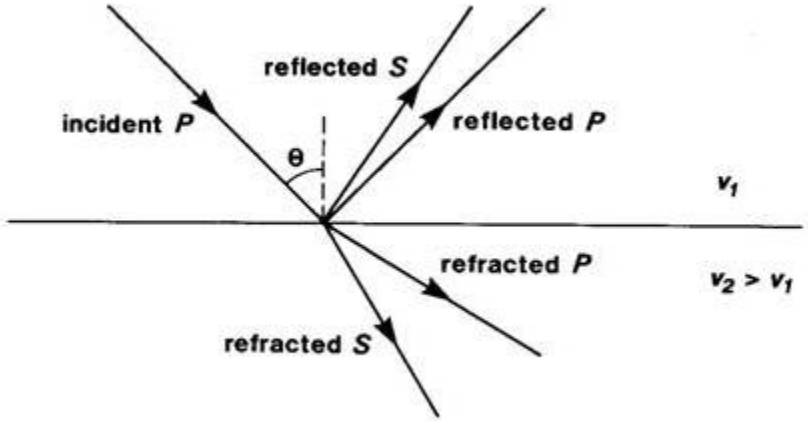


*Figure 3.1 Illustration of wave propagation. An incident P-wave generates a reflected wave and a refracted wave according to Snell's Law. Additionally, because some of the compressional energy is converted into shear energy, reflected and refracted S-wave is generated as well.*

The reflection strength at a boundary of 2 media can be determined as *reflection coefficient (R)*. By definition, "the *reflection coefficient* or *reflectivity* is the proportion of seismic wave

amplitude reflected from an interface to the wave amplitude incident upon it. If 10% of the amplitude is returned, then the reflection coefficient is 0.10" (SubSurfWiki, 2021)

$$\textit{Reflection Coefficient (R)} = \frac{v_2\rho_2 - v_1\rho_1}{v_2\rho_2 + v_1\rho_1}$$

Where: $v_1$, $\rho_1$ are velocity and density of upper rock

$V_2$, $\rho_2$ are velocity and density of lower rock

*Reflection Coefficient (R)* is limited between +1.0 and -1.0 range, with positive *R* shows a transition from softer, less dense rocks to harder, denser rock and vice versa for negative *R*. An interface between a porous sand and dense shale will have high *R* and produce clear reflecting surfaces. In contrast, a boundary between two tight limestones will produce an inconsiderable *R* and little energy reflection.

In actual processed seismic datasets, seismic signals are shown in amplitudes, which are deviation of wave from zero crossing. The value of a seismic amplitude is equal to the value of *seismic trace* at a specific depth and the *Seismic Trace* equals *wavelet x Reflection Coefficient.* Maximum positive amplitudes are referred to *peaks*, while maximum negative amplitudes are referred to *troughs.* An abrupt increase in seismic amplitude can indicate a drastic change in subsurface lithology or the presence of hydrocarbon in the rock.

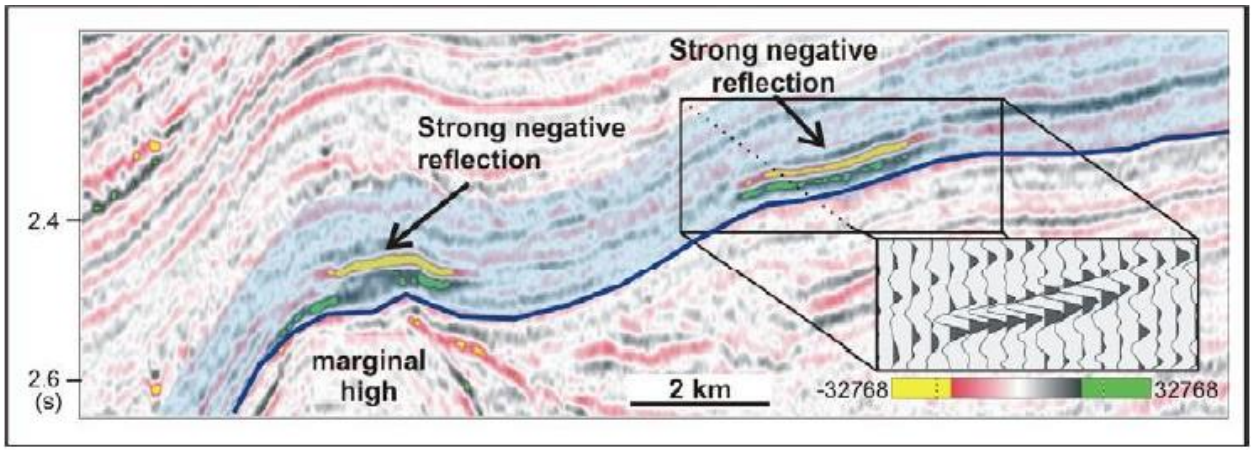


*Figure 3.2 Seismic amplitude shown in the dual polarity display. Positive amplitudes are marked in black and abnormally high positive amplitudes are marked in green; negative amplitudes are marked in red and extra negative amplitude are marked in yellow. The display uses the SEG polarity standard, zero-phase wavelet with wiggle display in addition. Andreassen, 2009 (modified from Andreassen et al. 2007)*

A local sharp increase or decrease of seismic amplitude along a seismic horizon is called an *amplitude anomaly*. Amplitude anomalies may be caused by hydrocarbon accumulation, geometric focus, velocity focus, interference, possible processing error, ….

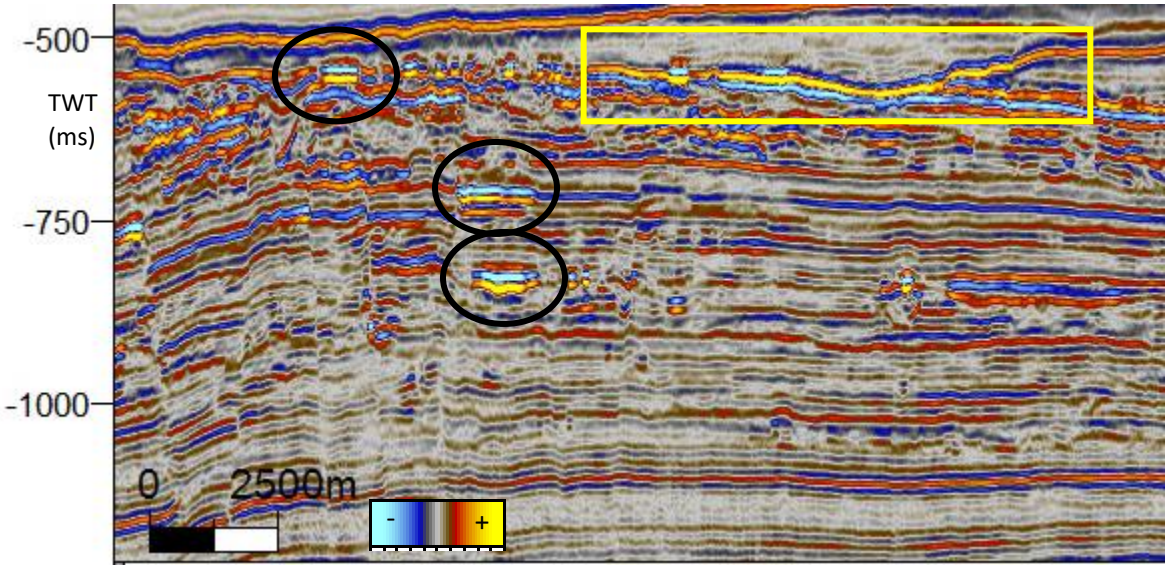


*Figure 3.3 An example of amplitude anomalies in inline 6811 from SG9803 3D seismic survey covering the Caurus/Langlitinden discovery. Negative amplitudes are marked in blue and extra-high negative amplitudes are marked in whiteish-blue; whereas, positive amplitudes are marked in red and extra-high positive amplitudes are marked in yellowish-red. The anomalies' absolute amplitudes value from 200-250 while ambient absolute amplitude only range about below 100. Anomalies in black circles may indicate the presence of fluid in sediments (e.g gas) or a different lithology compared to ambient lithology (e.g a sand pocket in shale beddings); the laterally extent of amplitude anomalies (in yellow rectangle), may indicate a drastic change in depositional condition, for example, an unconformity.*

To describe reflections in seismic data, the using of dual-polarity reference (peaks and troughs) following a phase convention is used. The convention of Badley (1985) and SEG (Society of Exploration Geophysicists) polarity standard of Sheriff (2006) is the most well-known and used regarding seismic interpretation. The SEG standard defines *normal polarity* as:

- For a *minimum-phase* wavelet, positive *R* or increasing acoustic impedance begins with a trough.
- For a *zero-phase* wavelet, positive *R* or an increase in acoustic impedance begins with a central peak.
- And vice versa for *reverse polarity*.

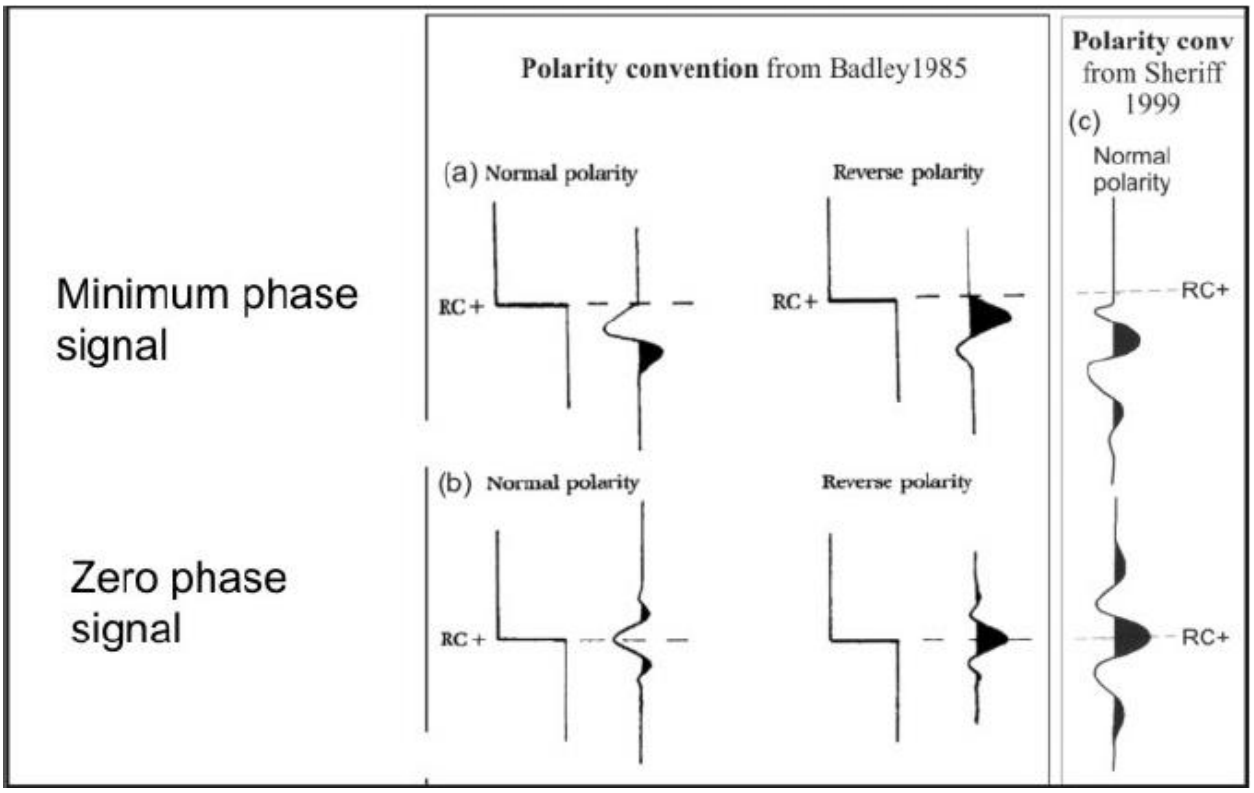


*Figure 3.4 Polarity conventions and signal phases for plotting of seismic signals. Andreassen, 2009.*

## 3.2 3D seismic surveys

The study area of this thesis focuses on South of Barents Sea, specifically follows the flare hunting cruise 20-2 from CAGE. The cruise line encountered geological elements and petroleum discoveries mentioned in Chapter 2.1. Within the study area, the student is authorized to use 3D and 2D seismic datasets to correlate the found flares in water column data with the on-site subsurface. Not all the datasets are in the same seismic phase, polarity and amplitude spectrum. For illustration, reflection at the seabed is usually the clearest and the most reliable due to the transition from water to the hard seabed. In such case, the wave's *reflection coefficient* should be outstandingly positive and according to that, by looking at the amplitudes, the survey's configuration can be determined.

The 3D seismic surveys within this thesis are listed in Table 1, the table includes general information of the surveys.

| Table 1. General information of the used 3D seismic surveys | | | | | | |
|---|---|---|---|---|---|---|
| **No.** | **Seismic survey** | **Sub type** | **Company - responsible** | **Completion year** | **Polarity configuration** | **Location** |
| 1 | SG9803 | 3D | Saga Petroleum ASA | 1998 | Zero phase - Reverse polarity | Caurus/Langlitinden |
| 2 | BG1002 | 3D | BG Norge AS | 2010 | Zero phase - Normal polarity | Samson Dome |
| 3 | NH0608 | 3D | Norsk Hydro Produksjon AS | 2006 | Zero phase - Reverse polarity | Arenaria |
| 4 | EN0702 | 3D | Eni Norge AS | 2007 | Zero phase - Normal polarity | Goliat |
| 5 | ST07M16 | 3D | Den Norsk Stats Ojleselskap AS | ? | Zero phase - Reverse polarity | Ververis |

*EN0702 (Figure 3.5)*

The 3D seismic survey EN0702 was operated by Eni Norge AS in 2007 in the South Barents Sea, covering about 1268km$^2$ over the Goliat field area. It is in Zero phase – Normal polarity configuration with reflection at the seabed showing middle-trough pattern. General amplitude spectrum of the survey is in range from -0.9 to 0.9 with positive amplitudes are in red, high positive amplitudes are in yellow; while negative amplitudes are in blue and high negative amplitude are in whiteish-blue. Background weak amplitudes (in grey) have absolute values of 0.01-0.02 whereas high amplitudes at reflectors have absolute values of 0.23-0.3.

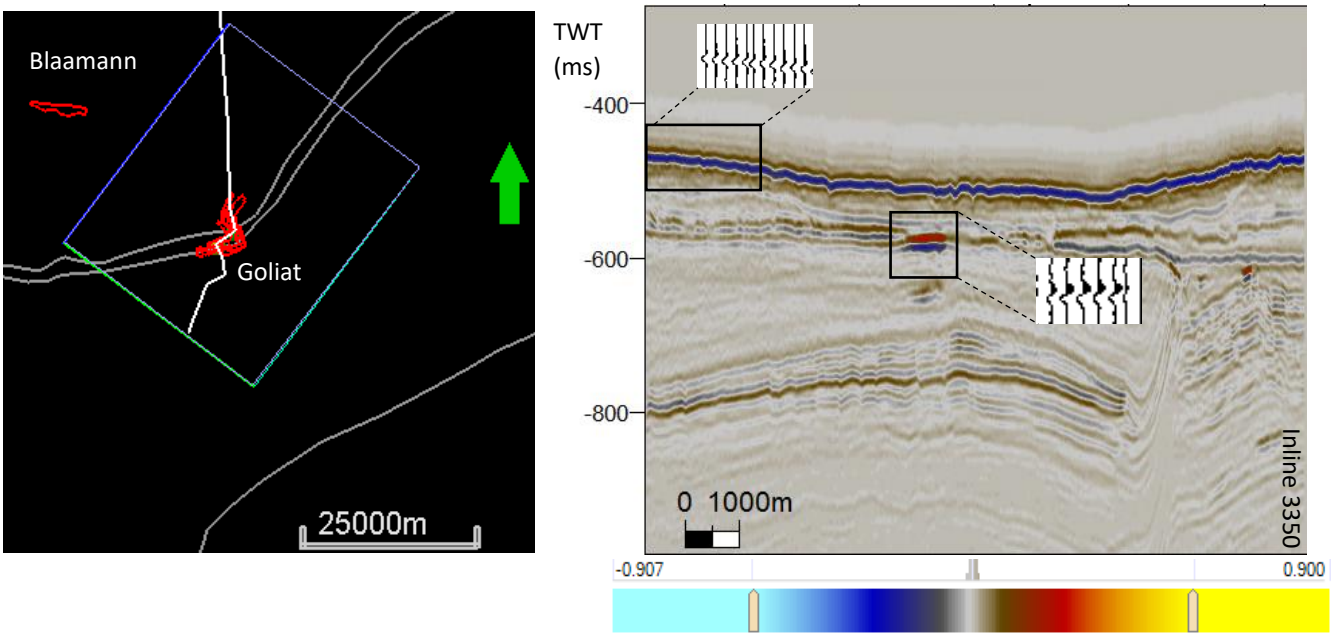


*Figure 3.5 EN0702 3D seismic survey coverage over Goliat field (figure to the left, within the rectangle); inline 3350 seismic profile from the EN0702 survey showing examples of the seabed reflection and an amplitude anomaly, also amplitude spectrum in the EN0702 survey is shown by the color bar.*

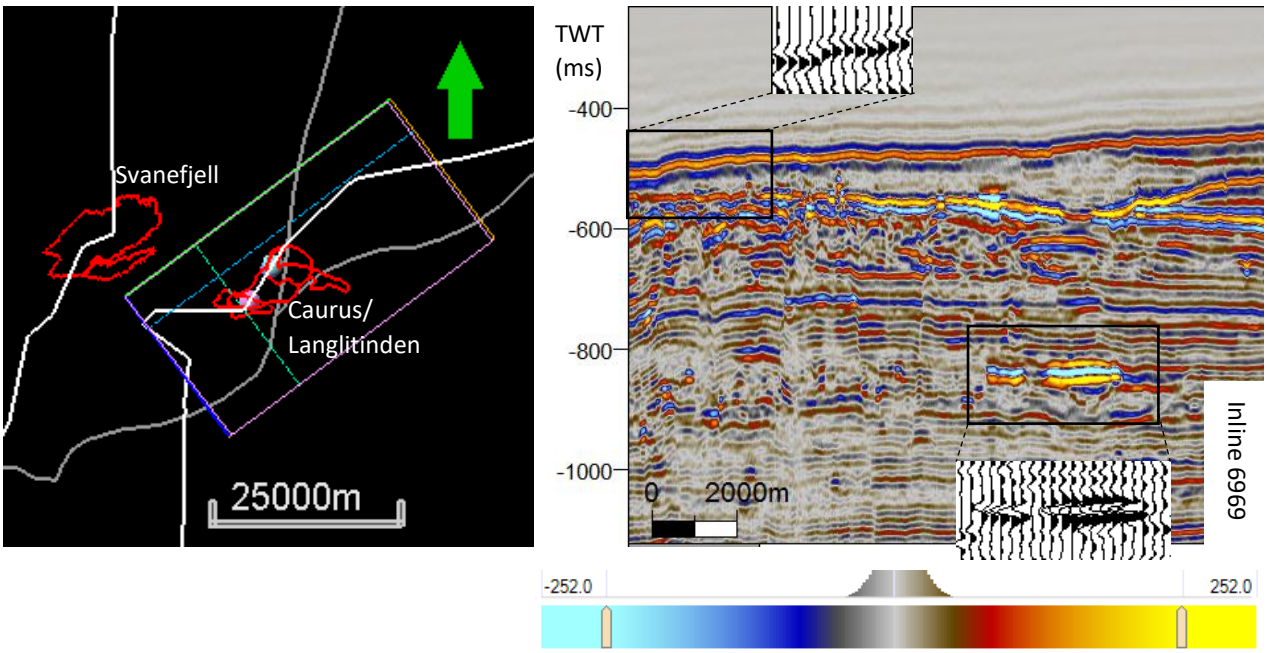


*Figure 3.6 SG9803 3D seismic survey coverage over Cauris/Langlitinden discoveries (figure to the left, within the rectangle); inline 6969 seismic profile from the SG9803 survey showing examples of the seabed reflection and an amplitude anomaly, also amplitude spectrum in the SG9803 survey is shown by the color bar.*

*SG9803 (Figure 3.6)*

The 3D seismic survey SG9803 was operated by Saga Petroleum ASA and finished in 1998 in the South Barents Sea. The survey covers the Caurus/Langlitinden discovery complex with area of about 940km$^2$. It follows Zero phase – Reverse polarity configuration according to the middle-peak reflection at the seabed, the survey's amplitude ranges between -252 and 252 with positive amplitudes (peaks) are marked in red, extra-high positive amplitudes are marked in yellow; while negative amplitudes (troughs) are marked in blue and extra-high negative amplitudes are marked in whiteish-blue. As a result, amplitude anomalies in SG9803 have absolute amplitudes of about 220-252 with weaker amplitudes in the background.

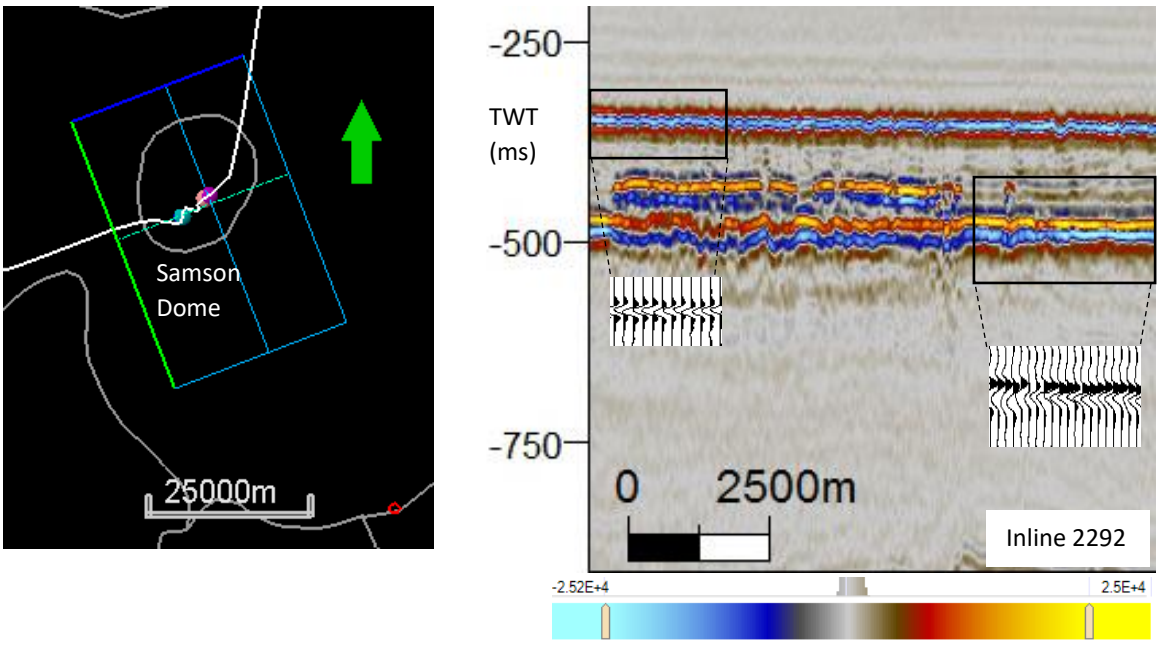


*Figure 3.7 BG1002 3D seismic survey coverage over Samson Dome (figure to the left, within the rectangle); inline 2292 seismic profile from the BG1002 survey showing examples of the seabed reflection and an amplitude anomaly, also amplitude spectrum in the BG1002 survey is shown by the color bar.*

*BG1002 (Figure 3.7)*

The 3D seismic survey BG1002 was operated by BG Norge AS and completed in 2010. The survey locates in the South Barents Sea, covers an area of 1170km$^2$ over the Samson Dome region. The survey was preprocessed using Zero phase – Normal polarity configuration defined by the seabed's reflection as central troughs in wiggle display. Amplitude spectrum is from -25000 to

25000, positive amplitudes are colored red, extra-high positive amplitudes are colored yellow; while negative amplitudes are colored blue and extra-high negative amplitudes are colored whiteish-blue. Amplitude anomalies' absolute values in BG1002 survey ranges 15000 to 24000 compared to background, non-anomalous amplitudes of around 300-500 absolute values.

*ST07M16 (Figure 3.8)*

The 3D seismic survey ST07M16 was operated by Den Norsk Stats Ojleselskap AS, the survey covers 920km$^2$ over the Ververis discovery. The seismic traces in this survey are in Zero phase – Reverse polarity as the seabed's reflection shows central-peak pattern in wiggle display. Amplitude spectrum ranges from -2.2 to 2.2 with positive amplitudes are marked in red and strong positive amplitudes are marked in yellowish-red; while negative amplitudes are marked in blue and high negative amplitudes are marked in whiteish-blue. Low background amplitudes (in grey) are about -0.03 to 0.03, whereas strong high amplitudes at reflectors are about -1.5 to 1.5.

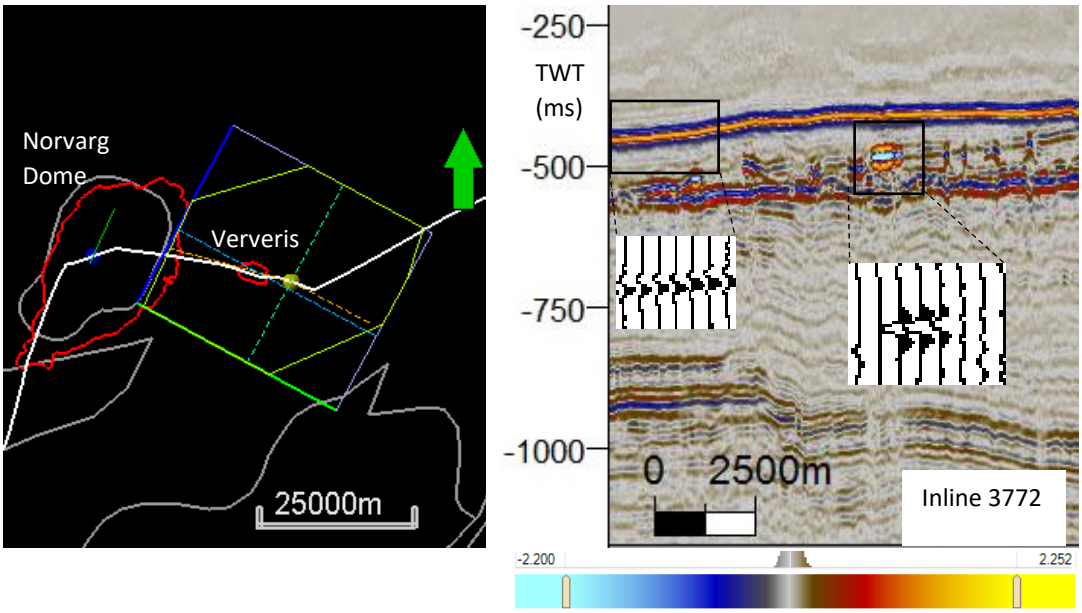


*Figure 3.8 ST07M16 3D seismic survey coverage over Ververis discovery (figure to the left, within the rectangle); inline 3772 seismic profile from the ST07M16 survey showing examples of the seabed reflection and an amplitude anomaly, also amplitude spectrum in the ST07M16 survey is shown by the color bar.*

## 3.3 Well data

At petroleum discoveries that are encountered by the cruise line within the study area, a set of hydrocarbon wells are available for investigation (Table 2). Well logs or well ties are not the

main purposes for using well data in this thesis, only general information of the wells is assessed to determine water depths, subsurface features that they penetrated, target formation and their contents. Moreover, gas may migrate along the well path due to "well integrity issues" (to be discussed further in Chapter 6) and pressure drop when penetrating subsurface formation and reach the seabed, therefore, it is necessary to regard well data when it comes to assessing gas flare in areas with petroleum activities.

**Table 2. Compilation of hydrocarbon wells used in this thesis and their general information**

| No. | Well | Operator(s) | Completion year | Discovery-Geology element | Water depth (m) | Content |
|---|---|---|---|---|---|---|
| 1 | 7122/7-1 (Goliat) | Norsk Agip AS | 2000 | Goliat | 381 | Oil |
| 2 | 7122/7-6 | Eni Norge AS | 2015 | | 380 | Oil/Gas |
| 3 | 7222/11-1 (Caurus) | StatoilHydro Petroleum AS | 2008 | Caurus | 356 | Oil/Gas |
| 4 | 7222/11-2 (Langlitinden) | Det Norske Ojleselskap AS | 2014 | Langlitinden | 338 | Oil |
| 5 | 7224/6-1 (Arenaria) | StatoilHydro Petroleum AS | 2008 | Arenaria | 266 | Gas |
| 6 | 7224/7-1 (Samson Dome) | Den Norske Stats Ojleselskap AS | 1988 | Samson Dome | 269 | Shows |
| 7 | 7225/3-1 | Total E&P Norge AS | 2011 | Norvarg | 377 | Gas |
| 8 | 7225/3-2 | Total E&P Norge AS | 2015 | | 381 | Gas |

| | | | | | | |
|---|---|---|---|---|---|---|
| 9 | 7226/2-1 (Ververis) | StatoilHydro ASA | 2008 | Ververis | 347 | Gas |
| 10 | 7324/7-2 (Hanssen) | OMV (Norge) AS | 2014 | Hanssen | 417.5 | Oil |
| 11 | 7324/8-1 (Wisting) | OMV (Norge) AS | 2013 | Wisting | 398 | Oil |
| 12 | 7324/8-2 | OMV (Norge) AS | 2015 | | 394 | Dry with shows |
| 13 | 7324/10-1 | Den norske stats oljeselskap a.s | 1989 | - | 408 | Dry with shows |

## 3.4 Multibeam echosounder

Multibeam echosounder systems (MBES) are powerful tools for seabed depth study as the systems use sonar pings to image a swath of subsea area (Urban et al., 2017). A *sonar* is a device used to record sound's behavior in water to determine objects in water. The concept includes two basic types: *active sonars* which produce sound waves at predefined frequencies and record the returned echoes from desired subsea objects; *passive sonars,* on the other hand, record emitted echoes from objects that produce sound on their own like ships, submarine creatures. (Street, 2000).

Apart from seabed depth determination, MBES systems are used for water column imaging (WCI) to search for gas bubble rising from the seabed by apply sound waves from a source. The operation of a sonar depth system is performed in a continuous cycle, naming the *ping cycle.* The system consists of four elements: a transmitter, a transducer, a receiver and a control and display system. The control and display system governs the transmitter to generate oscillating electrical sound pulses (or pings) with distinguishable frequencies. Those produced pings go through the transducer to convert the electrical energy into sound waves, the waves then travel to the subsea objects and reflect back to the receiver. The reflected sound waves on the way back are converted back into electrical signal by the transducer and reach the receiver. The ping cycle is depicted in Figure 3.9.

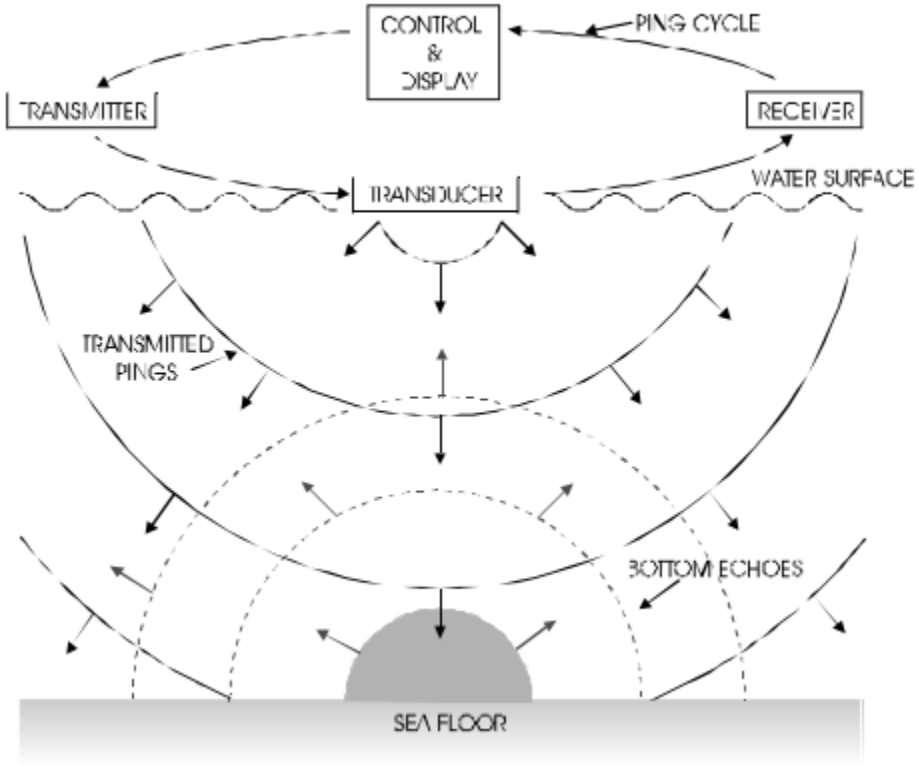


*Figure 3.9 Simplified scheme of the ping cycle in a single-beam echosounder system, including the four components of the system. Retrieved from Street, 2000.*

The scheme above is a simplified model of a single-beam echosounder, in this thesis, the water column data are acquired using a multibeam echosounder, which is essentially an instrument

that can image more than one location with a single ping. Multibeam echosounder can image a swath of contiguous areas perpendicular to the vessel direction (Figure 3.10) (Street, 2000).

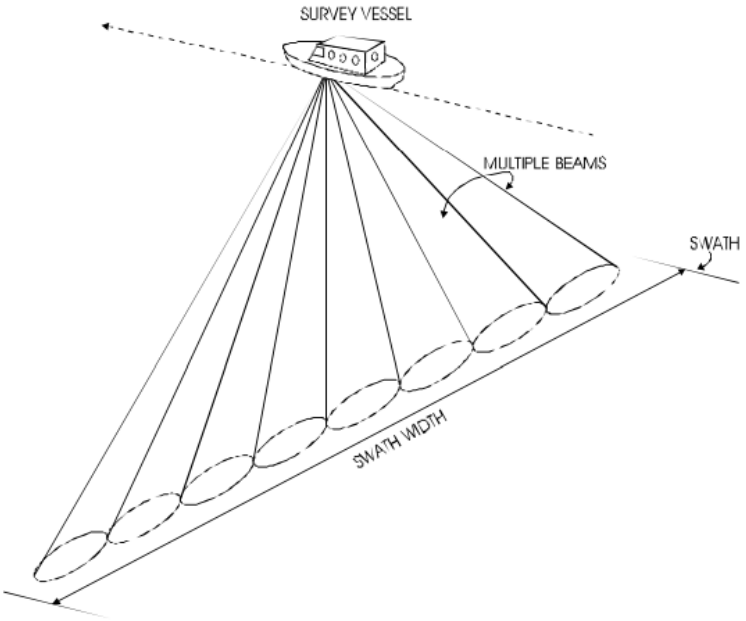


*Figure 3.10 Illustration of multibeam sonar swath. Retrieved from Street, 2000.*

Gas bubble released from the seabed come from different patterns in the water column, for example as single bubbles to mega size plumes (Leifer et al., 2006), in this thesis, bubble streams rooting from constant gas flux are concentrated. Because the gas streams appear as flare-shape features in acoustic echograms (or WCI) (Figure 3.11), they are referred as "gas flares" or "flares"(Urban et al., 2017). After processing, potential gas flares charactered by clouds of strong backscatter strength, which is a measurement of the reflected sound energy from materials in the water column. Urban et al., 2017 also defined the *minimum slant range*, "the shortest radial distance between the sonar transducer and the seafloor", if the gas flare is beyond the minimum slant range, the lower part of the gas flare where it connects with the seabed is challenging to detect due to the lack of data (Moen, 2020; Urban et al., 2017).

WCI may include unwanted features such as fish shoals and side lobe artefacts (Figure 3.12), when strong and direct enough, they may distort and mask the desired flare signals, making it challenging to detect the gas flare pattern. Therefore, criteria to decide whether the recorded signal is determined as gas flare or not suggested by Judd et al., 1997 are used in this thesis. The criteria are to be discussed further in chapter 3.2.2.

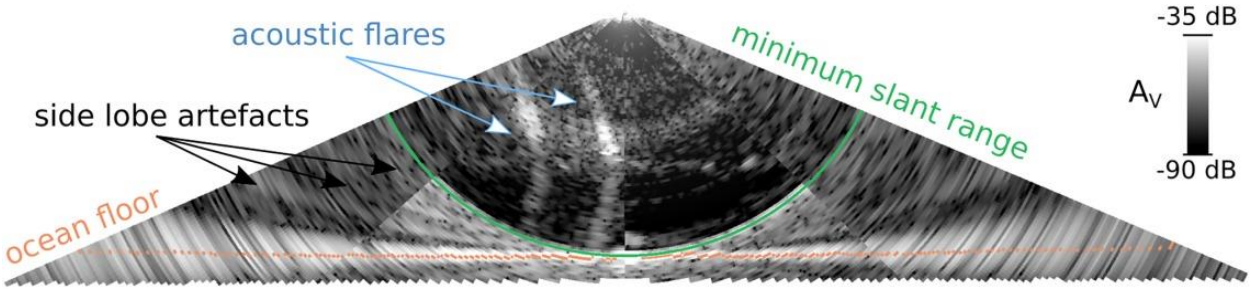


*Figure 3.11 A WCI from Kongsberg EM302. The WCI shows two acoustic flares within the minimum slant range and also side lobe artefacts which cause difficulties in detecting outside the minimum slant range. Retrieved from Urban et al., 2017.*

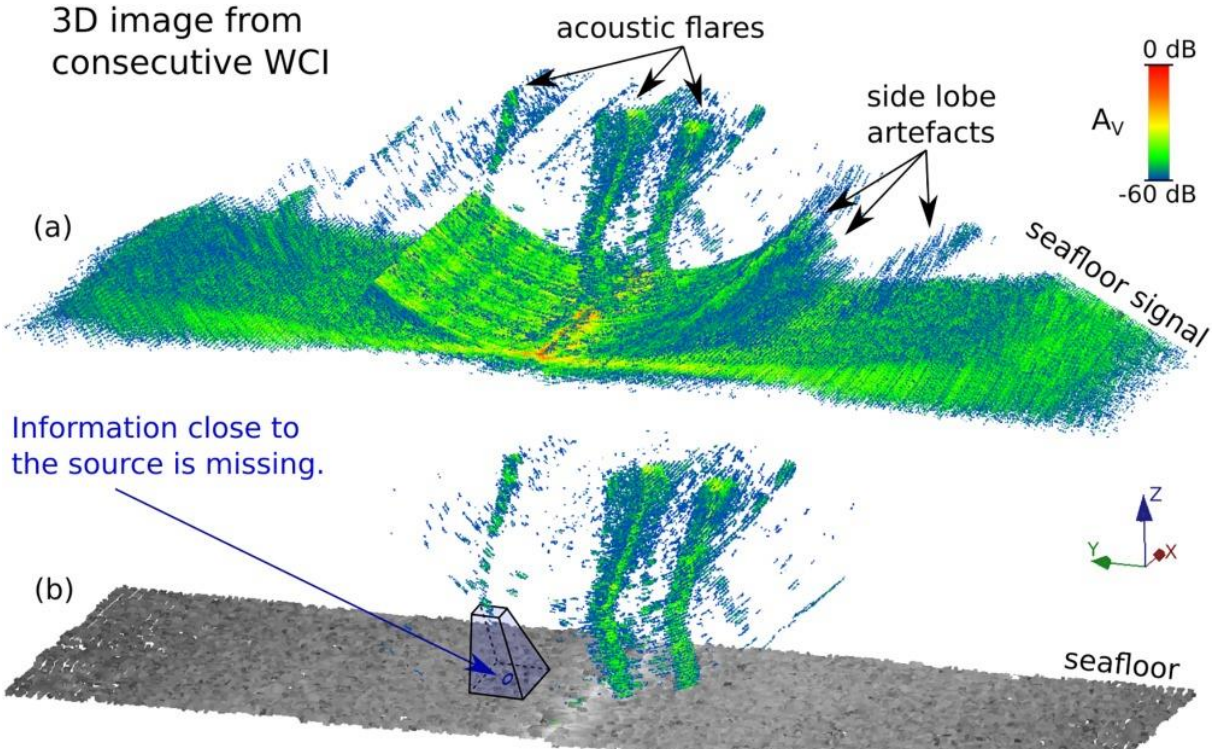


*Figure 5.12 (a) extracted cloud data from 120 consecutive WCIs, only backscattering strength signals of above -60dB are visualized. Three acoustic flares and side lobe artefacts are visible. (b) backscattering strength signals outside the minimum slant range are excluded because of the lack of data while the three flares remain clear. Retrieved from Urban et al., 2017.*

Within this thesis, multibeam echosounder data is from the *20-2 CAGE Cruise report "Hunting gas flares in Hopendjupet and glacial sediments in Sentralbankrenna"* (CAGE, 2020). The cruise covers the South Barents Sea region and include the study area of this thesis.

The cruise encountered some know petroleum discoveries and detected some flare locations. Within this thesis, because of the seismic datasets provided, gas flares in most of the discoveries

mentioned in the cruise log are assessed and corelated with subsurface seismic, excluding the flares in the Snohvit field and the Svanefjell discovery (Figure 3.13).

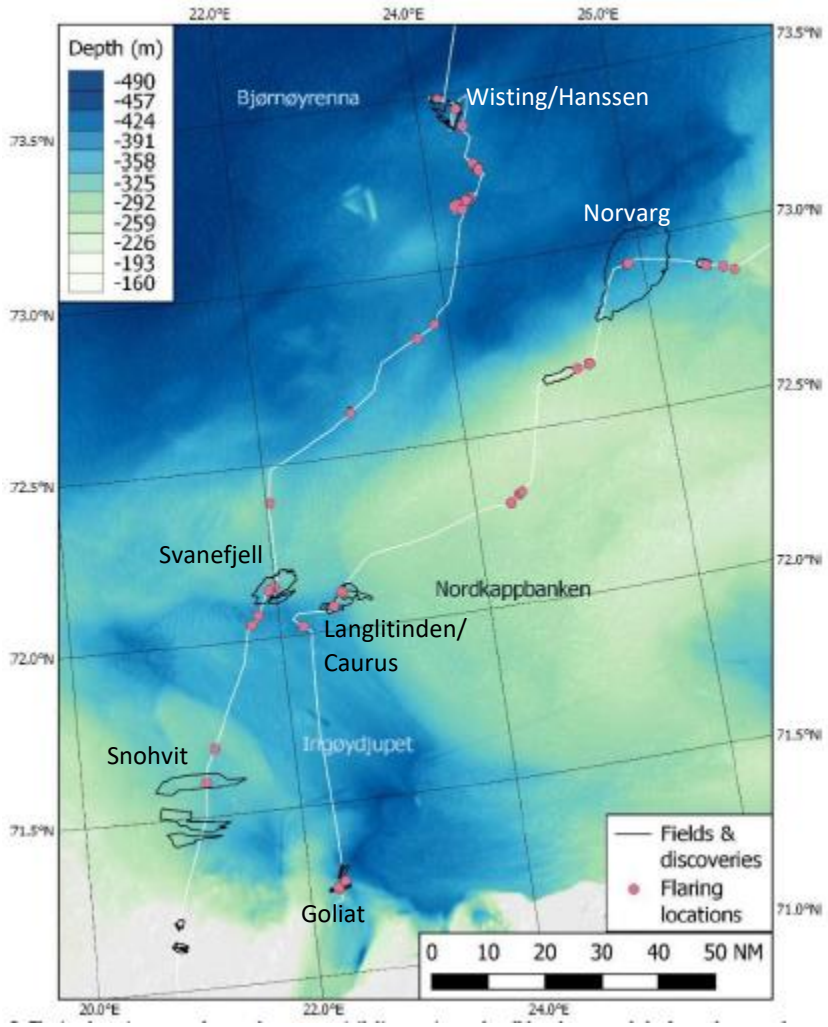


*Figure 3.13 The 20-2 Cruise track line (white line), the cruise encountered several petroleum discoveries and some flare locations are marked. Flares are detected at all the encountered discoveries. Because no seismic data is provided, the flares in Snohvit field and Svanefjell are excluded in this thesis. Modified from CAGE, 2020.*

# 4 METHODOLOGY

## 4.1 Software

The QPS's FM Midwater software is used to process raw multibeam data, pick out the desired range of wanted gas flare indicators and export the flares to ASCII format files.

For seismic assessment and interpretation, as well as gas flares (as ASCII format) visualization, Schlumberger's seismic software Petrel E&P Platform 2019 is used. The software utilizes seismic datasets to examine the datasets, interpret seismic horizons, make surfaces, apply seismic attributes, generate isochore maps and visualize the gas flares.

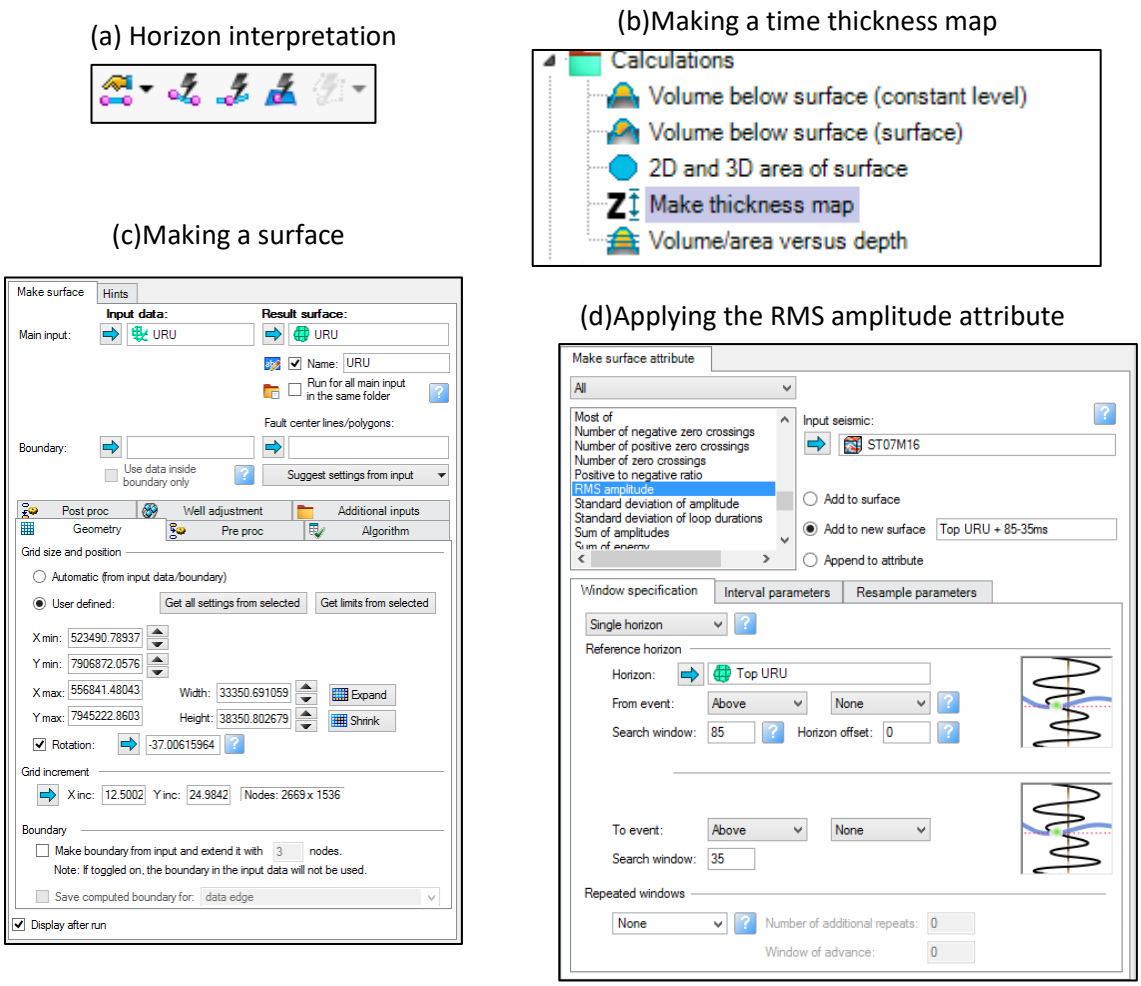


*Figure 4.6 Applications of the Petrel software in this thesis. (a) horizon interpretation, used to pick an event at a specific time elevation; (b) time thickness (isochore) map making, used to illustrate time thickness between two selected surfaces; (c) surface making from seismic horizon, with specific input data and parameters; (d) RMS amplitude surface attribute, used to illustrate seismic amplitude accumulations based on a reference surface.*

## 4.2 Seismic attributes

For the purpose of examining density changes of seismic amplitudes along a reference horizon, RMS amplitude is used to produce amplitude maps. The RMS Amplitude attribute

"computes the root mean square (RMS) of single-trace samples T(i), over a user-specified vertical window with a length of n samples, for each sample in an input trace" (Koson et al., 2014). In this thesis, several RMS amplitude maps were produced from the URU as reference surfaces, with varying search windows up to 90ms above the URU surfaces to visualize amplitude accumulations (for example, figure 4.1d).

Two-way-time isochore maps are generated in Petrel to illustrate the vertical time thickness between two selected surfaces (Figure 4.1b), in this thesis, time thickness maps from the seabed to the URU horizon are focused since the main objective is to determine potential gas source in shallow glaciogenic sediments which have gone series of glacial events since the last ice age.

## 4.3 Gas seepage

Natural gas seepage is defined by Giuseppe Etiope in his book "Natural gas seepage – The Earth's Hydrocarbon Degassing" as " the steady or episodic, slow or rapid, visible or invisible flow of gaseous hydrocarbons from subsurface sources to Earth's surface." He also mentioned the term "gas seepage" in petroleum mainly refers to methane ($CH_4$) and other minor organic gas such as ethane ($C_2H_6$), propane ($C_3H_8$) and butane ($C_4H_{10}$) (Etiope, 2015).

"Gas seepage" is a term of gas leakage that has been referred to marine environment, from "pockmarks" on the seabed, carbonate mounds and mud volcanoes on continental shelves and marine, sub-marine petroleum reservoirs (Alan Judd, 2000; Alan Judd & Hovland, 2007; Kvenvolden et al., 2001). The seepages' consequence is global methane ($CH_4$) – a GHG – emissions (Crutzen, 1991) which contribute to the climate change, therefore, the motivation of this thesis is to find out the relation between the gas seepages in the water column and subsurface geology, in order to explain how geology may influence natural and petroleum wells related gas seepages in the Barents Sea.

The origin of subsurface gas may vary in relation to the gas source. In general, there are 3 gas origins:

- Microbial (or biogenic) gas: the gas is produced during diagenesis, the phase occurring in the shallow subsurface at near normal temperatures and pressures. This is the phase when bacterial-aided biogenic decay happens. The process releases methane, carbon dioxide and water by organic matter.

- Thermogenic gas: this type of gas is produced during catagenesis phase, which is the petroleum generation phase of kerogen. Gas is produced by the thermal cracking of organic matter or oil at high temperatures and pressures.
- Abiotic gas: is produced by chemical reactions that do not require organic substances (Fischer Tropsch type reactions).

(Etiope, 2015; Richard C. Selley & Stephen A. Sonnenberg, 2015)

Under the effects of hypoxia in aquatic environments, which is the process of depleting oxygen in water around organic-rich area (in this case, at the seabed), methane is oxidized and gradually dissolved in water (Etiope, 2015). McGinnis et al. (2006) concluded that methane gas bubbles with diameter of 5.5mm released at 90m depth would reach the sea surface with no fraction of methane (Figure 4.2)(McGinnis et al., 2006). Despite that, methane is the third most important GHG after $H_2O$ and $CO_2$, in a 100-year time scale, methane is 28 times more potential to global warming than $CO_2$ because $CH_4$'s stronger capability to absorb infrared radiation per molecule compared to that of $CO_2$ (Ciais et al., 2013).

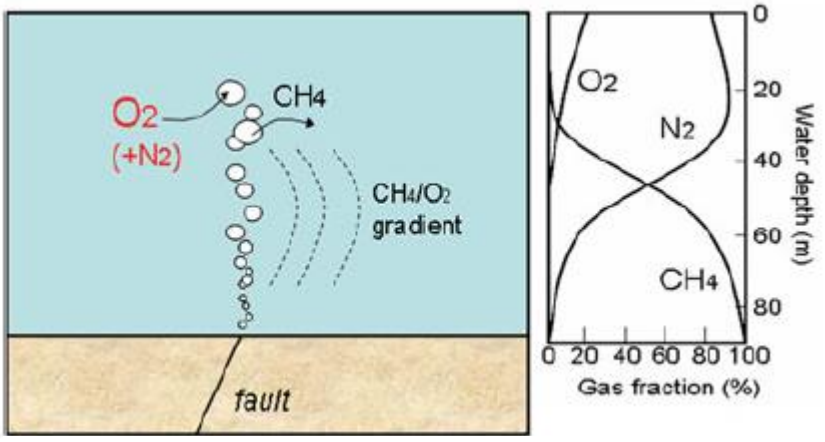


*Figure 4.2 Illustration of methane released from a fault on the seabed, oxygen decreases around the gas bubble plume. The plot line shows the exchange of gases between seawater and bubbles, the plot refers to the relation of modelled gases composition versus water depth, with gas bubbles diameter of 5.5mm. Sketch by Etiope (2015) and plot by McGinnis et al. (2006)*

Gas seepages to the Earth's surface may have migration sources from direct shallow gas accumulations, subsurface petroleum reservoirs or directly from the source rocks, and depending on surrounding rocks' permeabilities, gas can move in two mechanism:

- “Diffusion”: concentration gradients, gas molecules spread to the surroundings to equalize the gas concentrations in every part of the rock system (Etiope, 2015). This mechanism is also observed in the petroleum primary migration after the catagenesis process (Hunt, 1996).
- “Advection”: pressure gradients, gas movement from a high pressure zone to a low pressure zone. “Convection” is a form of advection-driven mechanism, in which fluid flows move with a pressure gradient generated by thermal gradients, or temperature gradients. (Etiope, 2015)

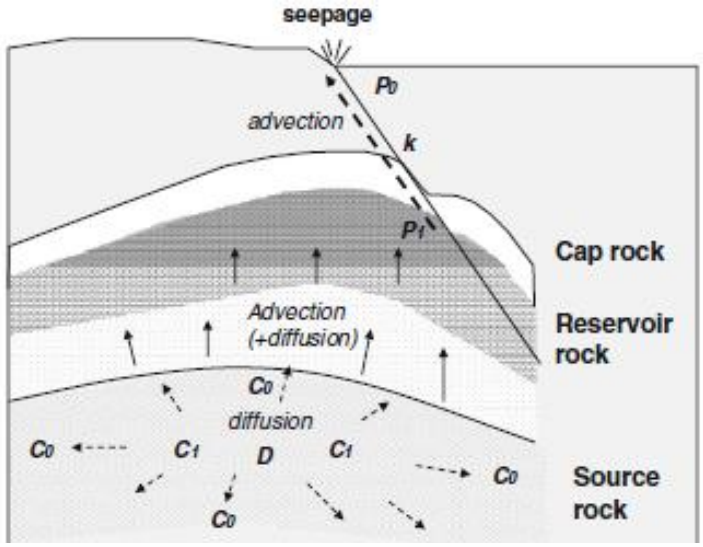


*Figure 4.3 The main factors in gas migration from source rocks to reservoirs and to the surface. P: gas pressure; k* permeability; *D* gas diffusion coefficient; and *C* gas concentration. Etiope, 2015.

Beside the migration mechanisms, gas seepages from subsurface formations require migration pathways. Link (1952) proposed five general types of stratigraphic and structural gas seepages:

1. Seeps on a homocline
2. Seeps caused by natural fracking of shallow source rocks
3. Seeps following along normal or thrust faults and fractured or eroded cap rocks
4. Seep over an unconformity
5. Seeps in fractured strata caused by intrusions/diapirs

(Link, 1952)

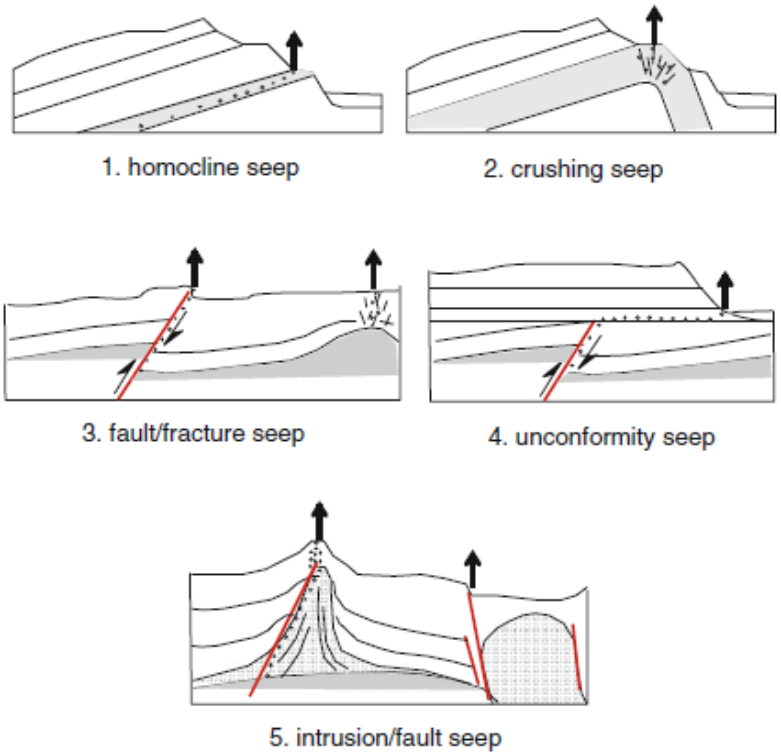


*Figure 4.4 The five hydrocarbon seeps suggested by Link (1952), in which type 1-2 is for oil seeping, type 3-5 is for gas seeping and type 5 is found in mud volcanoes. Comments by Etiope, 2015.*

## 4.4 Gas flares detecting in Multibeam Water Column Image (WCI)

Raw water column data were acquired by the Kongsberg Simrad EM302 multibeam echosounder system. The system's nominal sonar frequency of the sound waves is 30 kHz with coverage angle of up to 150º and 432 beams per ping, in practice, the system mainly used a 60º/60º opening angle. The ping rate varies with water depth and was switched frequently between 0.5 and 2 Hz (CAGE, 2020).

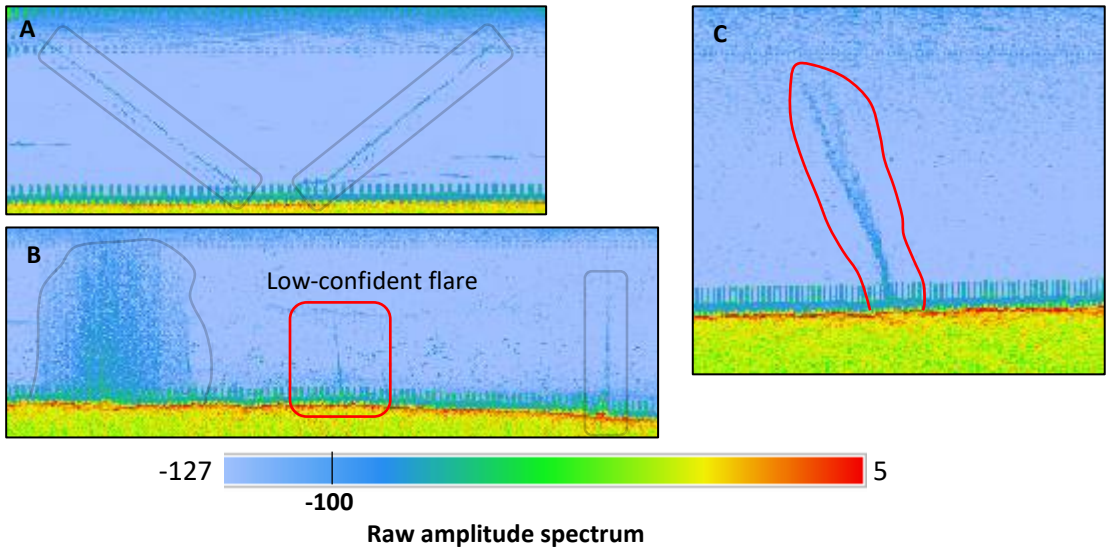


*Figure 4.5 (A) example of noise from CTD sensors; (B) the two noises from large on-ground infrastructure (black box to the left) and a well top (black box to the right) and a potential yet low-confident flare (red box); (C) an example of desired flare signals, which follows the criteria suggested by Judd et al., 1997.*

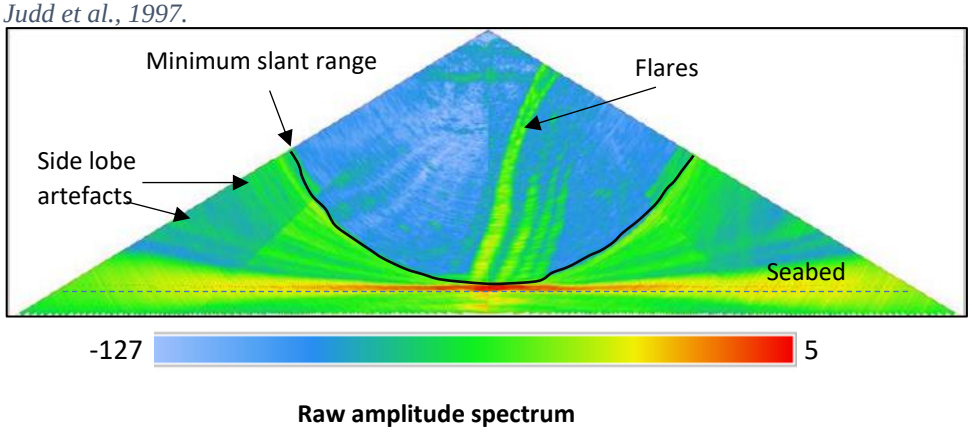


*Figure 4.5 A 5-stack fan view of multibeam WCI showing a potential flare. Modified from CAGE, 2020*

For acoustic behavior of gas flares can be confused with other unwanted objects (e.g fish shoal, ship noise) because "the reflection of an acoustic pulse occurs whenever a target is

encountered" (A Judd et al., 1997), a protocol of defining gas flare in WCI with following criteria is applied: (1) the potential gas flare must connect to the seafloor, which indicates the rooting of the flares, (2) the gas flares need distinguishing from fish schools, particularly the vertical to horizontal dimension ratio of the signals must be greater than two, (3) since gas bubbles do not occur singly, an isolated flare must be detected at least twice in the same location (Gentz et al., 2014; A Judd et al., 1997). Plus, under the effect of ocean currents, acoustic signals of the gas flares in R-stack view should bend upon the currents (Figure 4.5C), those absolutely vertical or clearly straight are associated with human-made noise such as signal interference with well tops at petroleum-active area (Figure 4.5B), gravity corer or CTD (conductivity, temperature, depth) sensors which were deployed from the ship to the seabed and retrieved back (Figure 4.5A).

The acquired data is imported and analyzed in QPS' FM Midwater software. Before processing the data, the provided sonar source files (*.all, *.wcd) need converting into generic water column file format (*.gwc). The procedure of detecting and extracting flare data in QPS' FM Midwater consists of the following steps:

- Playing back the data and identify the potential acoustic flares in fan view. In this thesis, a stack of 3 fans is used when viewing the data (Figure 4.6).
- Picking the flares: (a) locating a potential flare in fan view, (b) switch to R-stack view to identify the flare area, adjusting the amplitude range (Figure 4.7A, B), (c) delineate the flare amplitudes and export it as a ASCII file using WGS84UTM_34N coordinate reference system (Figure 4.7).
- Importing the ASCII into Petrel for visualization and correlation.

(CAGE, 2020)

The selected gas flares from water column data which were exported as ASCII files are imported into the Petrel software, matching with the chosen coordinates (for example, Figure 4.8). The gas flares are now visualized in 3D and interpretation windows to be correlated with their subsurface characteristics. The process of describing the gas flares includes the flares' directional orientation. However, because there is no navigation available in FM Midwater Fan view and R-stack window, the flares' orientation is relatively defined in Petrel's 3D window with low-confident accuracy (Figure 4.9A)

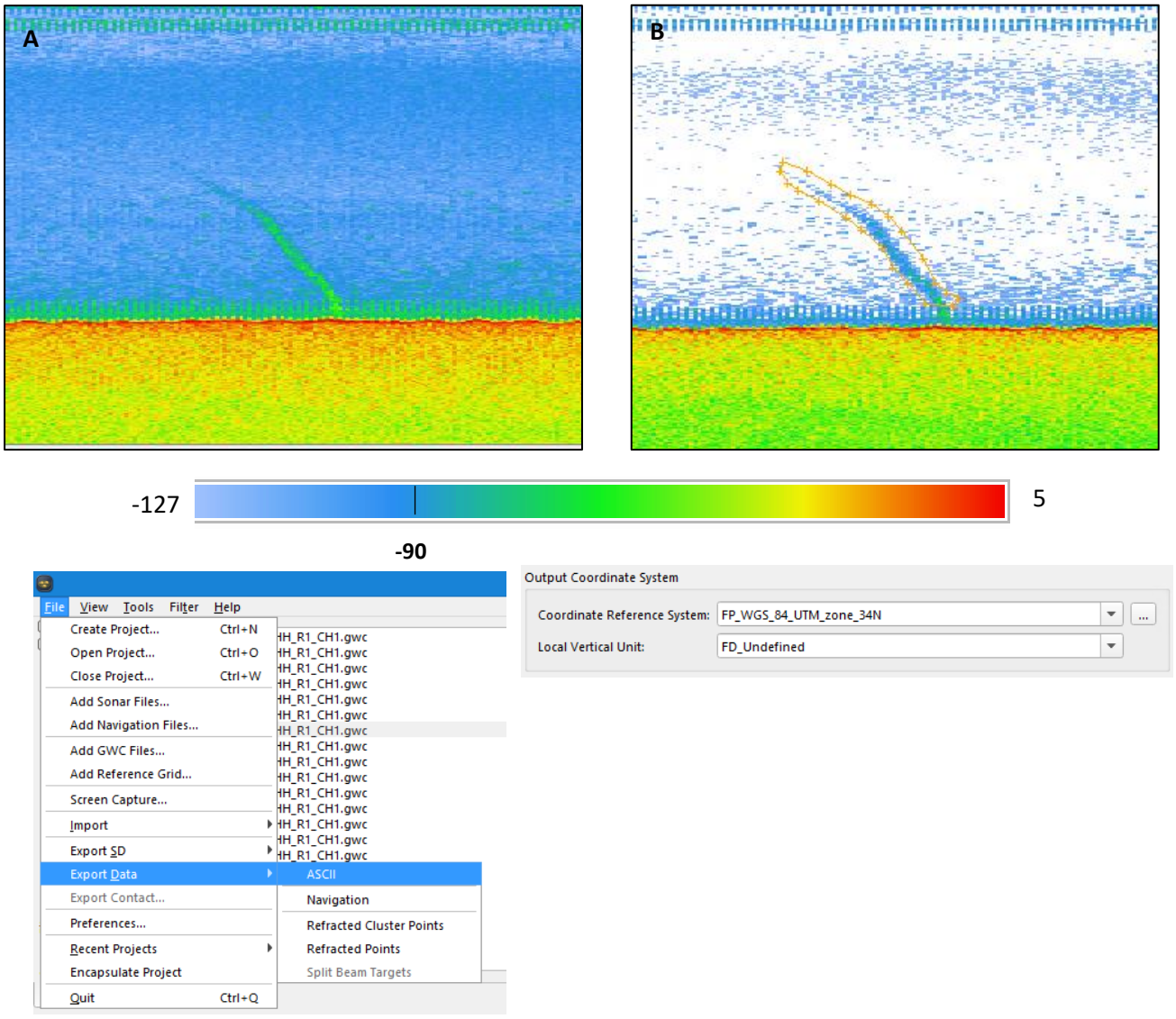


*Figure 4.7 Illustration of the gas flare in R-stack view and the process of exporting delineated flare amplitudes int o ASCII files. (A) gas flare in original raw amplitude spectrum; (B) gas flare in adjusted amplitude spectrum, excluding amplitudes that are lower than -90.*

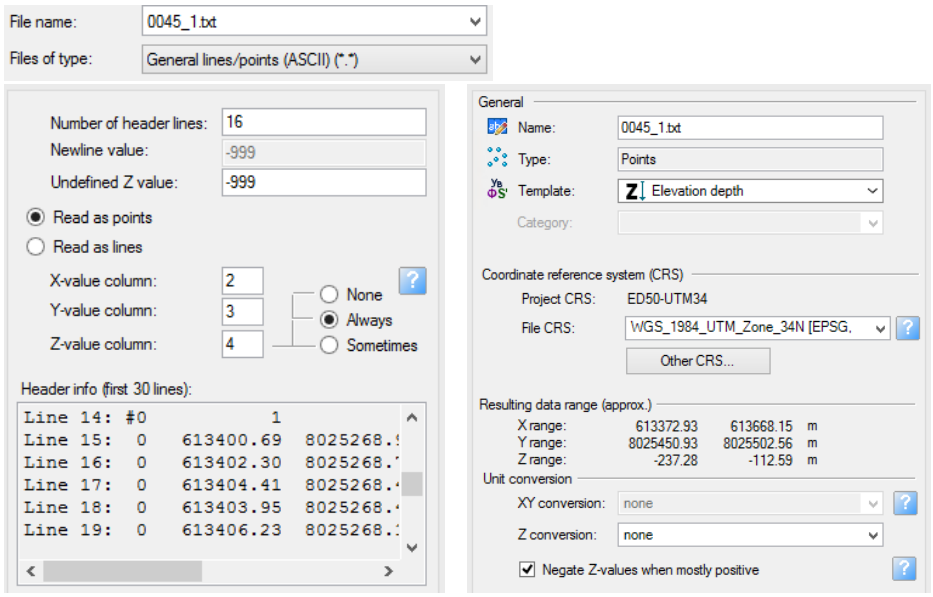


*Figure 4.8 Process and parameters of importing ASCII-formatted flares into Petrel*

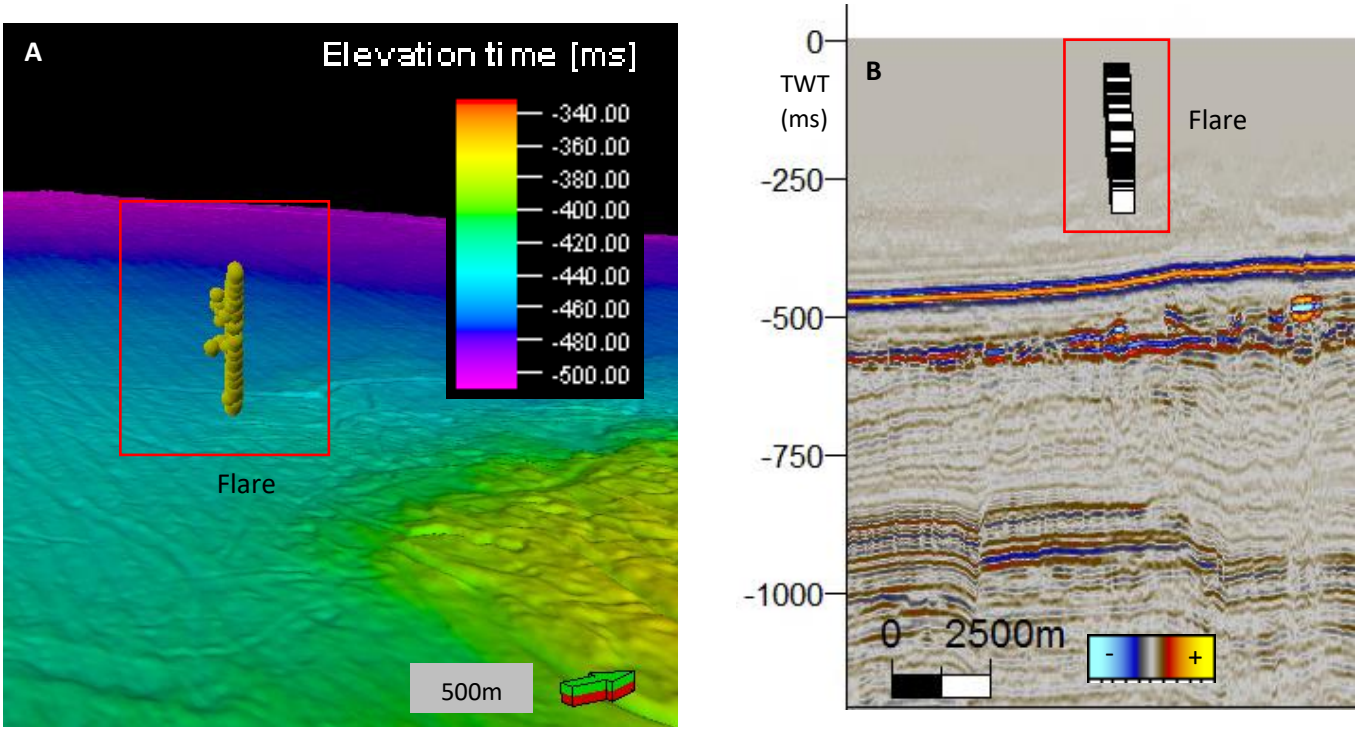


*Figure 4.9 Flare visualization in 3D window (A) and in Interpretation window (B). For the flares' relative orientation determination, the flare visualization in a 3D window is used.*

# 5 RESULTS

Within the available database, it will be assessed location by location to detect potential gas flares and correlate them with subsurface seismic data. The WCI data is used to pick up amplitude anomalies that satisfy the gas flare criteria mentioned in Chapter 4. Following that, seismic data is used to correlate them with the subsurface characteristics. The URU horizons represent the base surface of the glaciation events in the study area, whereas a regional reference horizon Top Mesozoic (TM) marks the top of Late Mesozoic sediments (as demonstrated in Figure 2.4).

## 5.1 Goliat field (7122/7-1)

The Goliat field is to-date an oil producing field in the Barents Sea. The reservoir is sandstone of Triassic age in the Kobbe and Snadd Formations, and in the Kapp Toscana Group (Realgrunne subgroup) of Triassic to Jurassic age. The field locates within the Troms-Finmark Fault Complex, 50km to the SE of the Snohvit field. The Goliat field corresponds to FMM line 0023of the cruise line. There are numerous of wells available at the site (Figure 5.1), in which, wells 7122/7-1 and 7122/7-3 are specifically used to examine the flare in FMM 0023. The wells determined water depth to be about 380m.

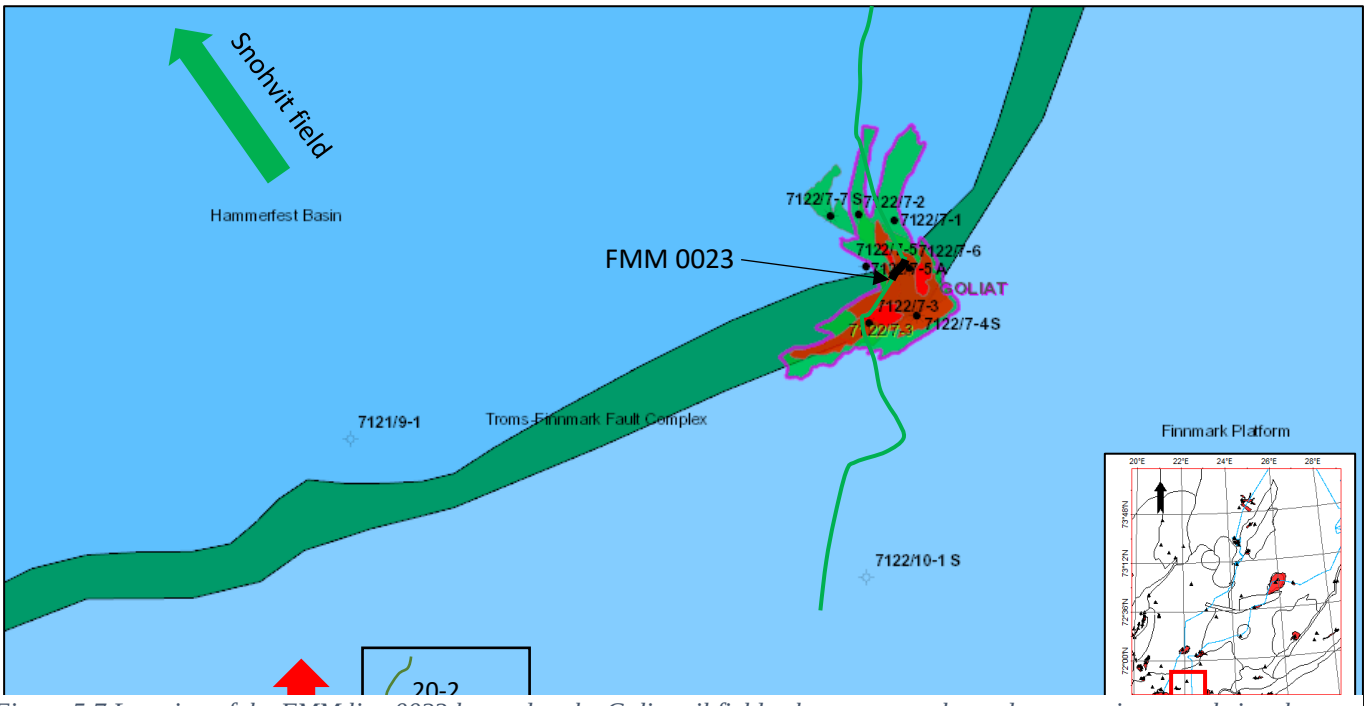


*Figure 5.7 Location of the FMM line 0023 located at the Goliat oil field, where water column data contain several signal noises caused by site infrastructure. A couple of low-confident gas flares are found at the location. The oil field lies within Troms-Finmark Fault Complex and is 50km to the SE of Snohvit field. Modified from npd.no*

On the account of massive on-ground petroleum producing infrastructure at the site, multibeam data in the water column are heavily disturbed and produce particular noise types (Figure 5.2):

- Distortions caused by on-ground pipeline (red dash line) appear below the seabed horizon.
- Reflected amplitudes of well heads, which is a completely vertical column of strong signals.
- Reflected signals of the other infrastructure at the site, which is a widespread area of amplitude anomalies shaping according to on-ground infrastructure.

However, a couple of low-confident flare indicators are picked. They are amplitude of -85 to -105 and do not clearly appear as strong flares but based on criteria for gas flares stated in Chapter 4.4, they are cynically regarded as gas flares. The one on the left in R-stack window is about 100m detectable height and slightly heading toward SW whereas the one to the right is just a weak indicator of flare that follow the criteria by Judd et al., 1997, with 60m detectable height and relatively vertical.

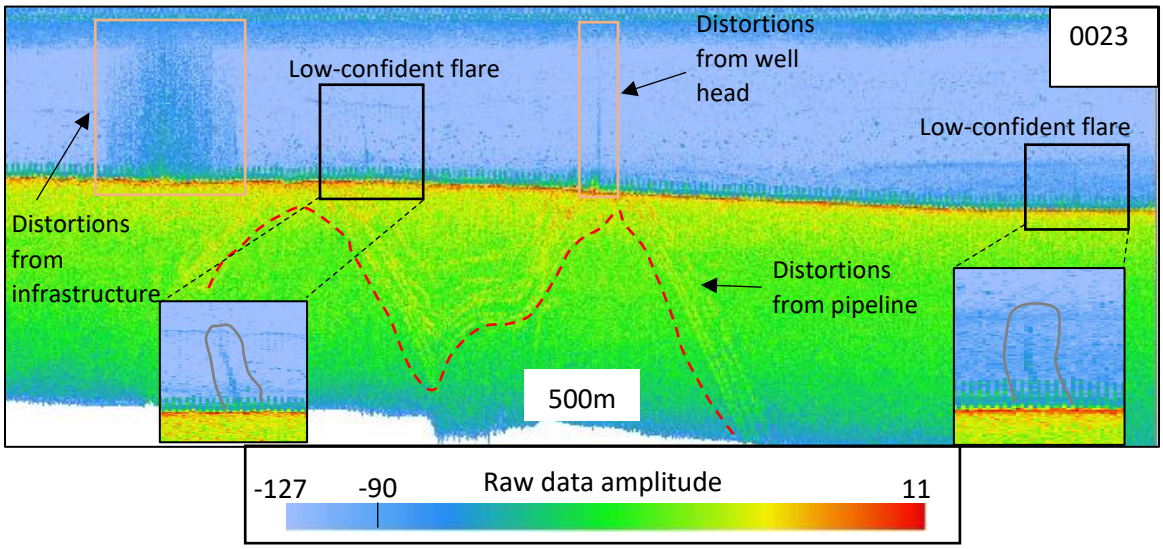


*Figure5.2 R-stack view of the FMM line 0023. Signal distortions caused by large infrastructure and well head are marked within orange rectangles; installed pipelines on ground pattern cause noise below seabed horizon (red dash line); 2 low-confident flares are found and delineated within black rectangles.*

The low-confident flares in FMM line 0023 at Goliat field are correlated with their subsurface seismic using 3D seismic survey EN0702. The seabed surface shows a descending morphology toward the NE of the survey. Thickness between the seabed and URU horizon

fluctuates from 120ms to 30ms TWT and is thinning northward. The thickness at the flare location is about 70ms TWT. There are no remarkably amplitude anomalies over the URU horizon, the URU is relatively continuous and slightly tilting toward NE. The flares found in FMM 0023 are located where wells 7122/7-1, 7122/7-3, 7122/7-5, 7122/7-5A and 7122/7-6 were drilled. Vertical profile at the flare location shows slight signal attenuations starting from the Top Mesozoic (TM) horizon at about -730ms TWT. The attenuated signals tend to associate with the well paths and directly connect to the flares in the water.

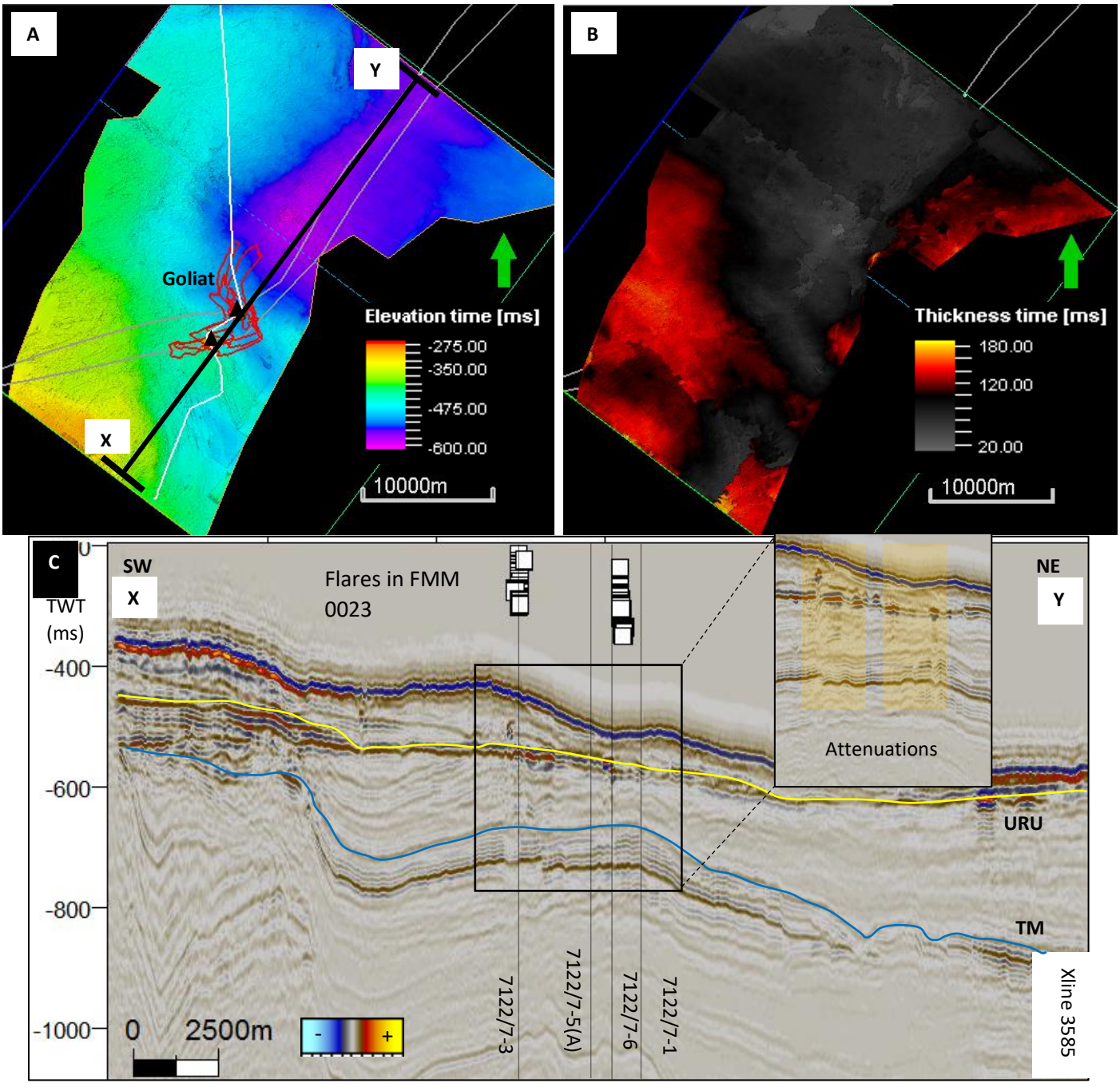


*Figure 5.8 A) Seabed surface showing location of the flares (black triangles) over the Goliat field (red delineation) and the descending morphology toward NE; B) Time thickness map from the seabed to the URU horizon; C) Vertical profile of the XY line in figure 3A, the flares appear right at the well locations and subsurface seismic shows attenuations of signals along the well paths.*

## 5.2 Caurus (7222/11-1) and Langlitinden (7222/11-2) discovery

Water column data from the cruise log line 0037 and 0038 on FM Midwater platform (FMM) reveals three gas flares in the water column, the features are observed at Caurus gas discovery and Langlitinden oil discovery complex. The complex locates at the trijunction of Loppa High, Bjarneland Platform and Hammerfest Basin (Figure 5.4). Two discovery wells were drilled in the complex to wildcat the petroleum potentials and provided oil shows in the discoveries. The flares in FMM line 0037 and 0038 strength is shown in amplitude, which ranges between -100 and -115 and their heights are about 200m from the seabed in the area with 330mwater depth (Figure 5.5).

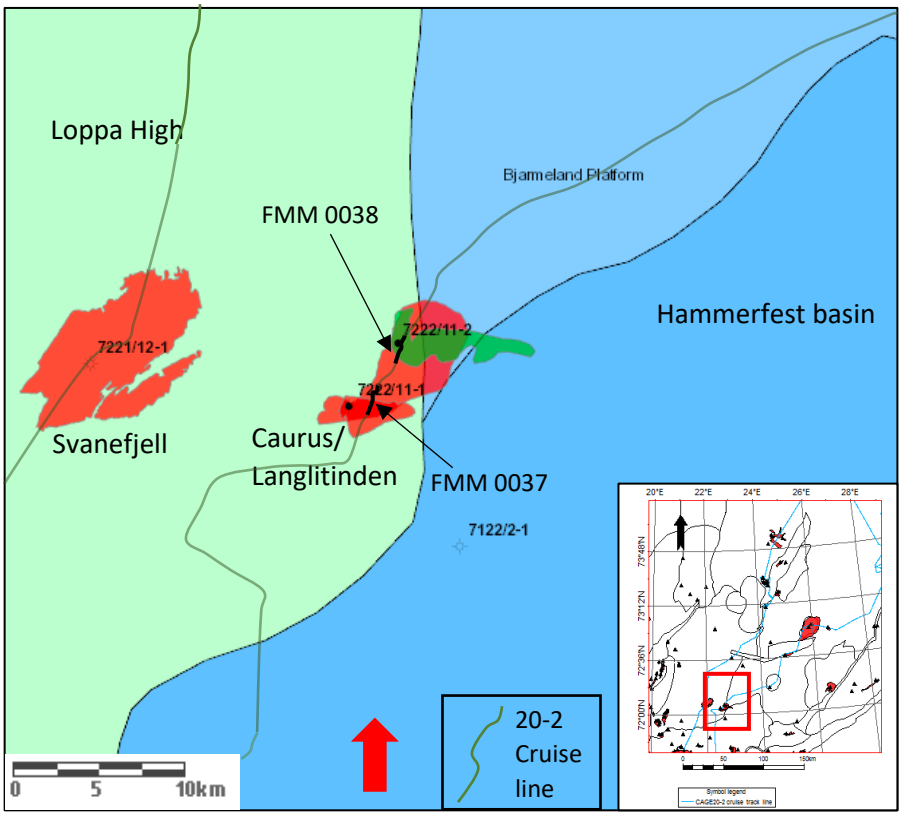


*Figure 5.4 Location of the FMM lines 0037 and 0038, which are located over Caurus/Lamglitinden complex, at the trijunction of 3 geology elements: Loppa High, Hammerfest Basin and Bjarneland Platform. The 20-2 cruise crossed the complex and found 2 flares at black-bolded sections. Modified from npd.no.*

FMM line 0037 contains numbers of amplitude anomalies, however, according to the mentioned characteristics of gas flares in Chapter 4.4, there is only one potential feature to be detected as a gas flare in an R-stack view of the line (Figure 5.5, 0037). A weak flux of vertical-

oriented amplitude anomalies appears as a probable gas flare in the water column. 3D illustration on Petrel shows that the flare is slightly heading SW from the seabed (Figure 5.6C). The other amplitude anomalies are assumed to be distortions caused by faunal activities in the water, most likely from plankton or fish.

FMM Line 0038 shows a double-flare feature coming relatively strong from the seabed, distancing about 550m from each other. The flare on the left is slightly heading southwest (Figure 5.5C) while the other one appears as two stacked flares next to each other, which is fairly vertical in the FMM R-stacked window (Figure 5.5, 0038). The flares' amplitude anomalies in FMM line 0038 are seen as strong fluxes of gas bubbles into the water from the seabed. A couple of amplitude distortions is also observed and assumed to be faunal activities as well.

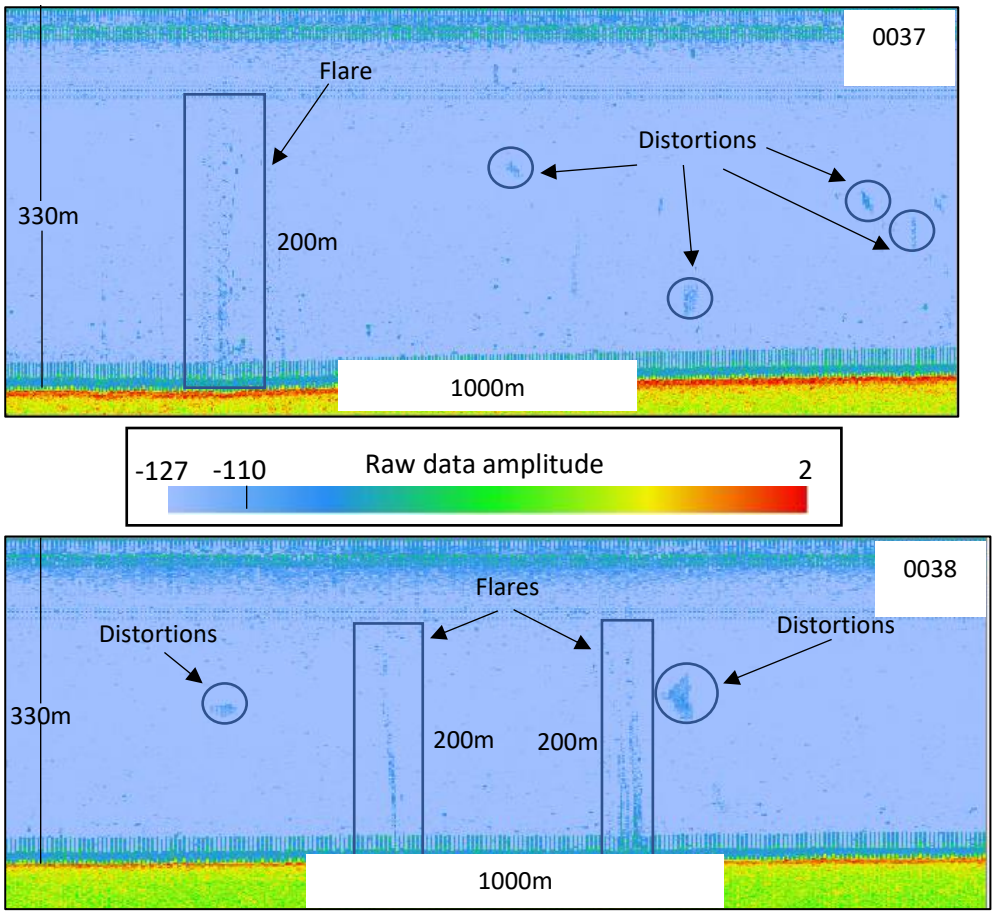


*Figure 5.5 R-stack view of the flares in FFM line 0037 and 0038, water depth stabilizes at 330m. Only hydroacoustic signals that follow flares' criteria suggested by Judd et al., 1997 are picked (black rectangles), other amplitude anomalies that do not root from the seabed are assumed to be distortions.*

Correlating the Midwater data with seismic data on Petrel, the flares are visualized in a 3D window and their relations with subsurface strata.

The flares in Caurus and Langlitinden discoveries are covered by the SG9803 3D seismic survey. The flares are shown in a 3D window, vertical exaggeration 5 over the seabed surface (Figure 5.6C). There is a region of deformed topography in the SW of the 3D survey (Figure 5.6B). Thickness from the seabed to URU horizon is about 100ms two-way-time travel (TWT) and thins down towards the deformed region (Figure 5.6D). Seismic profile of the flares area shows that strata below the TM horizon have anticline-like shape that moves up and are heavily affected by faults/fractures, the top of the anticline truncates the URU horizon (Figure 5.6A). Seismic amplitude anomalies are also spotted along the truncation on URU, which are channel-like

amplitude anomaly pockets at about -550ms TWT, and deeper formation, i.e the ones at -860ms and -900ms (TWT). Faults running into deep strata are present in the area as well. However, the flares are not over the deformed region, they are observed at a transition zone of the seabed depth topography. Also, according to the seismic profile in Figure 5.7, the flares in FMM line 0037 and 0038 are over the area where the TM horizon truncates with the URU horizon.

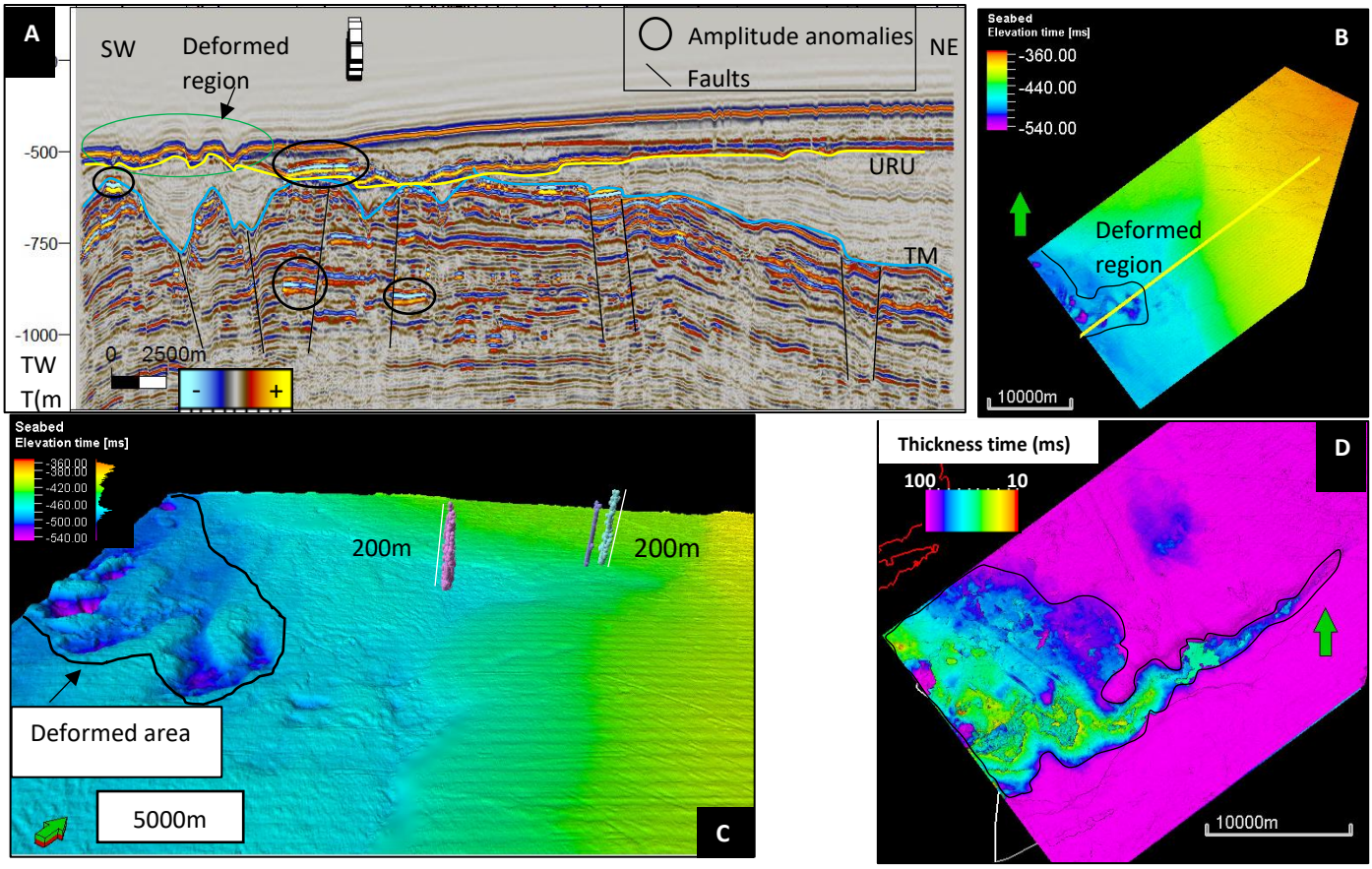


*Figure 5.6 Illustration of 3D view and seismic behavior of the flares in FMM line 0037 and 0038; A. Vertical profile of the flare area including seismic of the deformed area at the seabed (green circle); B. Seabed surface showing location of the deformed region at the SW of the survey; C. 3D view of the flares in a 3D window, vertical exaggeration 5, the flares locate at the flank of a descending slope on the seabed, not at the deformed region; D. Isochore map from the seabed to the URU horizon, showing the thinning thickness trend from NE to SW of the survey, towards the deformed region.*

In seismic profile of the flare in FMM line 0037, high amplitudes over the URU horizon and at a horizon at -850ms TWT are observed, together with their reversed polarity signals compared to the seabed. The amplitude anomalies cause acoustic masking to underlaying signals down to -880ms TWT. There are also indicators of faults starting from deep strata running to the URU horizon. Wildcat well 7222/11-1 (Caurus), which was drilled at water depth of 356m and to test

hydrocarbon presence in the Caurus discovery, it found gas samples in the shallow Snadd reservoir gas at 634.8m and 771.5m depth (npd.no).

In seismic profile of the flare in FMM line 0038, 3 amplitude anomaly points are found at the URU and on top of the TM horizon. A noticeable amplitude anomaly at -580ms TWT causes acoustic masking to underlaying signals, down to -800ms TWT. The discovery well 7222/11-2 (Langlitinden) is positioned where the flare is now located, at 338m water depth. The well was to investigate large scale channel system in the Kobbe Formation. Oil shows in cores were found in Kobbe Formation at below 2000m depth, the well was permanently abandoned and concluded to be technical oil discovery (npd.no).

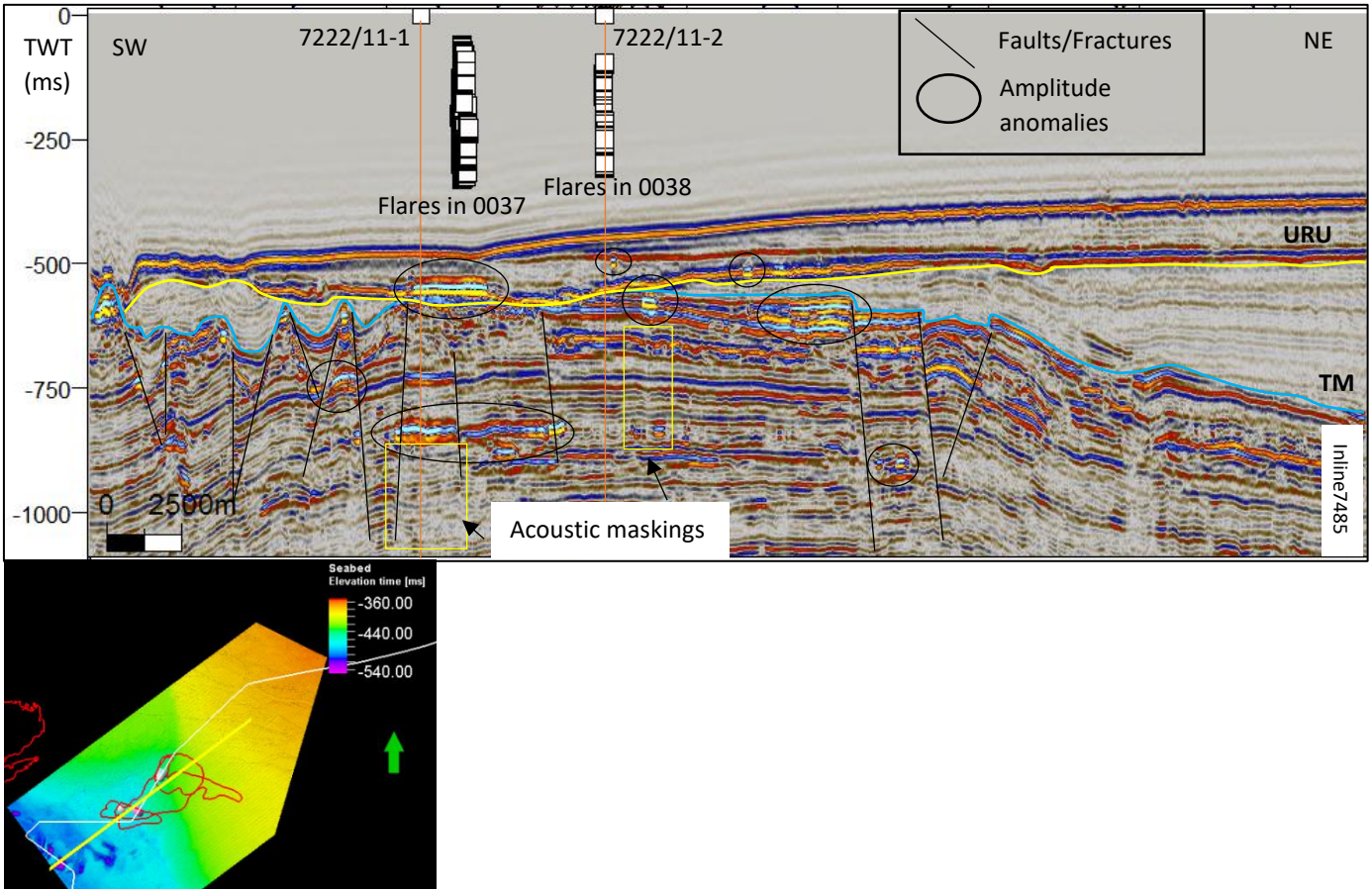


*Figure 5.7 Vertical profile of the flares in FMM line 0037 and 0038. Amplitude anomalies in varying sizes (from large pockets to small points) are spotted on top of the URU and the TM horizon. Exceptionally, 2 amplitude anomalies cause acoustic masking to the following signals (yellow rectangles). Faults/fractures indicators are present below horizon TM in considerable quantities and complex orders.*

## 5.3 Samson Dome (7224/7-1)

At FMM line 0045 and 0046 of the cruise, a set of small gas flares from the seabed is observed. The flares' location is over the Samson Dome salt structure, about 60km to NE of the Caurus/Langlitinden discovery complex (Figure 5.8). This area also includes the exploration wellbore 7224/7-1 drilled at 266m water depth and according to npd.no, the well was to test Early/Late Jurassic sandstone reservoir at the Samson Dome structure.

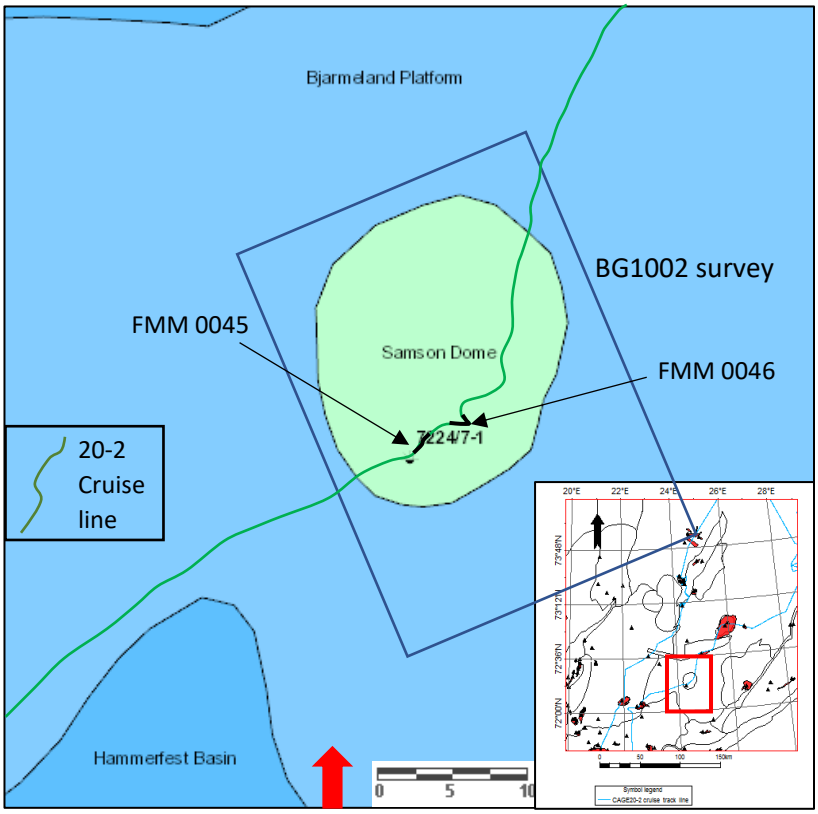


*Figure 5.8 FMM line 0045 and 0046 location, 2 flares are found just over the Samson Dome. The 20-2 cruise crossed the well 7224/7-1. Modified from npd.no.*

The flares in FMM line 0045 are examined in the R-stacked view in FMM window (Figure 5.9, 0045). There are 2 parts of the flares in this cruise line: the smaller flare to the left of the window is slightly heading toward NE with the detectable height of 80m; the other flare are laterally extent amplitude anomalies starting from the seabed, the anomalies column is 150m tall

and about 75m laterally extent. The 2 flares are about 70m distancing from each other. Amplitude spectrum of the target flares is in range of -90 to -115, other amplitude anomalies that do not root from the seafloor are assumed to be distortions.

Whereas in FMM line 0046 (Figure 5.9, 0046) there are two northeast-oriented flares from the seabed, with visual height of about 45m to 46m distancing about 720m to each other. The amplitude spectrum of the flares is between -80 to -110, they appear as weak output of gas bubbles into the water.

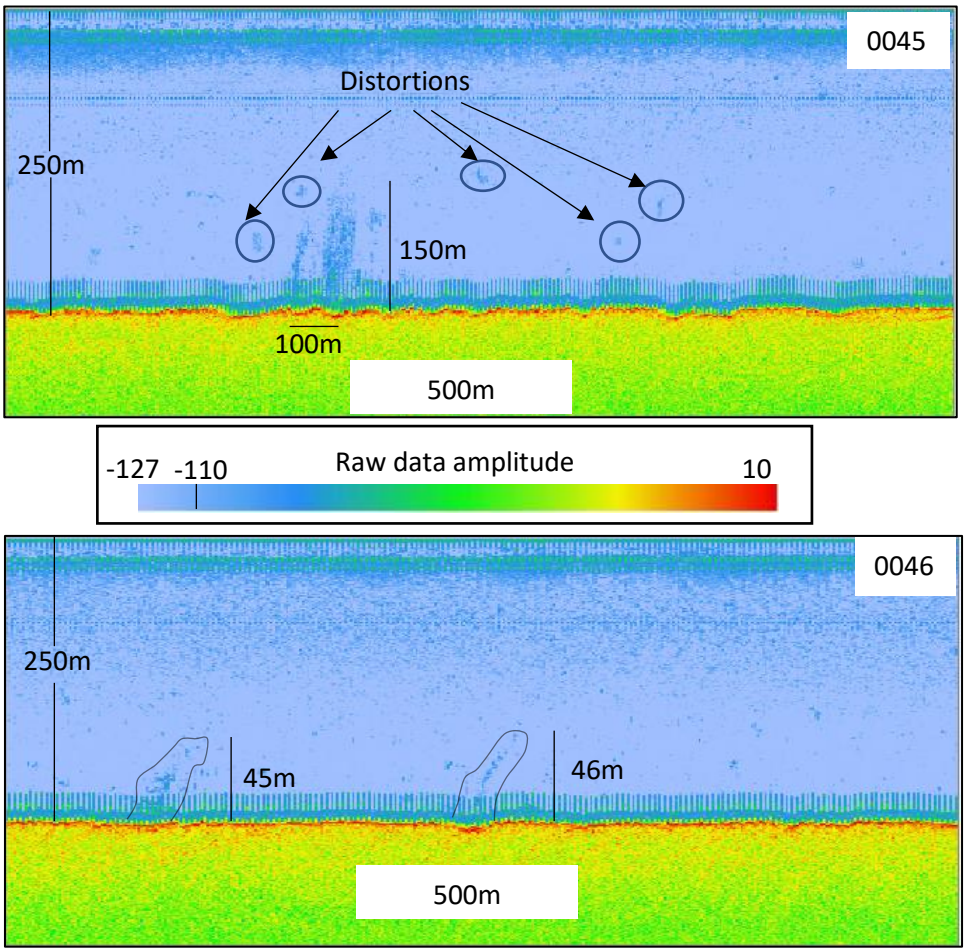


*Figure 5.9 R-stack view of the flares in FMM line 0045 and 0046, water depth is about 250m. The doubled-flare feature in FMM 0045 is measured in size, other amplitude anomalies (black circles) are considered distortions; the 2 flares in FMM 0046 are weak yet detectable amplitudes (black polygon, 0046.*

The flares in Samson Dome are covered by the 3D seismic survey BG1002 and 2D seismic lines NBR08-135996, NBR08-135652 and NBR08-136571. The seabed and URU horizon are relatively serene and the thickness from the seabed to URU is about 140ms throughout the survey (Figure 5.10). The 3D seismic profile shows a stable and continuous horizon of Top URU at -500ms TWT and local high amplitude anomalies at about 70ms above the Top URU horizon. An RMS map was made with search window of 70ms above Top URU down to 30ms above the horizon, the RMS amplitude map reveals an area of about 55km$^2$ of accumulated high amplitude anomalies of 6000 to 10000 (Figure 5.11A, within delineated red dash polygon).Additionally, a domal salt structure at around -1000ms TWT, which was determined as Samson Dome is shown in the seismic profile, well 7224/7-1 stated that peak of the structure is Middle Jurassic sandstone (Sto Formation) at 894m depth (npd.no).

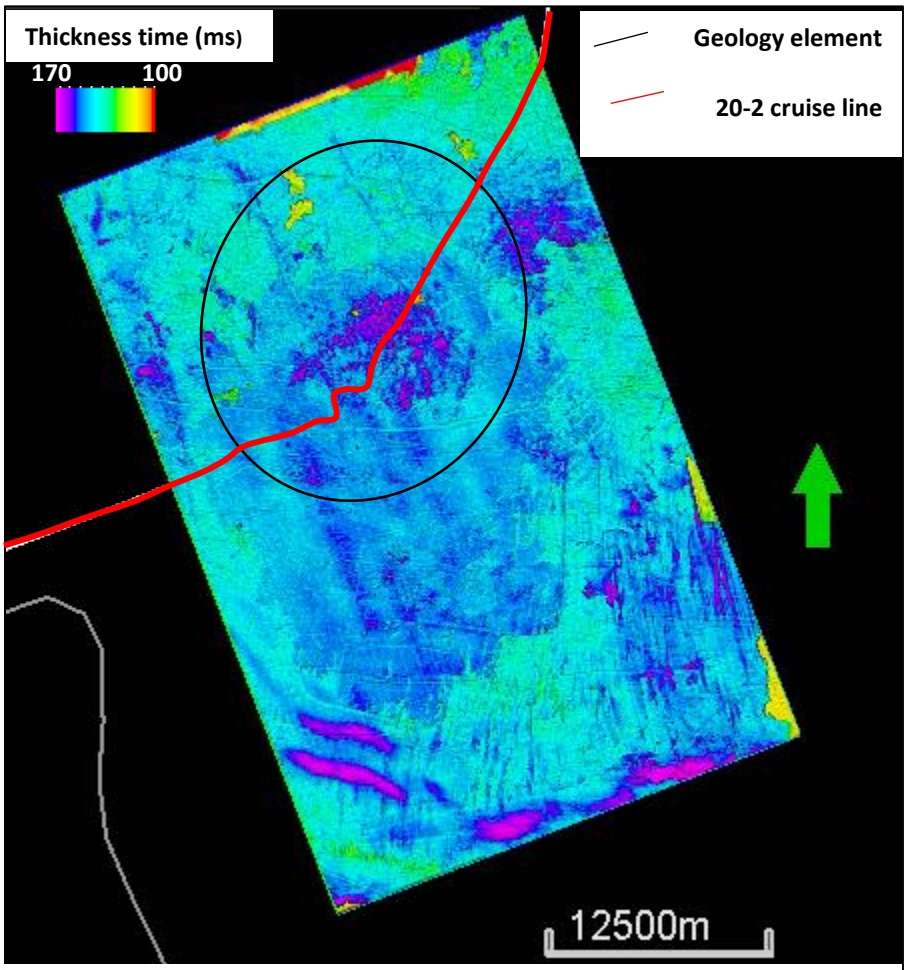


*Figure 5.10 Isochore map from the seabed to URU horizon showing relatively stable time thickness at 140ms, time thickness at the Samson Dome location is slightly increased to 170ms.*

Figure 5.11B illustrates a random line going over the high RMS amplitude area. The amplitude anomaly pocket spreads from 70ms above URU down to the horizon and causes some minor effects to underlaying signals.

Correlated subsurface seismic of the flare in FMM line 0045 shows an amplitude anomaly just 70ms above URU horizon (Figure 5.11C). The anomalies are outside the high RMS amplitude area and polarity-reversed to the seafloor's which causes weak push-down effects to underlaying signals. The wildcat well 7224/7-1 (Samson Dome), whose results had weak petroleum shows and were determined that the reservoir sandstone at 894m to 931m (consists of Sto, Nordmela and Tubaen FM) is water bearing. The well was abandoned when Statoil did not encounter expected reservoir sandstone.

Whereas, correlated seismic of the flare in FMM line 0046 includes amplitude anomalies at about 70ms above the URU horizon but in larger size and quantity. Several push-down effects to underlying signals are also observed (Figure 5.11B, C).

The salt dome structure peaks at the flares location and contains series of fractures. Seismic behaviors of strata between URU and the TM horizon suggest a top seal to the salt dome as no fractures/fault overcome the TM horizon (Figure 5.11B, C).

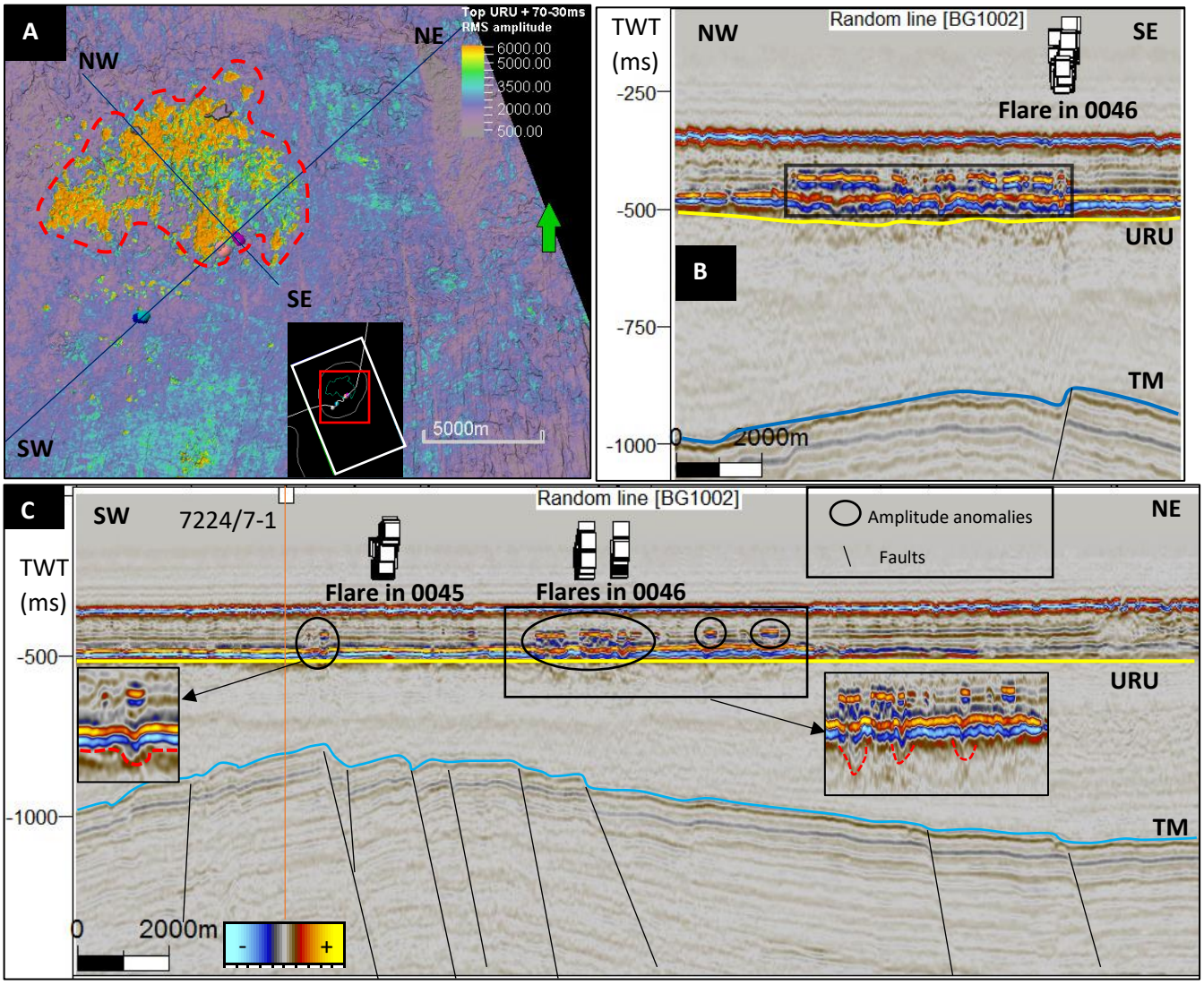


*Figure 5.11 A. RMS amplitude attribute map, search window from 70ms above URU down to the horizon, showing 55km$^2$ area of high RMS amplitude in the center of Samson Dome; B. Random seismic line showing high amplitude accumulation above the URU, which causes minor effects to underlaying signals; C. Random seismic line including the 2 flares in FMM line 0045 and 0046, amplitude anomalies at the flares' locations cause push-down effect to underlaying signals (red dash lines).*

## 5.4 Norvarg (7225/3-1) and Ververis (7226/2-1) discovery

FMM data over Norvarg and the neighboring Ververis gas discoveries reveal two gas flares. The Norvarg discovery locates at the Norvarg Dome structure with exploration wells 7225/3-1 and 7225/3-2 available. No 3D seismic survey is provided for the Norvarg Dome area, however, the 2D seismic line TEPN-12-2-10 which encounters the flare in FMM line 0061is used to examine the flare. On the other hand, the Ververis discovery locates roughly 11km to the west of the Norvarg discovery, the feature is covered by 3D seismic survey ST07M16 and one exploration wells 7226/2-1 was drilled to test the discovery. Water depth in the area is determined by the exploration wells to be in range from 347m to 381m (npd.no).

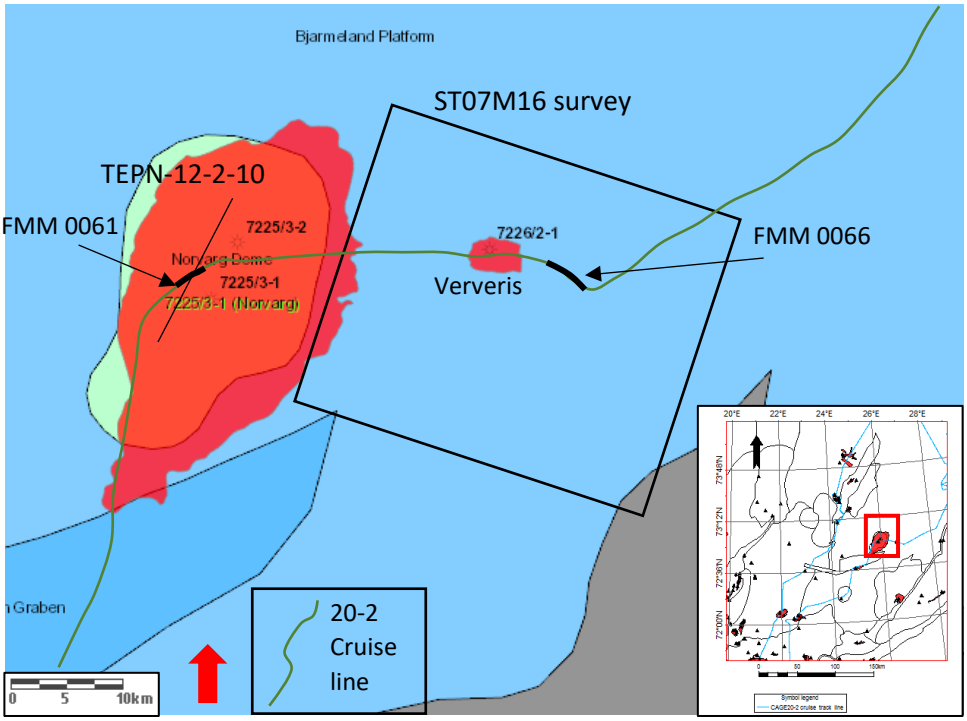


*Figure 5.12 Location of the FMM line 0061 and 0066, at Norvarg (7225/3-1) and Ververis (7226/2-1) discoveries. The 20-2 cruise line crossed the 2 discoveries and wells involved. Modified from npd.no*

At the Norvarg gas discovery, in FMM line 0061, a gas flare is detected with the height of 115m and heading SW (Figure 5.13, 0061). The gas bubbles indicate a strong release of gas from the seabed into water column but does not last long in the water, amplitude spectrum of the flare is from -85 to -106. Two other groups of amplitude to the right of the detected flare in the R-stack window are low-confident to be considered as flares because their weak connection to the seabed, therefore they are not regarded.

At Ververis gas discovery, in FMM line 0066, a powerful and elongated gas flare is observed, with vertical height of 210m (Figure 5.13, 0066). The feature is relatively tilting toward the SW with amplitude range lies between -90 and -115.

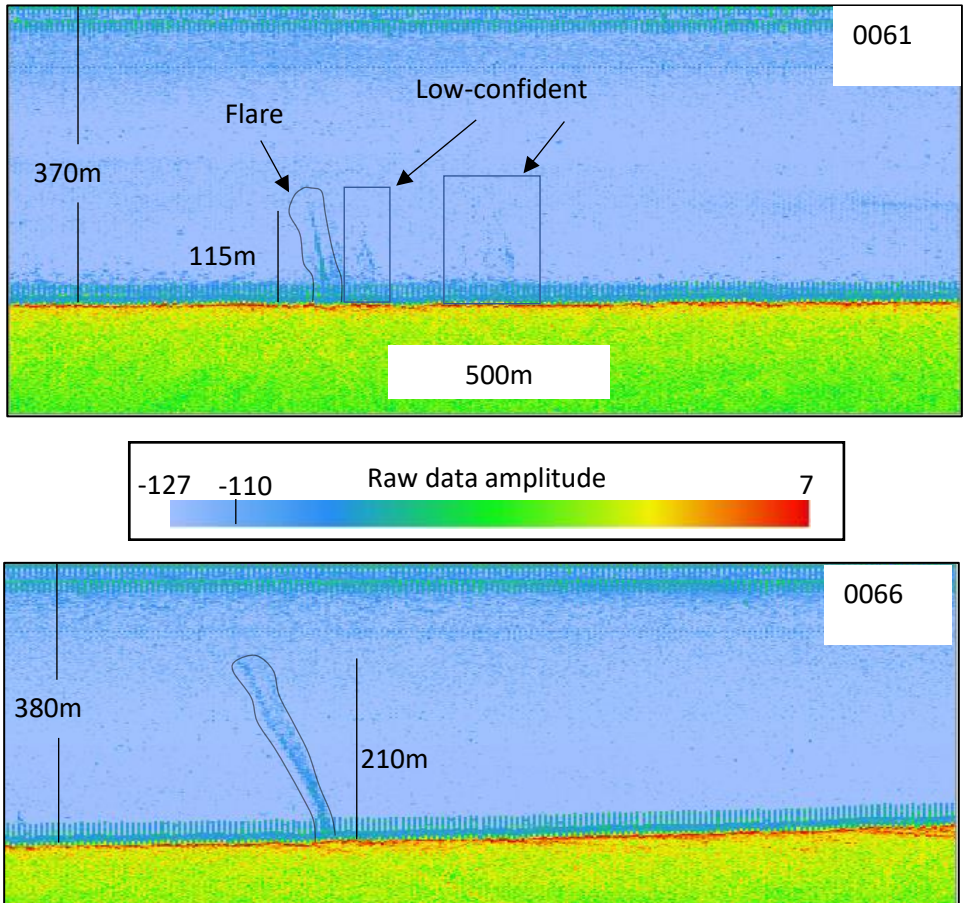


*Figure 5.13 R-stack view of the flares in FMM line 0061 and 0066. The target flares are delineated by black polygons while disregarded low-confident amplitudes in FMM line 0061 are covered in black boxes.*

Within provided data in this thesis, only a 2D seismic line is available for the flare at the Norvarg discovery (FMM line 0061), which is TEPN-12-2-10 2D line from the TEPN-12-2 survey acquired by Total E&P Norge AS in 2012. Wildcat well 7225/2-1 and 7225/3-1, whose purpose was to find hydrocarbon proof at Norvarg dome, has proven gas presence in Jurassic Stø Formation and determined Norvarg as a gas discovery. The literature data helped examine the subsurface strata of the flare in FMM line 0061. In the 2D seismic line TEPN-12-2-10, the flare is over a chaotic signal zone which roots from top of a domal structure (below the TM horizon) at -700ms TWT and reaches to the seabed. Strata below the TM horizon experience series of faults and the chaotic signals above appear to originate from one of the faults (Figure 5.14).

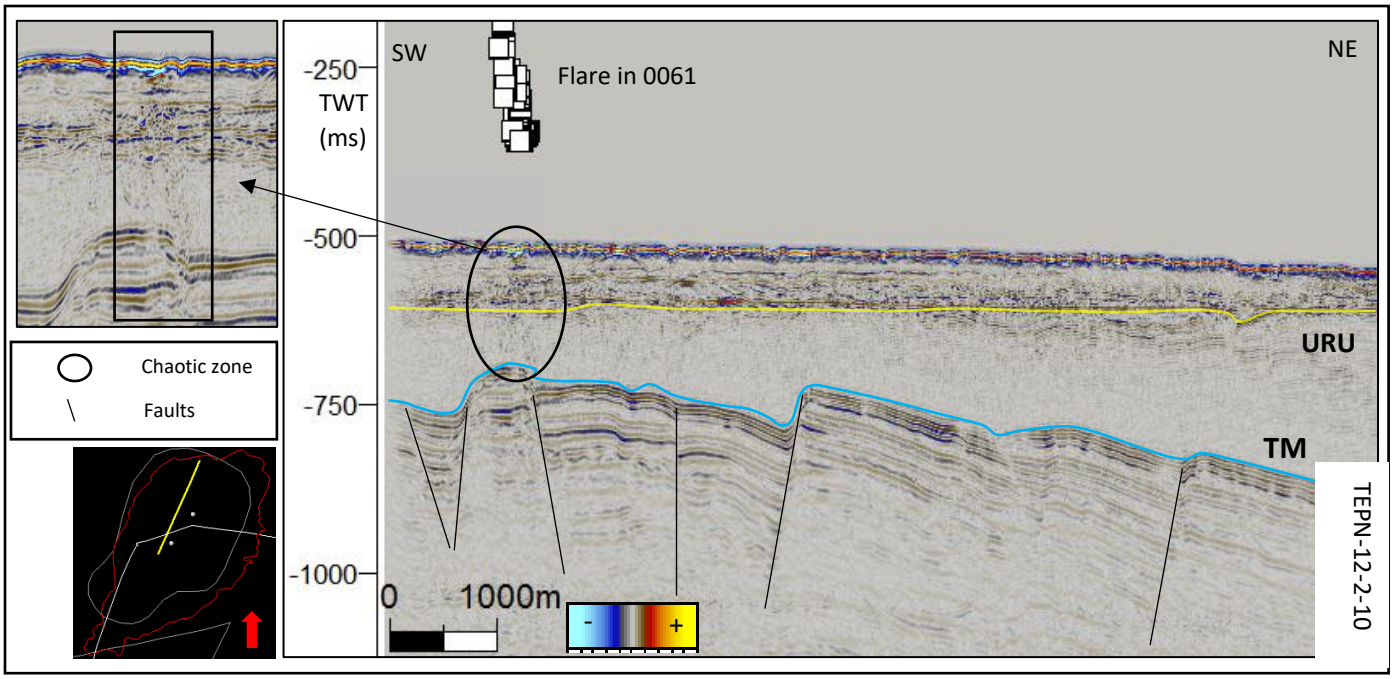


*Figure 5.14 2D line TEPN-12-2-10, which crosses the flare in FMM 0061, shows vertical profile of the flare's correlated subsurface. A chaotic zone rooting from one of the faults reaches the seabed and leaves high amplitudes at the seabed.*

The flare in FMM line 0066, at the Ververis discovery is examined using the 3D seismic survey ST07M16. The seabed has descending depth from -320ms in the east to -370ms toward the west and the flare locates at the flank of a slope, distancing about 6km to the SE of well 7226/2-1 (Figure 5.15C). A random line was made to include both the well's and the flare's vertical profile, running from NW border to SE border of the ST07M16 survey (Figure 5.15A). At about 85ms above URU, there is an amplitude anomaly in the profile which is polarity-reversed to the seabed and causes acoustic masking to underlaying signals.

An RMS amplitude map with search window of 85ms above URU to the horizon is made to assess the high amplitude distribution (Figure 5.15B). The RMS amplitudes gather in small groups at the flare location, and noticeably gather in large quantities in the NW and SE edges of the ST07M16 survey. Strata below the TM horizon shapes in anticline with top of the structure was

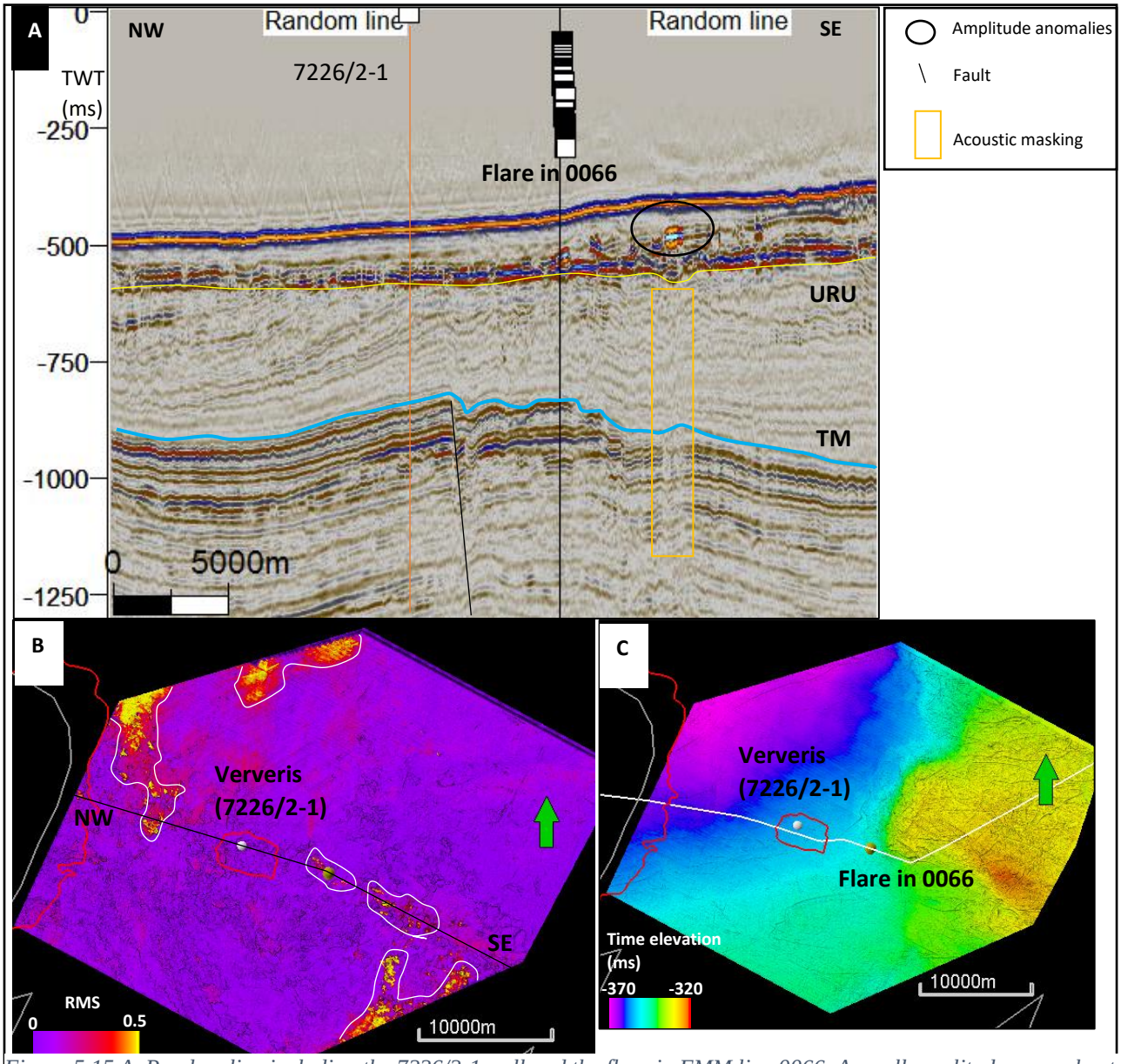


*Figure 5.15 A. Random line including the 7226/2-1 well and the flare in FMM line 0066. A small amplitude anomaly at 85ms above URU causes acoustic masking to underlaying signals. Strata below the TM horizon shows a peak of the structure, it is barely affected by faults/fractures; B. RMS map, search window 85ms above URU down to the horizon, shows high amplitude accumulations do not concentrate at the flare location, but at the survey's edges; C. Seabed surface within ST07M16 survey, showing descending depth of the seabed from east to west.*

encountered by the well 7226/2-1, the strata were slightly fractured and proved to have weak oil shows in Tubaen FM (at 905-952m interval) and in Kobbe FM (at 1746-1747m interval).

## 5.5 Hanssen (7324/7-2) and Wisting (7324/8-1) oil discovery

The cruise line crossing the Hanssen and Wisting oil discovery complex found 3 flares in FMM line 0780, 0787 and 0790. The area is at SW border of the Hoop Fault Complex in Bjarneland Platform (Figure 5.16). The flare in FMM line 0780 is observed to be over the Hanssen oil discovery, where the discovery well 7324/7-2 is located. Whereas the flare hunted in FMM line 0787locates over the Wisting oil discovery, specifically, just at the discovery well 7324/8-1 location. The complex was proven to contain oil in Sto FM and have a gas cap at 662m depth by OMV (Norge) AS in 2015. There is no 3D seismic provided to examine the area, instead 2D seismic lines from the OMV11300 survey are used, which includes both the flares in FMM line 0780 and 0787.

The flare in FMM line 0790 is roughly 6km to the SE of the oil discovery complex, it is just at where the discovery well 7342/8-2 is located. Similar to the flares at Wisting, with no 3D seismic provided, only one 2D seismic line NBR08-147482 is available to examine the flare.

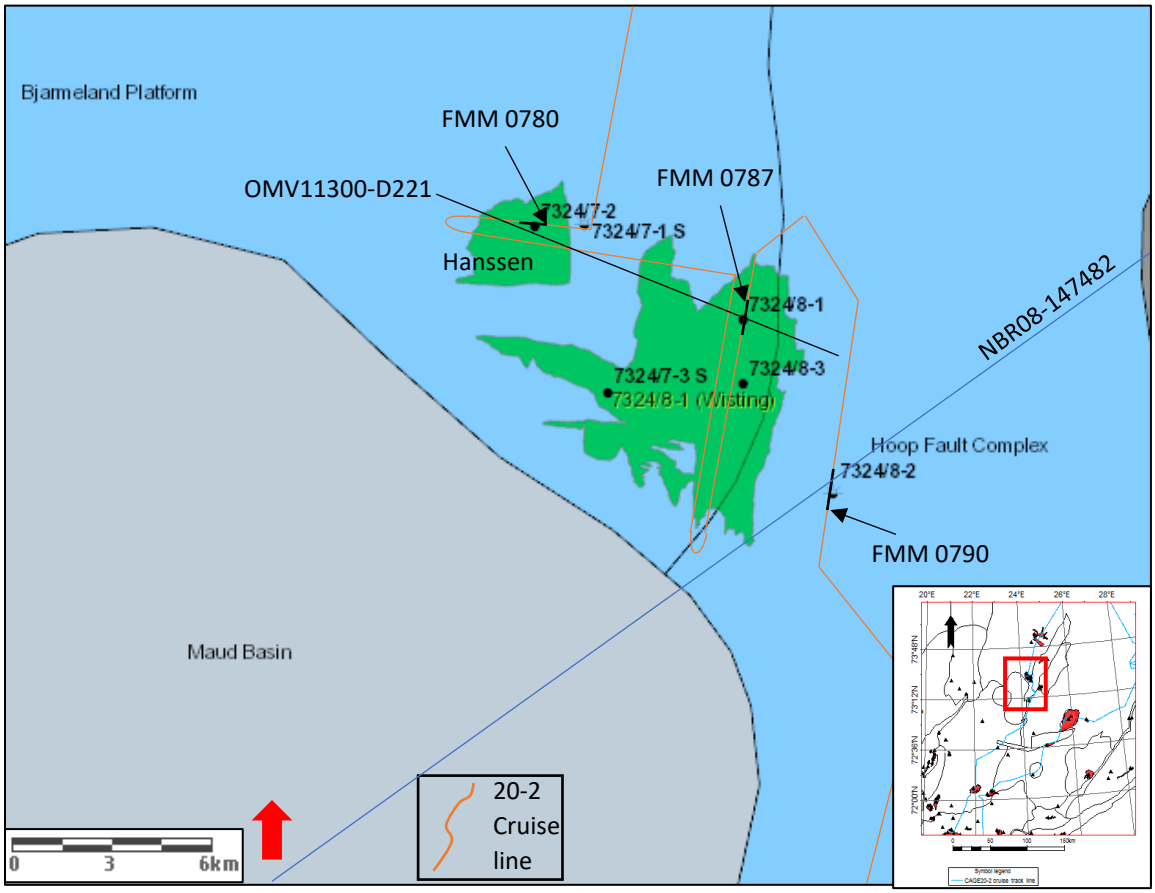


*Figure 5.16 Location of the flares in FMM line 0780, 0787 and 0790. Locating over Hanssen and Wisting oil discovery complex, just NE of Maud Basin. The 20-2 cruise line encountered the discoveries and wells involved. Modified from npd.no*

In FMM line 0780 (Figure 5.17, 0780), the flare is detected as a NW-tilted feature with vertical height of 250m, its amplitude spectrum stands out in range from -50 to -80. It appears as high flux of output gas into the water column but with a small exit in the seabed just on top of the Hanssen discovery.

In FMM line 0787 (Figure 5.17, 0787), the flare appears as a slim body of releasing gas into the water, with vertical height of160m and its amplitude varies from -55 to -80. The flare is slightly SW-oriented.

Line 0790 (Figure 5.17, 0790) also shows clear signals of a high flux of gas released into the water column which is strongly deviated towards NE direction. The flare is vertically 160m tall and ranges -55 to -80 in amplitude.

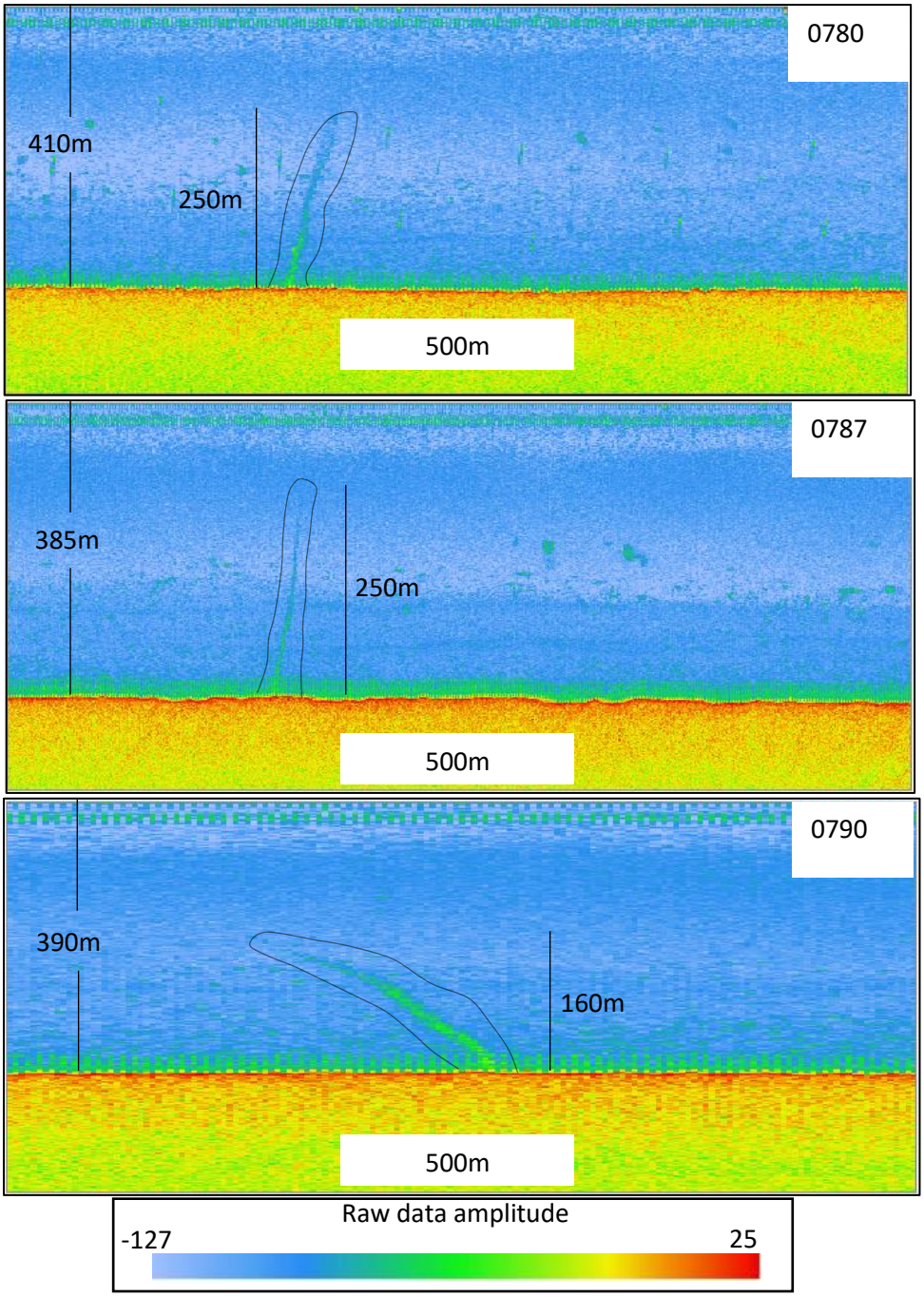


*Figure 5.17 R-stack view of the flares in FMM line 0780, 0787 and 0790. They are delineated within black polygons. Amplitudes that do not satisfy criteria made by Judd et al., 2017 are disregarded.*

There is only the OMV11330 2D seismic survey available when correlating the flares in FMM lines 0780 and 0787 with their subsurface characteristics. 2D lines OMV11300-D217 to OMV11300-D228 include the flares in FMM line 0780 and 0787 and some subsurface features

that can be linked to the flares. Thickness time from the seabed to URU horizon is determined in 2D line OMV11300-D221 to fluctuate bet ween 55-77ms, thickening toward the SE (Figure 5.18A). The flares' locations are right at where the wells 7324/7-2 and 7324/8-1 were drilled. No anomalously high amplitudes are observed in shallow subsurface (above URU horizon) in the 2D seismic lines. Strata below URU horizon show a series of fault blocks and the formations at -700ms TWT.

The flare in FMM line 0780 is observed right at the well 7324/7-2 (Hanssen) location, the well was to prove hydrocarbons in the Realgrunnen Subgroup. It encountered the primary target Sto FM at 712m and defined the formation as oil-bearing down to oil-water contact at 731.95 true-vertical-depth (TVD). There are no noticeable amplitude anomalies in seismic profile at the flare location, however, a couple of signal interferences and depressions are spotted at the seabed (Figure 5.18B).

The flare in FMM line 0787 is observed at the well 7324/8-1(Wisting), similarly to the well at Hanssen discovery, it was to test hydrocarbons in the Realgrunnen Subgroup. Top Sto FM was defined at 662m depth contains oil, oil-water contact was not clearly determined. No anomalously high amplitudes are observed in shallow seismic and interferences of signals and depressions at the seabed are also present in the flare location (Figure 5.18C).

Strata below the TM horizon are determined to be Middle Jurassic age, which were proven to contain hydrocarbons and affected by series of faults. The faulting appears, in the vertical profile, from deep strata and stops at URU horizon.

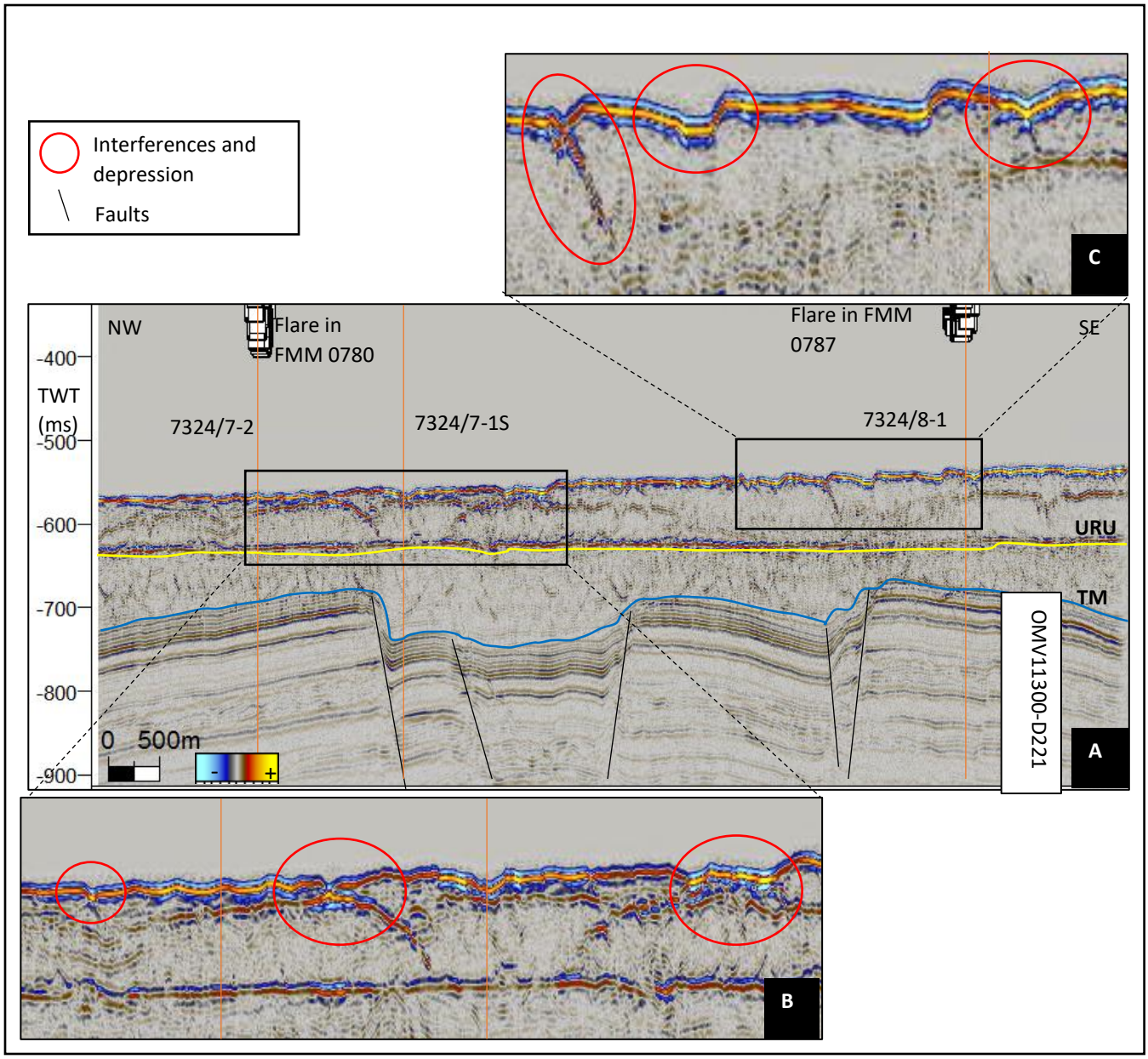


*Figure 5.18 A. 2D line OMV11300-D221 showing the flares in FMM line 0780 and 0787 and their correlated subsurface seismic; B, C. interferences and depressions on the seabed at the flares' locations.*

The flare in FMM line 0790 also locates at a well location, which is well 7324/8-2. The well was to primarily prove hydrocarbon in Middle Jurassic to Late Triassic Upper Realgrunnen Subgroup. Middle Jurassic Sto FM was determined at 668m depth and the well resulted in being dry. Correlated subsurface seismic of the flare in FMM line 0890, using 2D line NBR08-147482 (Figure 5.19), does not show high amplitude anomalies in shallow subsurface. A couple of

depressions on the seabed were observed, with potentially weak connection to deeper faulting. Fault indicators from a moving-up structure of strata below the TM horizon, at -750 to -800ms TWT. The strata, which were determined to be Sto FM, are heavily affected by fractures.

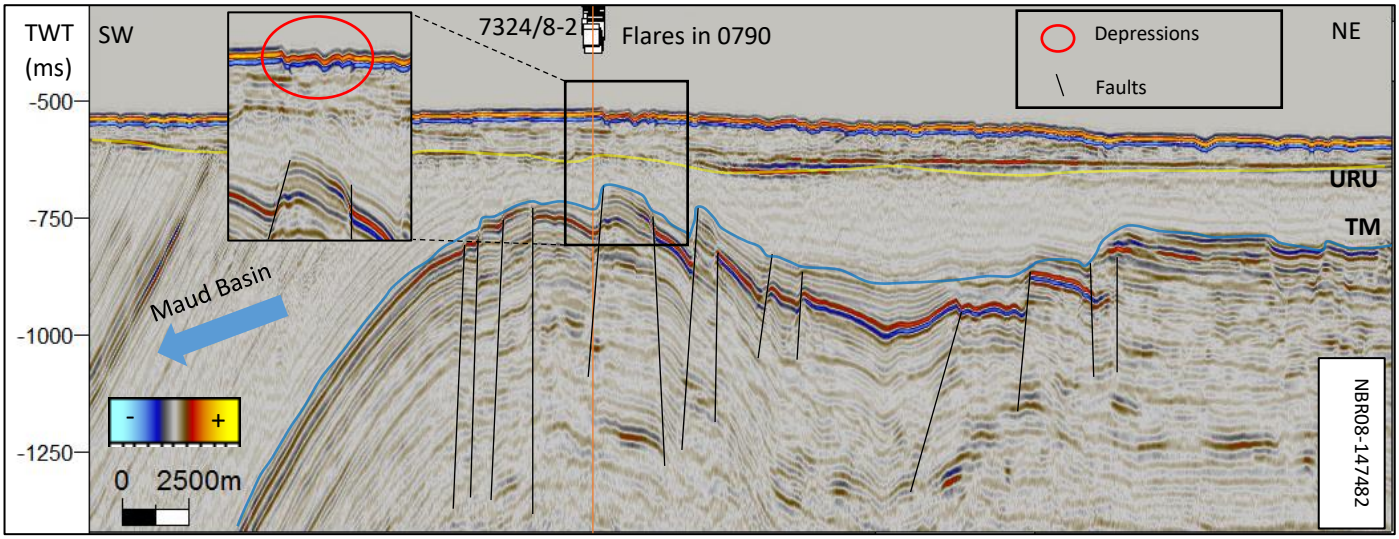


*Figure 5.19 2D line NBR08-147482 showing the flare in FMM line 0790 and its seismic profile. Slight interferences on the seabed at the flare location is observed (red circle). Strata below the TM horizon are heavily affected by faulting.*

# 6 DISCUSSION

The gas flares found in the study area are closely related to the location of petroleum fields/discoveries along the cruise line. each site of known hydrocarbon reservoirs encountered by cruise line provides at least one gas flare that can be observed in the WCI. After correlation with subsurface seismic data and regional geological data, three possible causes of the fluid leakage to the water column are proposed: (1) gas leakage due to petroleum activities, (2) the impacts of faulting/fracturing in the Barents Sea that opens up potential migration pathways and their connection with (3) historical uplift and erosion that lead to shallow fluid accumulations.

## 6.1 Source of the hydrocarbon flow

The petroleum source rocks in the south Barents Sea locate at stratigraphic levels from Carboniferous to the Cretaceous, in which the Hekkingen Formation (Upper Jurassic) is considered the most successful source rock. Wells that are used in this thesis is summarized in Table 3 with general information and the oldest penetrations, according to data from NPD.no, the Late Triassic – Early Jurassic Realgrunnen subgroup is the main reservoir. This setup draws a distinct petroleum layout in the south Barents Sea where the Hekkingen Formation source rocks overlaying the sand intervals of the Realgrunnen subgroup. The Hekkingen Formation might have matured prior to Cenozoic uplift and erosion, while deeper/older Triassic and Permian/Carboniferous source rocks are over the oil window or overmature (Argentino et al., 2021). Therefore, gas leakages in the area are suggested to be from the thermogenic source, mature hydrocarbon in deep source rocks may leak through faulting, fracture and/or drilling activities. Additionally, isotopic composition analysis of core samples from Leirdjupet Fault Complex, SW Barents Sea showed parts of biogenic origin of gas, along with the predominant content of thermogenic origin of gas, with secondary petroleum biodegradation to be ruled out (Argentino et al., 2021).

Apart from the apparent thermogenic gas from the working petroleum systems in the Barents Sea, microbial activities in shallow sediments that generate methane are also a source of gas. Moreover, because the microbial gas generation happens in such shallow sediments, it is more concerning that the gas would easily exit to the seafloor through soft, clastic and non-stratified sediments.

**Table 3. Hydrocarbon wells used to assess the gas flares**

| No. | Well | Discovery-Geology element | Water depth (m) | Content | Oldest penetration |
|---|---|---|---|---|---|
| 1 | 7122/7-1 (Goliat) | Goliat | 381 | Oil | Triassic Snadd Formation |
| 2 | 7122/7-6 | | 380 | Oil/Gas | Early Triassic Klappmyss Formation |
| 3 | 7222/11-1 (Caurus) | Caurus | 356 | Oil/Gas | Mid Triassic Kobbe Formation |
| 4 | 7222/11-2 (Langlitinden) | Langlitinden | 338 | Oil | Early Triassic Klappmyss Formation |
| 5 | 7224/7-1 (Samson Dome) | Samson Dome | 269 | Shows | Early Triassic Harvert Formation |
| 6 | 7225/3-1 | Norvarg | 377 | Gas | Permian Isbjorn Formation |
| 7 | 7225/3-2 | | 381 | Gas | Triassic Klappmyss Formation |
| 8 | 7226/2-1 (Ververis) | Ververis | 347 | Gas | Early Triassic Harvert Formation |
| 9 | 7324/7-2 (Hanssen) | Hanssen | 417.5 | Oil | Mid Triassic Snadd Formation |
| 10 | 7324/8-1 (Wisting) | Wisting | 398 | Oil | Late Triassic Snadd Formation |
| 11 | 7324/8-2 | | 394 | Dry with shows | Mid Triassic Snadd Formation |

## 6.2 Gas leaks related to petroleum activities

A publication from Böttner et al., 2020 assessed gas emission from offshore decommissioned hydrocarbon wells in the UK sector of the North Sea established some insights of how hydrocarbon wells may impact the leaking potential in regards of petroleum-prone area ("Greenhouse gas emissions from marine decommissioned hydrocarbon wells: leakage detection, monitoring and mitigation strategies" by Böttner et al., 2020). The source of the gas leaks in the paper is determined to root from both thermally matured fluids in the deep organic-rich source rocks and shallow gas accumulations (A Judd et al., 1997). The same scheme can be applied for the study area, the south of Barents Sea. As stated in chapter 5.1, the study area has prolific source levels from Carboniferous to Cretaceous, with the Upper Jurassic Hekkingen Formation standing out as the most successful source rock in the Barents Sea. Shallow gas accumulations in the study area

can be correlated to over the URU level, where numbers of reversed polarity seismic anomalies are spotted as shown in the Result chapter.

Results from Böttner et al., 2020 show 2 mechanisms that control the well-related fluid migration:

(i) Fluids migrate through "well-induced fractures surrounding the well path" (Böttner et al., 2020), the fractures will open anthropogenic routes through rock permeability or well barriers, therefore, form hydraulic connection between strata and the seabed (Aydin, 2000).

(ii) Leakages through "well integrity issues", in which fluids migrate through faulty, damaged or corroded well casings and/or annuli. The errors when cementing and casing wells may connect formation and casing, thus cause the leakage over the time (Böttner et al., 2020).

Well-induced fractures are focused on the shallow sediment. As concluded in the publication, gas migration in 1000m below the seabed is likely to be impacted by the well drilling procedure. Moreover, the paper showed that geological background conditions are also crucial, specifically, the distance from an indicated well to potential shallow gas accumulations matters. Statistic results from Böttner et al., 2020 show that if there is any shallow accumulation/seismic anomaly within a radius of 300m from the well, the leakage possibility is 100%, while the radius of 300-1000m from the well generates 44% chance of leakage and if the accumulations are further than 1000m from the well, the leakage is not likely (0%). Fractures opening by wells mechanically depressurize overburden and increase permeability in regards of vicinity rocks, hence promote fluid migration. The process of vertical fluid migration is up to 10 times more intensive in areas where pre-existing fluid-concentrated elements present, such as gas chimneys, pipe structures (Böttner et al., 2020).

Petroleum wells that are included in this thesis mainly penetrated hydrocarbon-potential strata and the main subsurface targets to examine in this thesis are shallow sediments. Therefore, the impacts of wells in hydrocarbon leakage in the study area is apparent.

The wells in Figure 5.3 at the Goliat field penetrated the proven sandstone reservoirs, thus might cause potential leakage along the wellpath. As shown in the figure, evidence of seismic attenuations and acoustic masking are spotted along the wells position and just at the flare location,

although there are not many clear seismic accumulations observed. Gas leakage to the seabed might occur from the penetration of hydrocarbon - rich reservoirs in relatively shallow depth (about -700ms TWT) and escape to the surface through well-induced fractures.

In the Caurus/Langlitinden area, both the 2 well mentioned in Figure 5.7 directly encounter or is located close to bright spots and the flares are also observed just at the well positions. The well 7222/11-1 contacted 2 large reversed - polarity seismic accumulations at -500ms and -800ms TWT, while the well 7222/11-2 is located roughly 600m to the SW of a small bright spot that causes acoustic masking. The gas flares available at the well locations might support the conclusion by Böttner et al., 2020 that hydrocarbon leakages within 1000m below the seabed are attached to well-induced fractures for fluid accumulations within 1000m radius from the well.

On the other hand, well 7224/7-1 at Samson Dome and well 7226/2-1 at Ververis do not give any evidence of well-related seepages. At Samson Dome (Figure 5.11C), the gas flares are at an immense area of high RMS amplitudes, however, none of the flares are related to the well 7224/7-1 since it distances roughly 900m to a minor bright spot and too far away from the other considerable accumulations. Similarly, at Ververis (Figure 5.15A), there is not a significant accumulation close to the well 7226/2-1 and no indicator of signal attenuations along the wellpath, hence the gas flare in this location is not related to well drilling. The gas flares at Samson Dome and Ververis are rather due to fluids escaping through shallow minor faults and uncompact, soft sediments, which will be discussed further.

## 6.3 The impacts of faulting/fracturing

The South Barents Sea has gone through series of geological events along its history. As stated in Chapter 2, the geological background in the study area includes the extensive process consisting of orogeny, seafloor expanding, uplifts/erosions and episodes of glaciation. All the indicated rock-mass movements create faults/fractures in the in-place rocks, and due to varying timing of the geological events in the Barents Sea, the area's fault system was thus active, inactive and reactivated accordingly. Faults can characterize as either conduits or barriers for fluids migration depending on the properties of the fault. Shearing and fracturing can increase porosity, permeability and promote fluids migration. On the other hand, diagenesis, mineralization crystallization,… that is related to faults can seal the permeability contacts and become subsurface fluid barriers (Ferrill & Morris, 2001; Yielding et al., 1997). Additionally, to the case in the study

area, severe uplift and erosion removed the overburden pressure, which results in gas expansion and oil flush to the fault zones. This mechanism of re-migration and leakage is also a key process in the south Barents Sea.

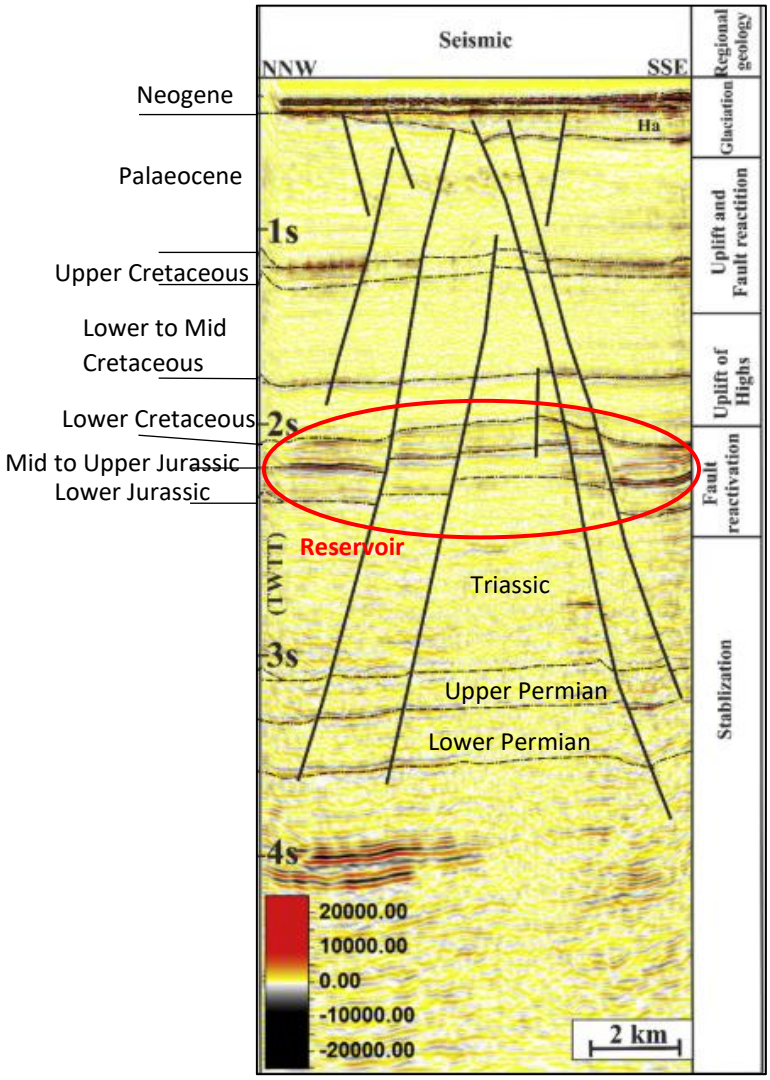


*Figure 6.1 Interpreted major stratigraphic tops and summarized tectonic history at the Snohvit field, showing the timing of the fault reactivation and uplift at the reservoir levels and at glaciation time. Retrieved and modified from Mohammedyasin et al, 2016 and Ostanin et al., 2013.*

Formations below the reference the TM horizon in Figure 5.6A at the Caurus/Langlitinden discovery are heavily impacted by deep faults, seismic anomalies are also observed near or on the faults. Those anomalies are polarity-reversed to the seabed's reflection hence they can be assumed to be hydrocarbon-related accumulations. This is an indication that these faults might be leaking.

A publication discussing hydrocarbon leakage by Mohammedyasin et al., 2016 proved the fault reactivation mechanisms in the Hammerfest Basin as well as fluid migration phases, whose results can be used to correlate with the case at Caurus/Langlitinden. The deep faults in Figure 5.6A and Figure 5.7 can be the result of the Late Jurassic – Early Cretaceous fault reactivation in the Hammerfest Basin, followed by Early Paleocene faulting and subsequent uplift and erosion (Figure 6.1). The fault reactivations may connect faults at different levels by the dip linkage and open migration pathways for fluids. The paper also concluded two fluid migration phases during Late Jurassic and Late Cretaceous – Paleocence times (Mohammedyasin et al., 2016), therefore, fluids at Caurus/Langlitinden might have migrated into the accumulations (seismic anomalies) prior to the Paleocene uplift and erosion.

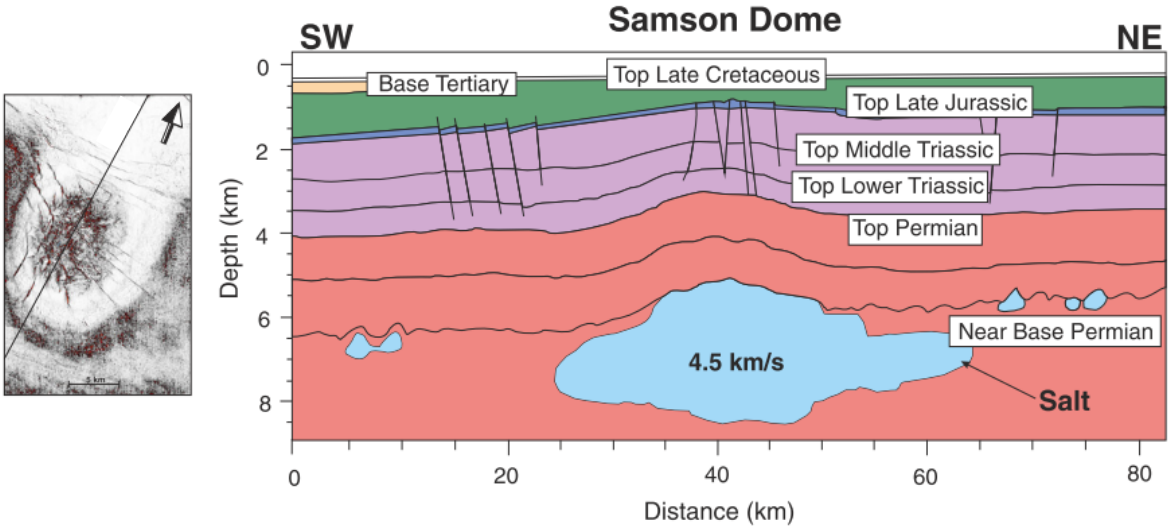


*Figure 6.2 An interpreted model of the Samson salt body and the surrounding strata. Open faults/fractures were opened by the salt tectonics during the process and subsequent uplift/erosion in the area. Retrieved from Mattos et al., 2016, which is modified from Breivik et al., 1995.*

The faulting/fracturing in domal areas, specifically at Samson and Norvarg Dome within the study area is well related to halokinesis (salt tectonics) that offsets overlaying strata and open faults/factures. A simplified model of the salt at the Samson Dome and open fractures in the area is shown in Figure 6.2. The halokinesis of the Samson Dome will be discussed more in chapter 6.4. Shortly, the salt tectonics of the Samson Dome includes series of salt development resulting in forming an open anticline, salt dissolution and a collapse of the dome. The process created faults in the uppermost Mesozoic strata in the area, including petroleum-prolific plays such as the Sto,

Nordmela and Tubaen Formations (Mattos et al., 2016), hence promotes petroleum secondary migrations in this area. Subsequently, under the effect of uplift and erosion, parts of the fluids continued migrating and accumulating over the URU horizon as shown in Figure 5.11B, C and Figure 5.14. The fluids may then migrate and leak towards the surface through shallow open faults in agreement with a similar migration pattern in the Loppa High (Chand et al., 2012) or the fluids moved into shallow sediments and leaked towards the surface through polygonal faults like in the Hammerfest Basin (Ostanin et al., 2012).

## 6.4 The impacts of uplift and erosion

Uplift and erosion is one of the distinct characteristics in the Barents Sea, as stated and summarized by Lasabuda et al., 2021, net erosion of the Hammerfest Basin is about 1500, while the number in Loppa High and Bjarmeland Platform is roughly 2000m. The removal of ~1500m of ice after the last glacial period and the indicated net sediment erosion significantly decreased the overburden stresses, hence lowered the Temperature – Pressure conditions of the reservoir, which results in the expansion of existing reservoir gas cap and subsequently building up overpressure conditions in the reservoir, leading to fluids spill out of the closure (Ostanin et al., 2017). Additionally, the erosion event would create unconformity traps over the URU surface for fluids to migrate into. Well data in the study area show that most of the Paleogene sediments are absent from the profile due to erosion and along the URU horizon, indicators of fluid accumulations (gathered reversed-polarity seismic amplitude anomalies) are also observed. Therefore, there is high chance hydrocarbon fluids would escape towards the seabed through pore space in shallow, uncompact sediments or through shallow faults.

Data from well 7222/11-2 (Langlitinden), 7224/7-1 (Samson Dome), 7226/2-1 (Ververis), 7324/7-2 (Hanssen) and 7324/8-1 (Wisting) reveal the absence of Paleogene Sotbakken Group sediments. The URU horizon, which is the erosional bottom of multiple glacial events, marks the start of Mesozoic sediments, Late Cretaceous Adventdalen Group particularly. Indicators of pockmarks on the seabed and along the URU horizons are also present. According to a study in Loppa High, the simultaneous presence of non-active pockmarks and active gas flares may propose two fluid migration processes after the glacial retreat: (1) the release of methane hydrates when the seabed temperature increased, which amplifies the making of pockmarks and (2) gas escaping

from open faults/fractures, which were caused by glacial isostatic adjustment during the last Ice age (Chand et al., 2012).

One remarkable feature to demonstrate the pockmarks is from the "deformed region" on the seabed in Caurus/Langlitinden discovery in the Loppa High (Figure 5.6A). The depressions on the region's seabed are possibly pockmarks that are connected to amplitude anomalies over the reference the TM horizon and the URU horizon. The reversed - polarity to the seabed signals of the anomalies suggests that those are hydrocarbon accumulations over the URU surface, which root from Mesozoic sediments (below the TM horizon) and migrate along deep faults. The pockmarks and gas seepage in Figure 5.6A may root from fluid flows from the shallow gas accumulations which are only 60-65ms below the seabed, suggesting that there potentially is a working fluid flow in the area, either through shallow faults or through sediment pore space.

The uplift – erosion impacts the domal structures in the Bjarmeland Platform (Samson and Norvarg Dome) in a similar way, and since they possess a similar evolutional history, Samson Dome is described as a representative. Seismic profile in Samson Dome reveals potential pockmark indicators on the seabed and over the URU horizon, just at the flare location. Exceptionally, possible pockmarks over the URU horizon in this area are closely connected to high amplitude accumulations in shallower sediments. This might be a sign of an on-going fluid system that is gradually transporting gas from source rocks to the seabed seepages, as shown by gas flares in the area. The evolution and fluid migration potential of the Samson Dome was well studied by Mattos et al., 2016, the dome initiated its halokinesis during Late Mesozoic, progressing to following salt growth cessation, salt dissolution, domal collapse and post-salt sediment loading. Subsequently, the dome went through Late Cretaceous – Paleogene uplift - erosion. The fluid migration in the Samson Dome was suggested by authors to be the reduction in overburden stresses resulted from the erosion of Upper Cretaceous units, which leaked fluids towards the surface and fluids migrating through faults in shallow sediments to reach the seabed (as in Figure 6.2). Moreover, the area was concluded to have a "likelihood of failure seal" derived from leakage factor calculations, which leads to more possibility for fluid leakages (Mattos et al., 2016).

## 6.5 Wisting/Hanssen discovery, the anomaly in the Barents Sea

Wisting discovery and its sub-structure Hanssen at the Hoop Fault Complex stands an exceptional case in petroleum exploration in the Barents Sea. The Wisting discovery is an ultra-

shallow structure with thin overburden sealing lithology, the discovery has reservoir of highly segmented and containing oil in sandstones of the Fruholmen, Nordmela and Sto Formations (NPD(g), 2018). Although the Wisting petroleum system has been proven work, its relatively shallow depth of 250m from the seabed is considered risks of leaking. The faults below reference the TM horizon in Figure 5.18A and Figure 5.19 may have made ways for petroleum secondary migration in the system, for hydrocarbon from the Upper Jurassic Hekkingen Formation source rock to migrate into the indicated reservoir sandstones. Since the petroleum system is too shallow in terms of usual required overburden pressure, the Wisting discovery's retention is still considered a major risk. However, recent wells have proven the thin overburden shales at Wisting have capacity to seal both oil and gas in numbers of structures (Aatisha Mahajan et al., 2014).

A study in caprock capability by Hansen et al., 2020 determined from well 7234/8-1(Wisting) that the caprock section here is soft, clay-rich, little silty, little brittle, therefore little fracture-prone. The authors concluded that the Upper Jurassic seal at Wisting is able to retain significant oil column, additionally, clay-dominated Lower Cretaceous strata also acts as a secondary seal for the structure. Moreover, uplift-generated fracturing to cause hydrocarbon leakage was concluded unlikely since intermediate gas accumulations were discovered in areas with high net erosion (~2km). The leakage risk at Wisting was assumed to be leakage through potential conductive faults in-place rather than the caprock risk (Hansen et al., 2020).

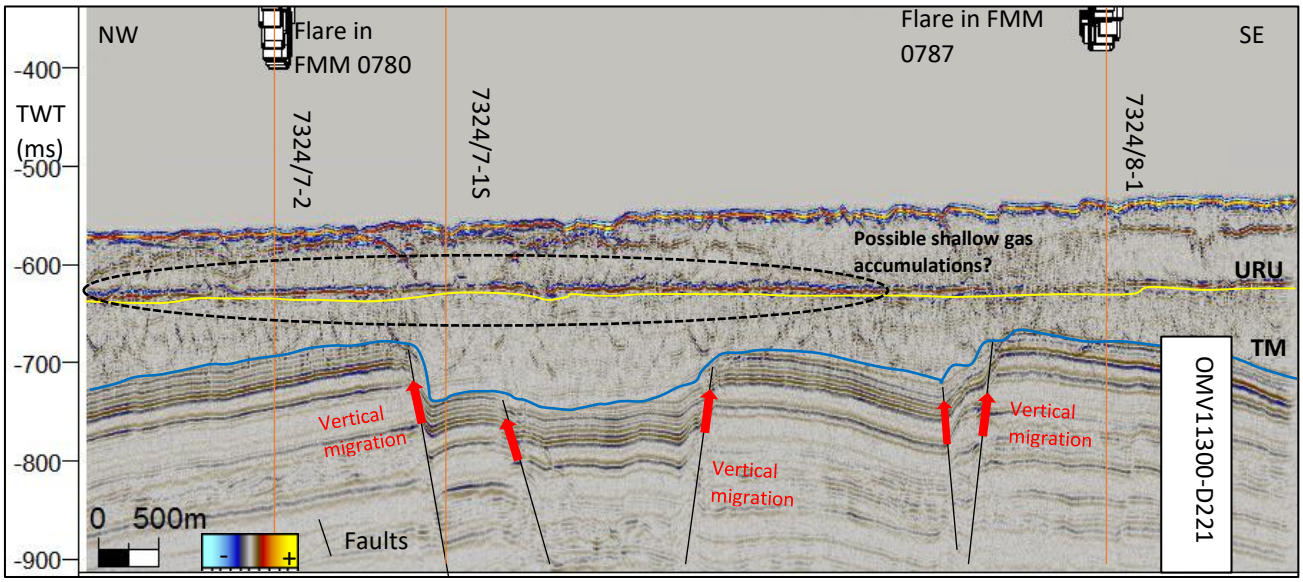


*Figure 6.3 Petroleum system of the Wisting Discovery showing potential vertical migration from inductive faults (red arrows). The migration might reach the URU horizon and accumulate over the URU.*

Discarding the sealing risk in the Wisting discovery, the gas seepages in the area are suggested to root from shallow sediments, which are above the URU horizon in Figure 5.18A. Numbers of amplitude anomalies and seabed depressions are of observed at the gas flare locations. The reflections over the URU are not anomalously high and gathered to be considered fluid accumulations, however, seabed reflections in Figure 5.18B, C show the depressions on the seabed that may act as the connection to the URU horizon. The depressions appear to be pockmarks, ploughmarks or seabed furrows suggesting that there is a fluid migration system over the URU horizon. Since hydrocarbon leakage from pre-Paleocene sediments has been proved unlikely, the fluid might come from yet-to-know sources in surrounding areas.

Considering well-induced fracturing that may cause hydrocarbon leakages, seismic signals along the 7324/7-2, 7324/81 and 7324/8-2 wellpaths are not attenuated or disturbed. There are no significantly high amplitude accumulations close to those wells, yet the gas flares appear right at the well positions. This scenario enforces the suggestion of a fluid flow over the URU horizon and when the wells penetrate such shallow flow, leaking is inevitable.

To sum up the thesis, a model by Mattingsdal & Knutsen, 2021 is used to illustrate the relation between geology and the gas flares (natural and anthropogenic) (Figure 6.4). Tectonic movements and uplifts create faults that open migration pathways from reservoir intervals to upper

formations. Under the effects of uplift/erosion and repeated glaciation in the Cenozoic reactivated the faulting systems and created a shallow unconformity surface (the URU) which is a good place with good conditions to form shallow gas accumulations. The fault reactivation and removal of overburden pressure (by erosion) enhances the fluid migration into the shallow accumulations, the fluid then naturally escape towards the seabed through young faults or directly through pore space in shallow sediments. Whereas, for the gas flares that are related to well drilling activities, leakages through well-induced fractures along the wells happen if they encounter the shallow accumulations. However, according to Mattingsdal & Knutsen, 2021, it is still uncertain about the relationship between the natural gas flares and well-related gas flares. A remaining question is that whether the wells triggered the leakages or the leakages have been already there and the wells just amplify the leakages (Mattingsdal & Knutsen, 2021). Further study will be needed to thoroughly understand the case to better assess the gas leaking process.

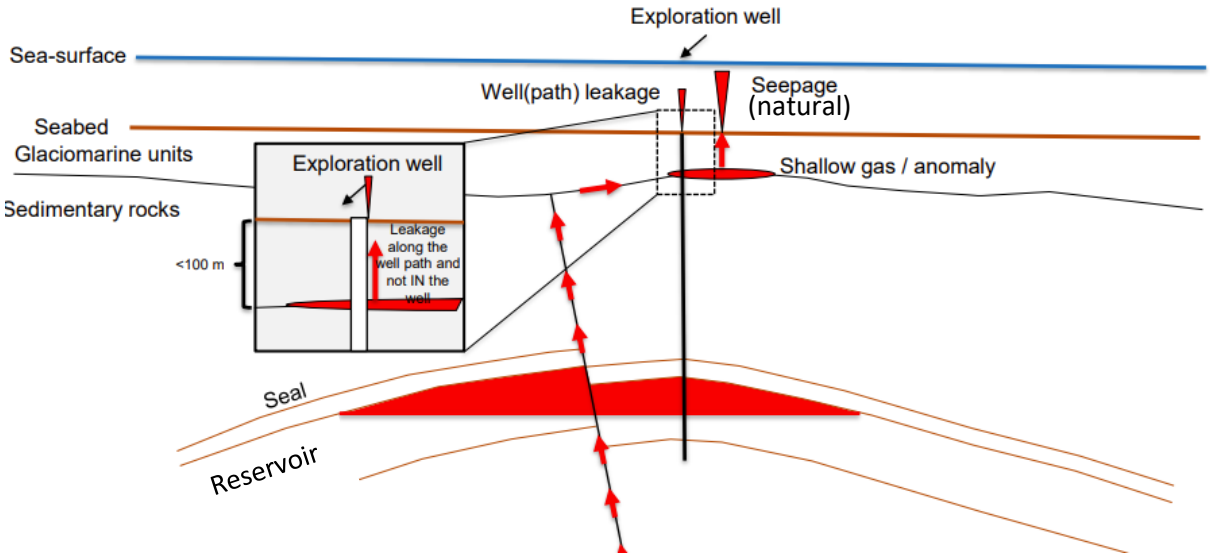


*Figure 6.4 Natural and Wellpath leakage model. Modified from Mattingsdal & Knutsen, 2021.*

# 7 CONCLUSION

The thesis used Water Column Imaging (WCI) from the Cruise line 20-2 from CAGE to detect gas flares over known hydrocarbon discoveries and along the cruise line. The gas flare data was then correlated with subsurface seismic data, well data and regional literature data to find out how geology impacts the gas flares in the water column.

- The study location is in a hydrocarbon-prone area and the cruise line crossed the known hydrocarbon discoveries, gas flares are found over most of the structures.
- The source of the gas flares may be from both thermogenic origin from deep, mature source rocks (for example the Hekkingen Formation) and biogenic origin from microbial activities in shallow hydrocarbon-rich sediments.
- The geological processes in the study area (south of Barents Sea) includes series of faulting and uplift/erosion, which are the most important factors that govern the fluid leakage in the area. Tectonic processes open faults in deep prolific source rocks promoting secondary migration and occasional fault activation cause possible fluid leakages in different intervals. Whereas uplift/erosion and glaciation in the Barents Sea created shallow fluid accumulations over the URU surface. Fluids may escape from such accumulations, through young, shallow faults or directly through sediment pore space.
- In the Late Mesozoic and older strata (below the TM horizon), where most of the known petroleum systems locate, faulting plays a role in making ways for secondary migration of fluids into reservoir, and potentially leakages towards younger sediments due to sealing integrity problems.
- For young sediments (Paleocene and younger), the effects of uplift-erosion and glaciation predominates. The indicated processes removed as much as 2km of sediments, which in turn reduce the overburden pressure, causing the reservoir fluids to expand and escape. Fluid leakages in shallow sediments are mostly through minor faults/fractures and/or directly through the pore space.
- Hydrocarbon wells may cause leakage through well-induced fractures along the wellpath. If there is a shallow accumulation/seismic anomaly within the 300 – 1000m radius of a well, it is likely to leak through the well.
- The gas flares at Wisting/Hanssen raise a question where the fluid flow in the area could come from. Since the sealing risk of the main petroleum system is excluded, understanding the fluid flow origin over the URU is necessary for future development of the discovery to enhance the prospecting confidence and minimize the leaking risk.

# 8 REFERENCES


Argentino, C., Waghorn, K. A., Vadakkepuliyambatta, S., Polteau, S., Bünz, S., & Panieri, G. (2021). Dynamic and history of methane seepage in the SW Barents Sea: new insights from Leirdjupet Fault Complex. *Scientific Reports*, *11*(1), 1–13. https://doi.org/10.1038/s41598-021-83542-0

Aydin, A. (2000). Fractures, faults, and hydrocarbon entrapment, migration and flow. *Marine and Petroleum Geology*, *17*(7), 797–814. https://doi.org/10.1016/S0264-8172(00)00020-9

Berglund, L. T., Augustson, G., Færseth, R., & Ramberg-Moe, H. (1986). The evolution of the Hammerfest Basin. *Habitat of Hydrocarbons on the Norwegian Continental Shelf, January 1986*, 319–338.

Böttner, C., Haeckel, M., Schmidt, M., Berndt, C., Vielstädte, L., Kutsch, J. A., Karstens, J., & Weiß, T. (2020). Greenhouse gas emissions from marine decommissioned hydrocarbon wells: leakage detection, monitoring and mitigation strategies. *International Journal of Greenhouse Gas Control*, *100*(July), 103119. https://doi.org/10.1016/j.ijggc.2020.103119

Breivik, A. J., Gudlaugsson, S. T., & Faleide, J. I. (1995). Ottar Basin, SW Barents Sea: a major Upper Palaeozoic rift basin containing large volumes of deeply buried salt. *Basin Research*, *7*(4), 299–312. https://doi.org/https://doi.org/10.1111/j.1365-2117.1995.tb00119.x

CAGE. (2020). Hunting gas flares in Hopendjupet and glacial sediments in Sentralbankrenna. In *CAGE Cruise report*.

Chand, S., Thorsnes, T., Rise, L., Brunstad, H., Stoddart, D., Bøe, R., Lågstad, P., & Svolsbru, T. (2012). Multiple episodes of fl uid fl ow in the SW Barents Sea ( Loppa High ) evidenced by gas fl ares , pockmarks and gas hydrate accumulation. *Earth and Planetary Science Letters*, *331–332*, 305–314. https://doi.org/10.1016/j.epsl.2012.03.021

Ciais, P., Sabine, C., Bala, G., Bopp, L., Brovkin, V., Canadell, J., Chhabra, A., DeFries, R., Galloway, J., Heimann, M., Jones, C., Quéré, C. Le, Myneni, R. B., Piao, S., & Thornton, P. (2013). The physical science basis. Contribution of working group I to the fifth assessment report of the intergovernmental panel on climate change. *IPCC Climate Change*, 465–570. https://doi.org/10.1017/CBO9781107415324.015

Crutzen, P. J. (1991). Methane ' s sinks and sources. *Nature*, 380–381.

Etiope, G. (2015). Natural Gas Seepage - The Earth's Hydrocarbon Degassing. In *Natural Gas Seepage*. https://doi.org/10.1007/978-3-319-14601-0_2

European Environment Agency. (1999). *Environment in the European Union at the turn of the century-3.1. Greenhouse gases and climate change*. 79–98.

Ferrill, D. A., & Morris, A. P. (2001). Displacement gradient and deformation in normal fault systems. *Journal of Structural Geology*, *23*(4), 619–638. https://doi.org/10.1016/S0191-8141(00)00139-5

Gabrielsen, R. H., Faerseth, R. B., & Jensen, L. N. (1990). Structural elements of the Norwegian continental shelf. Pt. 1. The Barents Sea region. *Norwegian Petroleum Directorate*.

Gentz, T., Damm, E., Schneider von Deimling, J., Mau, S., McGinnis, D. F., & Schlüter, M. (2014). A water column study of methane around gas flares located at the West Spitsbergen continental margin. *Continental Shelf Research*, *72*, 107–118. https://doi.org/10.1016/j.csr.2013.07.013

Gudlaugsson, S. T., Faleide, J. I., Johansen, S. E., & Breivik, A. J. (1998). Late Palaeozoic structural developments of the south-western Barents Sea. *Marine and Petroleum Geology*, *15*(1), 73–102. https://doi.org/10.1016/S0264-8172(97)00048-2

Hansen, J. A., Mondol, N. H., Tsikalas, F., & Faleide, J. I. (2020). Caprock characterization of Upper Jurassic organic-rich shales using acoustic properties, Norwegian Continental Shelf. *Marine and Petroleum Geology*, *121*(July). https://doi.org/10.1016/j.marpetgeo.2020.104603

Hjelmervik, K., Hjelmervik, K. T., & Ostenstad, P. (2015). Estimation of oceanographic profiles and climatological regions in the Barents Sea. *MTS/IEEE OCEANS 2015 - Genova: Discovering Sustainable Ocean Energy for a New World, June 2016*. https://doi.org/10.1109/OCEANS-Genova.2015.7271512

Hunt, J. M. (1996). *Petroleum geochemistry and geology*. W.H. Freeman and Co.

IEA. (2005). *A Review of Natural Co2 Occurrences and Releases and Their Relevance To Co2 Storage*.

Judd, A, Davies, G., Wilson, J., Holmes, R., Baron, G., & Bryden, I. (1997). Erratum : Contributions to atmospheric methane by natural seepages on the U.K continental shelf [Mar. Geol. 137 (1997) p165-189]. *Marine Geology*, *Vol. 140*(96), 427–455.

Judd, Alan. (2000). Geological sources of methane. In *Atmospheric methane: its role in the global environment* (pp. 280–303). Springer-Verlag.

Judd, Alan, & Hovland, M. (2007). *Seabed fluid flow: impact on geology, biology and the marine environment*. Cambridge University Press. https://doi.org/doi.org/10.1017/CBO9780511535918.009

Koson, S., Chenrai, P., & Choowong, M. (2014). Seismic Attributes and Their Applications in Seismic Geomorphology. *Bulletin of Earth Sciences of Thailand*, *6*(1), 1–9. file:///E:/copied%0Afrom%0AD/endnote%0Alibrary%0Adocuents%0Afor%0Apublication/Seismic%0AAttributes%0Aand%0ATheir%0AApplications%0Ain.pdf

Kvenvolden, K. A., Lorenson, T. D., & Reeburgh, W. S. (2001). Attention turns to naturally occurring methane seepage. *Eos*, *82*(40), 457. https://doi.org/10.1029/01EO00275

Lasabuda, A. P. E., Johansen, N. S., Laberg, J. S., Faleide, J. I., Senger, K., Rydningen, T. A., Patton, H., Knutsen, S. M., & Hanssen, A. (2021). Cenozoic uplift and erosion of the Norwegian Barents Shelf – A review. *Earth-Science Reviews*, *217*(March), 103609. https://doi.org/10.1016/j.earscirev.2021.103609

Leifer, I., Luyendyk, B. P., Boles, J., & Clark, J. F. (2006). Natural marine seepage blowout: Contribution to atmospheric methane. *Global Biogeochemical Cycles*, *20*(3), 1–9. https://doi.org/10.1029/2005GB002668

Link, W. K. (1952). Significance of oil and gas seeps in world oil exploration. *AAPG Bulletin*, *36*(8), 1505–1540. https://doi.org/doi.org/10.1306/5CEADB3F-16BB-11D7-8645000102C1865D

Mahajan, A., , Gabrielsen, R. H., & , Faleide, J. . (2014). Structural analysis of 3D seismic for Hoop Fault Complex, SW Barents Sea. In *NGF Abstracts and Proceedings* (Vol. 2).

Mahajan, Aatisha, Gabrielsen, R., & Faleide, J. I. (2014). *Structural Evolution using 3D Seismic of Hoop Fault Complex, SW Barents Sea Norway* (Issue February 2015). https://doi.org/10.13140/2.1.2390.0968

Mattingsdal, R., & Knutsen, S. (2021). The chicken and the egg : The relation between leakage from hydrocarbon wells and natural sea-bed seeps. *Presentation at Norwegian FORCE. June 11th 2021*.

Mattos, N. H., Alves, T. M., & Omosanya, K. O. (2016). Crestal fault geometries reveal late halokinesis and collapse of the Samson Dome, Northern Norway: Implications for petroleum systems in the Barents Sea. *Tectonophysics*, *690*, 76–96. https://doi.org/10.1016/j.tecto.2016.04.043

McGinnis, D. F., Greinert, J., Artemov, Y., Beaubien, S. E., & Wüest, A. (2006). Fate of rising methane bubbles in stratified waters: How much methane reaches the atmosphere? *Journal of Geophysical Research: Oceans*, *111*(9), 1–15. https://doi.org/10.1029/2005JC003183

Mitrovica, J. X., & Vermeersen, B. L. A. (2002). Glacial Isostatic Adjustment and the Earth System. In *Ice Sheets, Sea Level and the Dynamic Earth (eds J.X. Mitrovica and B.L. Vermeersen)* (pp. 1–2). https://doi.org/https://doi.org/10.1002/9781118670101.ch1

Moen, J.-E. K. (2020). *Gas migration and sealing modelling in the Haapet Dome area, Norwegian Barents Sea – analysis of seismic anomalies and water column data*. The Arctic University of Norway.

Mohammedyasin, S. M., Lippard, S. J., Omosanya, K. O., Johansen, S. E., & Harishidayat, D. (2016). Deep-seated faults and hydrocarbon leakage in the Snøhvit Gas Field, Hammerfest Basin, Southwestern Barents Sea. *Marine and Petroleum Geology*, *77*, 160–178. https://doi.org/10.1016/j.marpetgeo.2016.06.011

Müller, R., Klausen, T. G., Faleide, J. I., Olaussen, S., Eide, C. H., & Suslova, A. (2019). Linking regional unconformities in the Barents Sea to compression-induced forebulge uplift at the Triassic-Jurassic transition. *Tectonophysics*, *765*(March), 35–51. https://doi.org/10.1016/j.tecto.2019.04.006

NPD(a). (2014). *Geology of the Barents Sea*. https://www.npd.no/en/facts/publications/co2-atlases/co2-atlas-for-the-norwegian-continental-shelf/6-the-barents-sea/6.1-geology-of-the-barents-sea/#

NPD(b). (2014). *The Sassendalen Group*. https://www.npd.no/en/facts/publications/co2-atlases/co2-atlas-for-the-norwegian-continental-shelf/6-the-barents-sea/6.1-geology-of-the-barents-sea/the-sassendalen-group/

NPD(c). (2014). *The Kapp Toscana Group*. https://www.npd.no/en/facts/publications/co2-atlases/co2-atlas-for-the-norwegian-continental-shelf/6-the-barents-sea/6.1-geology-of-the-barents-sea/the-kapp-toscana-group/

NPD(d). (2014). *The Adventdalen Group*. https://www.npd.no/en/facts/publications/co2-atlases/co2-atlas-for-the-norwegian-continental-shelf/6-the-barents-sea/6.1-geology-of-the-barents-sea/the-adventdalen-group/

NPD(e). (2014). *Sotbakken Group*. https://factpages.npd.no/en/strat/PageView/Litho/Groups/154

NPD(f). (2014). *Nordland Group*. https://factpages.npd.no/en/strat/PageView/Litho/Groups/113

NPD(g). (2018). *Wisting*. https://factpages.npd.no/en/discovery/pageview/all/23761893

Ostanin, I., Anka, Z., & Di Primio, R. (2017). Role of faults in hydrocarbon leakage in the hammerfest basin, SW barents sea: Insights from seismic data and numerical modelling. *Geosciences (Switzerland)*, *7*(2), 1–29. https://doi.org/10.3390/geosciences7020028

Ostanin, I., Anka, Z., di Primio, R., & Bernal, A. . (2012). Hydrocarbon leakage above the Snøhvit Gas

Field, Hammerfest Basin SW Barents Sea. *First Break*, *30*, 55–60. https://doi.org/10.3997/1365-2397.2012018

R.H. Gabrielsen, I. Grunnaleite, & S. Ottesen. (1993). Reactivation of fault complexes in the Loppa High area, southwestern Barents Sea. *Elsevier*, *2*, 631–641. https://doi.org/https://doi.org/10.1016/B978-0-444-88943-0.50041-1

Richard C. Selley, & Stephen A. Sonnenberg. (2015). Chapter 5 - Generation and Migration of Petroleum. In Richard C. Selley & Stephen A. Sonnenberg (Eds.), *Elements of Petroleum Geology (Third Edition)* (pp. 191–253). Academic Press. https://doi.org/https://doi.org/10.1016/B978-0-12-386031-6.00005-9

Sayago, J., Di Lucia, M., Mutti, M., Sitta, A., Cotti, A., & Frijia, G. (2018). Late Paleozoic seismic sequence stratigraphy and paleogeography of the paleo-Loppa High in the Norwegian Barents Sea. *Marine and Petroleum Geology*, *97*(May), 192–208. https://doi.org/10.1016/j.marpetgeo.2018.05.038

Street, W. (2000). Multibeam Sonar Theory of Operation L-3 Communications SeaBeam Instruments. *L-3 Communications SeaBeam*, 107.

SubSurfWiki. (2021). *Reflection Coefficient*. https://subsurfwiki.org/wiki/Reflection_coefficient

Urban, P., Köser, K., & Greinert, J. (2017). Processing of multibeam water column image data for automated bubble/seep detection and repeated mapping. *Limnology and Oceanography: Methods*, *15*(1), 1–21. https://doi.org/10.1002/lom3.10138

Vorren, T. O., Kristoffersen, Y., & Andreassen, K. (1986). Geology of the inner shelf west of North Cape, Norway. *Norsk Geologisk Tidsskrift*, *66*(2), 99–105.

Vorren, T. O., Lebesbye, E., Andreassen, K., & Larsen, K. B. (1989). Glacigenic sediments on a passive continental margin as exemplified by the Barents Sea. *Marine Geology*, *85*(2–4), 251–272. https://doi.org/10.1016/0025-3227(89)90156-4

Yielding, G., Freeman, B., & Needham, D. T. (1997). Quantitative fault seal prediction. *AAPG Bulletin*, *81*(6), 897–917. https://doi.org/10.1306/522b498d-1727-11d7-8645000102c1865d